

M.Sc. Thesis

Experimental study on the operational efficiency of modified sandwich filters for pesticides and phosphate removal from tile drainage water

Master of Science

Environmental Engineering

Faculty of Civil Engineering & Geoscience

Delft University of Technology

By

4226011

10-1-2025

Graduation Committee;

Dr. Ing. Kim Maren Lompe
Dr. Boris van Breukelen
Dr. Ir. Ralph Lindeboom
Dr. Ir. Bas Heijman

Tu-Delft
Tu-Delft
Tu-Delft
Tu-Delft

Acknowledgement

I would like to extend my gratitude to Kim Lompe, who has for the full duration of this thesis been an amazing support, listening ear and has continuously provided insight and ideas. Furthermore, I'd like to thank the lab staff of the Waterlab, specifically Jane and Patricia for their help, coffee and laughter.

Abstract

Pilot aquifer storage and recovery (ASR) systems are currently being built and operated to capture agricultural run-off water during wet seasons in an attempt to increase the availability of water during the dry seasons. The collected water requires treatment prior to infiltration due to its high fertilizers and pesticides concentrations in order to adhere to Dutch legislation surrounding underground storage. This study investigated the performance of two different carbon types which are currently in use in a pilot ASR plant in Texel, which used slow sand granular activated carbon (SSF-GAC) sandwich filters. The GACs used in this study, one mesoporous, Eversorb 520 (GAC-E), one microporous, Norrit PK1 (GAC-N), were compared through isotherm experiments and lab scale SSF-GAC sandwich filters, constructed for the first time in a way to allow for sampling in between layers, during a 14 week period. Additionally, one sandwich filter was augmented for the first time with an Iron Oxide Coated Sand (IOCS) top-up layer to assess its ability to remove phosphate and natural organic matter (NOM) from agricultural water. The water was doped with 10 µg/L for 5 pesticides commonly found in Dutch agricultural water: Atrazine, Bentazone, Chloridazon, Imidacloprid and Tebuconazole. Of these compounds, Bentazone showed extremely weak adsorption during all studies. It is unclear if the weak adsorption to both carbon types is contained to Bentazone as a compound or due to its positive charge. The isotherm experiments in high NOM water ($C_0 = 13.85$ mg/L) resulted in similar NOM loading on both carbon types, despite their difference in pore size distribution. The adsorption of pesticides was favored by GAC-E over GAC-N with higher loading (40 – 300 % in q_e) where it appeared that the surface functional groups of the GAC were the dominant factor in the difference in adsorption. Isotherm studies with the microporous GAC-N in two water types with varying NOM concentrations ($C_0 = 13.85$ mg/L vs 23.35 mg/L) found limited reduction in sorption capacity (30 – 40 % in q_e) for all compounds despite the fact that NOM loading on the GAC increased by 117 %.

During the column experiments the NOM loading was higher for the microporous carbon in contrast with the isotherm experiments, despite equal performance of the SSF in both columns. The adsorption of pesticides (EBCT 11.2 min) showed similar correlations as during the isotherm experiments, with 20 - 35 % higher breakthrough observed for GAC-N. Compensated for carbon density, the overall loading (µg/gGAC) was on average 45 % higher for GAC-N ($\rho = 250\text{kg/m}^3$) than GAC-E ($\rho = 500\text{kg/m}^3$), contradicting the isotherm experiments. Due to problems with gas accumulation between the GAC in combination with wall effects the empty bed contact time (EBCT) was negatively impacted, resulting in a mass transfer zone (MTZ) that was too short for the compounds to reach equilibrium over the columns. If GAC-N has higher adsorption kinetics than GAC-E it could explain the overall higher pesticide loading. The reduction in EBCT resulted in immediate breakthrough from week 1 onwards, with breakthrough curves showing linear patterns. As a result, it was not possible to accurately predict the sorption capacity of the columns or translate lab-scale performance to pilot data. Modelling with fixed bed adsorption software using homogenous surface mass diffusion (HSMD) and linear driving force (LDF) models was attempted but did not yield usable data for all pesticides.

The IOCS isotherms ($C_0 = 50$ mg PO_4^{3-} /L) showed Freundlich type adsorption of phosphate ($k_f = 5.39$ & $n = 2.04$), with additional high removal of calcium (37%), magnesium (27%) and potassium (10%), though these did not show Freundlich or Langmuir type adsorption. Phosphate removal

was successfully modelled with HSDM models which predicted breakthrough at 700 - 2000 bed volumes (BV) depending on the diffusion coefficients. The column experiments showed significantly faster initial breakthrough at 400 BV despite maintaining 55 min EBCT. The column maintained a significantly higher sorption capacity after initial breakthrough for longer than predicted, losing only 50% capacity over the course 2500 BV. During the column studies high removal of calcium was observed and it was theorized that phosphate formed calcium precipitation complexes at pH of 8. The removal of magnesium and potassium was absent during column studies. At the conclusion of the experiments, the IOCS had sorbed 12.8 mg PO_4^{3-} /gIOCS after 2573 BV with roughly 50% residual sorption capacity remaining.

As a result of pre-loading during production, the IOCS leached NOM during the isotherm experiments. Subsequent column experiments did not show NOM (UV254) desorption but rather showed NOM removal at higher rates than the SSF (10% vs 5%) which resulted in additional higher removal of NOM in the following GAC-E layer vs a column without the IOCS layer, exhibiting synergies between the layers.

The IOCS layer was successful in the removal of Imidacloprid from the influent, which started after 1100 BV or 6 weeks and is suspected to occur through biodegradation, peaking at 70 % removal at conclusion of the experiments. The SSF layer following the IOCS was presumably inoculated with the biomass and additionally removed 70 % of the Imidacloprid from the IOCS effluent. The combined IOCS-SSF removed 90 % of the Imidacloprid influent ($\mu\text{g/L}$), which has not been seen in these filters at such short EBCT to date for any compound. The SSF-GAC columns that did not contain IOCS did not show Imidacloprid removal, indicating that the biomass can only form on selective substrate. It is unclear at this point whether removal is contained to Imidacloprid or if additional compounds are susceptible for removal in IOCS layers. The combined influence of lower NOM and lower total pesticide loading on the GAC-E layer resulted in a 8 – 10 % increase in total pesticide adsorption vs the column that did not contain an IOCS layer, with 5 – 10 % lower breakthrough for all compounds. Chloridazon and Tebuconazole were likewise removed after 1100 BV or 6 weeks through suspected biodegradation in both the IOCS and SSF layers, peaking at 25 % and 40 % removal respectively. Though the biodegradation of these compounds has been proven in literature, it has not been observed in column studies at such high concentrations & removal rates at these low EBCT. It is hypothesized that the abundance of nutrients allowed for rapid bio growth and subsequent pesticide degradation.

The results of this study indicate that the augmentation of SSF-GAC sandwich filters with IOCS columns aid in the removal of phosphate, NOM and Imidacloprid, thereby extending the filters bed life and improving overall performance. While the removal of other pesticides remains to be investigated, the findings of this thesis underpin the use case of IOCS as a top up layer for SSF-GAC sandwich filters used to treat agricultural waters.

Contents

Acknowledgement.....	ii
Abstract.....	iii
List of abbreviations.....	viii
List of equations.....	viii
List of figures.....	ix
List of tables.....	xi
Introduction.....	xiii
Background.....	xiii
Problem description.....	xiv
Approach	xvii
Literature Review.....	1
Chapter 1: Slow sand filtration	2
1.1.1 Slow Sand filter design	2
1.1.4 Slow Sand Filter Ripening.....	2
1.1.5 Removal mechanisms for slow sand filtration	3
1.2 Physical treatment	3
1.2.1 Transport Mechanisms.....	3
1.2.2 Detachment Mechanisms	4
1.3 Degradation mechanisms	4
1.4 Slow Sand filter maintenance	6
1.5 Advantages and limitations of SSF treatment.....	7
Chapter 2: Water treatment by activated carbon.....	8
2.1 Properties of Granular Activated Carbon.....	8
2.2 Design and operation of GAC filters.....	10
2.3 GAC Removal Mechanisms	12
2.3.1 Adsorption	12
2.3.2 Biodegradation.....	15
2.4 GAC Adsorption Models.....	18
2.5 Advantages and limitations of GAC filters.....	20
Chapter 3: Multimedia Filters	21
3.1 Design and operation.....	21

3.2 Additional filter materials and top up layers.....	22
3.3 Advantages and limitations of multimedia filters	25
Chapter 4: Materials and Methods	25
4.1 Materials and Methods.....	25
4.1.1 Granular Activated carbon	25
4.1.2 Iron Oxide Coated Sand.....	26
4.1.3 OMP Selection.....	27
4.1.4 Water Matrix.....	31
4.1.5 Sampling and analysis	32
4.2 Isotherm experiments.....	33
4.2.1 GAC Isotherms	33
4.2.2 IOCS Isotherms.....	36
4.3 Colum experiments.....	37
Chapter 5 Results and Discussion	39
5.1 Physical characteristics of GAC	39
5.1.1 Surface Area.....	39
5.1.2 Grain size distribution	40
5.1.3 Observations during washing.....	40
5.2 GAC Isotherm results	41
5.2.1 Quality Control.....	41
5.2.2 Ion adsorption.....	43
5.2.3 NOM adsorption	44
5.2.4 Pesticide adsorption.....	46
5.3 IOCS Isotherm results.....	51
5.4 Column Results	56
5.4.1 Water Matrix.....	58
5.4.2 NOM adsorption	59
5.4.3 Phosphate adsorption on IOCS.....	63
5.4.4 Pesticide adsorption.....	66
6. Conclusion and Recommendations.....	73
Bibliography.....	76
Appendix 1 MSDS GAC.....	87

Appendix 2 Particle size distributions	89
Appendix 3 correction factor	91
Appendix 4 IOCS isotherms.....	92
Appendix 5 Pesticide Isotherms.....	93
Appendix 6 Column studies	96

List of abbreviations

Abbreviation	Definition
AC	Activated Carbon
BAC	Biologically Activated Carbon
BOC	Biologically Organic Carbon
BV	Bed Volume
CAPEX	Capital Expenditures
CUR	Carbon Usage Rate
DO	Dissolved Oxygen
DOC	Dissolved Organic Carbon
EBCT	Empty Bed Contact Time
GAC	Granular Activated Carbon
GAC-N	GAC type Norit PK1
GAC-E	GAC type Eversorb 520
IOCM	Iron Oxide Coated Media
IOCO	Iron Oxide Coated Olivine
IOCS	Iron Oxide Coated Sand
MTZ	Mass Transfer Zone
NOM	Natural Organic Matter
NTU	Nephelometric Turbidity Unit
OMP	Organic Micro Pollutants
OPEX	Operating Expenditures
PPCP	Pharmaceuticals and Personal Care Products
SSF	Slow Sand Filter
TOC	Total Organic Carbon
TSS	Total Suspended Solids

List of equations

Equation 1 EBCT formula	11
Equation 2 Carbon equilibrium loading	18
Equation 3 Langmuir equation.....	18
Equation 4 Freundlich equation.....	19

List of figures

Figure 1 Schematic overview of tile drainage pipes (Sands, 2024)	xiii
Figure 2 Schematic overview of a slow sand granular activated carbon sandwich filter (Li, Campos, Zhang, & Xie, 2022).....	xiv
Figure 3 General overview of a slow sand filter, along with component indications. From (Huisman, 1974).....	2
Figure 4 Conceptualized representation of ozonated DOC removal by adsorption and biological degradation over time (Dussert & Van Stone, 1994)	17
Figure 5 Particle size distribution IOCS. Shaker parameters: T=10mins. Amplitude=0.5mm/g. Interval 10 seconds.....	27
Figure 6 Cluster analysis of OMPs present in Zuid-Holland surface waters	28
Figure 7 Schematic overview of column setup (A) and full column setup (B)	38
Figure 8 Particle size distribution for Norit PK1-3M and Eversorb 520.....	40
Figure 9A-B Difference in TOC (A) and UV254 adsorption (B) for the Boskoop and Schie waters on the same type of carbon (Norit PK-1). Error bars depict variance between control bottles.	45
Figure 10A-B Difference in TOC (A) and UV254 (B) adsorption for the two different carbon types (Eversorb and Norit PK-1) in an identical water matrix (Schiewater). Error bars depict variance between control bottles.	45
Figure 11A-D Comparison of adsorption of GAC-N and GAC-E in Schiewater for 4 pesticides. Error bars as variance in control bottles (too small to be observable).....	48
Figure 12 IOCS Isotherm results for the 3 week set. PO_4^{3-} (blue, left axis) TOC (Red, right axis) and Nitrate (Purple, right axis). Measurement error too small to depict.....	51
Figure 13A-B phosphate isotherm results for normal (A) and log (B) scales, derived with Freundlich equations. Measurement error too small to depict.....	54
Figure 14 Modelled breakthrough curve for phosphate removal ($\text{C}_0 = 10\text{mg/L}$) from the IOCS column. Parameters can be found in table 19. Conversion of Weeks to BV in Appendix Column studies.	55
Figure 15A-B Air entrapment in (A) column 1 (GAC-N) and (B) column 2 (SSF) observed during week 5.5	56
Figure 16 flow rate over time for each column. Dashed lines indicate start and end of weekly flushing .	57
Figure 17 A-B UV254 absorbance, TOC influent and effluent concentrations for SSF and IOCS layer over each column layer versus influent concentrations during the 14 week study. Error bars indicate variance between control bottles.	60
Figure 18A-B UV254 absorbance, TOC influent and effluent concentrations for the GAC layer over each column during the 14 week study. Error bars indicate variance between control bottles.....	61
Figure 19A-B UV254 absorbance, TOC influent and effluent concentrations for all columns during the 14 week study. Vertical lines indicate start and end of weekly flushing Error bars indicate variance between control bottles.	62
Figure 20 Breakthrough curve for phosphate on the IOCS column during the 14 week column study ($\text{C}_0 = 10\text{mg/L}$) together with the modelled breakthrough curve.	64

Figure 21A-D Breakthrough curves for the SSF and IOCS layer in each column during the 14 week study. Vertical lines indicate start and end of weekly flushing. Error bars indicate variance between influent measurements (Table 23).	68
Figure 22A-D Breakthrough curves for the GAC layers in each column during the 14 week study. Vertical lines indicate start and end of weekly flushing. Error bars indicate variance between influent measurements (Table 25).	70
Figure 23 A-D Breakthrough curves for each column during the 14 week study. Vertical lines indicate start and end of weekly flushing. Error bars indicate variance between influent measurements (Table 26).	71
Figure 24A-B Bentazone C_e/Q_e (A) and log-log (B) plots. Plots where not suitable to model Freundlich or Langmuir isotherm parameters.	94
Figure 25A-D log-log plots for the 4 compounds used for Freundlich modelling	95
Figure 26 Salt tracer test (1mg/L NaCl) for all columns performed prior to the column experiments	96
Figure 27 Phosphate breakthrough modelled with BV instead of weeks.	97
Figure 28 Nitrate and phosphate levels in the SSF and IOCS layers of the columns. Dashed lines indicate start and end of weekly flushing. Variance too small to be visible. Note the difference in C/C_0 axes.	98
Figure 29A-C bentazone breakthrough curves for column studies. Breakthrough over SSF/IOCS (A), over GAC layer (B), over whole column (C)	99
Figure 30 biogrowth on sand column. Photos taken after weeks 4,8,14	100

List of tables

Table 1 General properties of selected GAC's (Calgon Carbon Corporation, 2024; EVERS GmbH & Co. KG, 2024).....	8
Table 2 GAC types and properties used	25
Table 3 selection of OMP's proposed by Acasia. From: (University of Hertfordshire, 2023).....	29
Table 4 Selection of OMP's used in this research. From: (University of Hertfordshire, 2023)	29
Table 5 Molecular structures influencing adsorption of OMPs used in this research	30
Table 6 Comparison between tile drainage water from Texel (sampled March 2023), Thames feedwater(Data from (Bauer, et al., 1996) for their sandwich filters, Schiewater (sampled June 2023) and Boskoop water (sampled July 2023). Data labelled N/A was either not available (Thames Water) or below the detection limit (rest)	31
Table 7 GAC isotherm reactor set	35
Table 8 IOCS Isotherm reactor set	36
Table 9 Content of each column in the column study including weight and size of column units.	37
Table 10 Pore volume and density parameters of both carbon types	39
Table 11 Ions leached from the washed GAC, soaked for 2 weeks ultrapure water.	40
Table 12 Variability in duplicate reactor uptake	42
Table 13 Selective bottles from TOC measurements. Low concentration GAC reactors often returned higher TOC values than control bottles.....	42
Table 14 Ionic water composition and ion adsorption by GAC for each isotherm	44
Table 15 7 Day isotherm sample to check if equilibrium had been attained	50
Table 16 Kf and N values for pesticides used in the Isotherm experiments derived using Freundlich equation kf in $(\mu gmg)/\mu gLn$	50
Table 17 IOCS reactors in ultrapure water to determine NOM release due to selective displacement by phosphate.....	52
Table 18 Cation removal during IOCS isotherms. Note that P1-6 is marked as outlier	53
Table 19 Parameters set for modelling phosphate breakthrough on the column experiments.	55
Table 20 Average NOM and ion concentration of the influent water during the column experiments. ...	58
Table 21 Average pesticide concentration of the influent water during the column experiments, in $\mu g/L$	58
Table 22 Phosphate vs calcium removal in the IOCS column	64
Figure 22A-D Breakthrough curves for the SSF and IOCS layer in each column during the 14 week study. Vertical lines indicate start and end of weekly flushing. Error bars indicate variance between influent measurements (Table 23).	68
Table 24 Mass pesticide removed in each GAC layer, both absolute and per gram of GAC used. Note that the majority of Imidacloprid is removed in the IOCS layer, resulting in a low total loading.	69
Figure 23A-D Breakthrough curves for the GAC layers in each column during the 14 week study. Vertical lines indicate start and end of weekly flushing. Error bars indicate variance between influent measurements (Table 25).	70

Figure 24 A-D Breakthrough curves for each column during the 14 week study. Vertical lines indicate start and end of weekly flushing. Error bars indicate variance between influent measurements (Table 26).....	71
Table 27 Particle size distribution for both carbon types.....	89
Table 28 PSD for the IOCS.....	90
Table 29 Theoretical vs measured concentration of pesticides in the stock solution and the correction factor derived	91
Table 30 IOCS Isotherm data table.....	92
Table 31 Conversion of weeks to BV for IOCS breakthrough simulation based on Freundlich Isotherm data.....	92
Table 32 Raw LC-MS data for all compounds. Note; values are not corrected for the correction factor (Table 29).....	93
Table 33 Salt tracer test data for all columns.....	96
Table 34 Bed volumes for all layers during the 14 weeks of operation of the column experiments.....	97

Introduction

Background

In recent years, the effects of global warming have been causing more extreme fluctuations in seasonal weather, which resulted in either excess or shortage of water available for agriculture in any given season. While there is still a net surplus of water during the year, the majority of the rainfall occurs during the autumn season, when water is diverted away to ditches and rivers. During the summer season there is a shortage of groundwater for agricultural use due to increased evaporation and decreased precipitation (van Gaalen, et al., 2024). This disconnect is expected to increase further in the coming decades as climate change progresses (Verweij, van der Wiele, van Moorselaar, & van der Grinten, 2010). One possible solution to this problem that has been investigated recently is the development of aquifer storage and recovery (ASR) systems that collect and store excess water underground during the wet season, allowing for recovery and irrigation during the dryer summer months. It is expected that around 70 % of the injected water can be recovered, with the rest migrating through the aquifer (Maliva, Guo, & T.M., 2006). Water intended for underground storage is subjected to treatment requirements in accordance with Dutch legislation regarding water quality (Omgevingswet, 2024). This is especially needed for water collected from agriculture due to the high pesticide and fertilizer use in the Netherlands (Table 6). In the Netherlands, an ASR pilot study has been built in Texel, where agricultural runoff water is collected via the tile drainage channels underneath the agricultural fields and subsequently treated before being stored underground. The water collected with this method is referred to as tile drainage water (TDW). The systems themselves are referred to as tile drainage systems as they used to be comprised of permeable ceramic tiles installed 1 - 2 meters below the surface. Nowadays, this is done with perforated HPDM pipes installed several meters apart (Figure 1). These channels are commonly present in Dutch agricultural fields as a method of rainwater diversion and to help control the naturally high groundwater level. In addition to the pilot in Texel, a second ASR-pilot which utilizes similar treatment is currently being constructed in Boskoop, which plans to use water collected from various sources around a horticultural company, such as rainfall collection and the re-use of irrigation water.

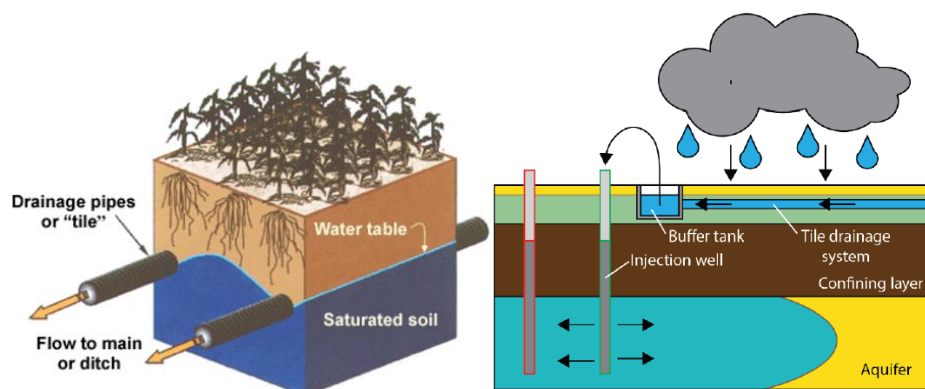


Figure 1 Schematic overview of tile drainage pipes (Sands, 2024)

Problem description

TDW generally has high nutrient concentrations and can contain various pesticides, which differ from site to site, depending on local pesticide use. In accordance with the “Omgevingswet” the concentration of the sum of all organic micropollutants (OMPs), the overarching class that also contains pesticides, should fall below 0.5 µg/L, where the maximum allowable concentration of an individual OMP has a limit of either 0.05 µg/L or 0.1 µg/L depending on the substance. The maximum allowable concentrations for fertilizers are 0.4 mg PO₄³⁻/L and 5.6 mg NO₃²⁻/L. For Texel, pesticide types and concentrations can vary significantly and are dependent on what the farmers use in a given year. Fertilizer concentrations of 4.502 mg PO₄³⁻/L and 43.02 mg NO₃²⁻/L have been reported, severely exceeding maximum allowable concentrations.

The treatment method used in the Texel pilot consists of a slow sand filter (SSF) with a layer of granular activated carbon (GAC) in the middle, a type of multimedia filter also commonly referred to as sandwich filters (Figure 2). This type of filter was first implemented in the 1990s by Thames Water and where designed to remove nutrients, natural organic matter (NOM), and OMPs from the influent water (Bauer, et al., 1996). The first layer (SSF) acts as both a physical strainer and biofilter as it will form a schmutzdecke over time, removing nutrients and NOM by physical and biological treatment, filtering solid particles, and additionally serving as a protective layer for the brittle activated carbon (AC) beneath. While there is some biological activity in the AC, the main removal of OMPs occurs through adsorption (Bauer, et al., 1996; Gimbel, Graham, & Collins, 2006). The sandwich filters are known to have a higher OMP removal rate than standalone SSF or GAC filters due to the combination of NOM removal and selective biodegradation of OMPs, which extend the GACs bed life (Li, Zhuo, & Campos, 2018).

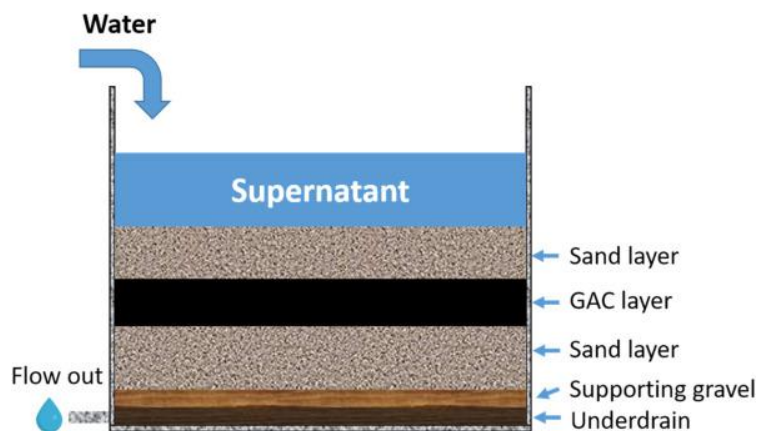


Figure 2 Schematic overview of a slow sand granular activated carbon sandwich filter (Li, Campos, Zhang, & Xie, 2022)

If the pilots in Texel and Boskoop prove to be successful, it could lead to the implementation of ASR systems utilizing SSF-GAC sandwich filters nationwide. While all treatment locations have to adhere to the same legislation, the water matrices between locations differ significantly and even vary from field to field for a given location, as is the case in Texel (Table 6). If it is possible to use the sandwich filters as a “one system fits all” solution, it would reduce project complexity both in construction as well as maintenance. TDW is naturally high in NOM, which is problematic for GAC filters as it can lead to pore blockage and preloading of the carbon, severely reducing the performance and lifetime of the filter. While GAC in drinking water treatment is subjected to a maximum of 4-8 mg NOM/L, concentrations in TDW have been

reported up to 23 mg/L (Table 6) and far exceed the filters' design values (Bauer, et al., 1996). As such, the concentration of NOM reaching the GAC layer should be reduced as much as possible to extend the filters' lifetime. While the sandwich filters are known to be resilient to variations in influent water, as is the case with Thames water (Bauer, et al., 1996), is it unknown how well they perform with different variations of much higher nutrient, higher NOM containing agricultural water matrices as seen on Texel and Boskoop (Table 6). This can make it difficult to determine the impact of varying water matrix compositions on GACs performance for pesticide removal. The first research question of this thesis research can thus be formulated as:

What is the influence of differences in high nutrient, high NOM water compositions on GAC adsorption for sandwich filters?

While the sandwich filters were efficient in the removal of OMPs from influent water for drinking water treatment, their popularity fell out of grace after the 1990s with the onset of modern treatment methods such as ozonation. This resulted in little to no publication of research up until the early 2020s. Due to the long absence of interest in sandwich filters and the quick rise of OMPs, there remain a large number of unknowns regarding the exact optimal working of the filters in the context of high nutrient, high NOM containing waters. The main physical components that can be optimized for the sandwich filters are the type of filter sand and GAC used. GAC can be created from a large range of precursor materials, each with its own characteristics and optimal removal rates tailored to the treatment of specific groups of substances. These material differences can range from density, adsorption affinity as a result of the GACs surface chemistry, pore size distribution, and available surface area. These base GAC properties already have a large influence on the adsorption of OMPs in conventional drinking water treatment, where several pre-treatment steps are present to prevent the rapid loading of the GAC with NOM. In TDW, there are no pretreatment steps except for the preceding SSF layer, exposing the GAC not only to the OMPs, but also to significantly higher NOM concentrations. This high NOM load can lead to preloading and pore blockage, which can quickly deplete filter capacity. Furthermore, the use of fertilizers results in a high ionic strength water matrix (Table 6), which is theorized to negatively influence the adsorption of OMPs onto AC (Youcef & Abdelkader, 2017; Abdelkader & Youcef, 2016; Heo, Lee, Koh, & Chang, 2007). At the pilot site on Texel, three different GAC types have been installed in two parallel sandwich filter pilots, though it is too soon to conclude what their performance is. While each carbon type is marketed for OMP treatment, the question remains as to which carbon performs best in the treatment of TDW. The second research question can thus be formulated as:

What is the effect of the type of GAC on the OMP pesticide adsorption in a multimedia sandwich filter?

While it has long been known that in a sandwich filter, the upper sand layer acts as a biological and physical treatment step (Weber-Shirk & I. Dick, 1997), little is known about the effects of adding top-up layers to sandwich filters to aid the removal of specific compounds. Previous research advised further investigation into other treatment technologies and materials to combine with conventional SSF layers for SSF-GAC filters but have so far not yielded suitable replacements (Li, Campos, Zhang, & Xie, 2022).

An older study performed with standalone SSFs found that swapping out the sand for an iron oxide coated olivine (IOCO) greatly improved the removal efficiency of NOM by adsorption onto the IOCO while also noting that the adsorption sites were bio-regenerated over time due to the low hydraulic rate. The difference in performance between sand and IOCO was especially prevalent in colder environments (McMeen & Benjamin, 1997). These findings have yet to be tested or implemented in combination with multi-media filters such as the proposed sandwich filters or in combination with other layers outside of the conventional drinking water treatment (McMeen & Benjamin, 1997). While these authors did not mention the removal of phosphate, more recent studies have found that iron oxide coated sand (IOCS) was also effective at the removal of phosphorus from wastewater (Zhang, Wang, Lakho, Yang, & Depuydt, 2022). Likewise, iron slag from steel production has previously been suggested for phosphorous removal from TDW (Edgar, Hamdan, Morales, & Boyer, 2022). IOCS is produced as a waste product from drinking water operations in the Netherlands/Belgium and, as such, is an abundant material. The TDW at the pilot study in Texel has exceptionally high NOM and nutrient content (phosphate and nitrate; Table 6), for which treatment is warranted, as mentioned before. This is both to prevent the quick depletion of the GACs sorption capacity but also to adhere to the Dutch laws regarding subsurface storage of water (Omgevingswet, 2024). Using IOCS as a top-up layer has not yet been tested in a sandwich filter setup nor with the exceptionally high nutrient / NOM containing TDW. The third research question is thus formulated as:

What is the influence of using iron oxide containing media (IOCM) as a top layer on the performance of the sandwich filter?

These research questions will need to be answered to obtain more information around the optimal composition of SSF-GAC filters and to investigate what the influence of differing water matrix compositions at various locations is. A “one filter fits all” would be ideal as it allows for a simple to implement, simple to maintain solution. The potential augmentation of the IOCS layer could further increase its removal capacity of phosphate and NOM, increasing the overall filter performance. Combining these research questions posed above with the use case for the sandwich filter in the Texel and Boskoop pilots results in the overarching thesis question that can be formulated as:

Can a SSF-GAC sandwich filter be tailored with IOCS to remove both pesticides and nutrients from TDW?

Approach

This thesis will focus on the operational efficiency of lab-scale pilot SSF-GAC sandwich filters for pesticide and nutrient removal using different configurations. A literature study will be conducted to determine the extent of past research on the topic and to properly understand the current state of knowledge for the different components that make up the SSF-GAC sandwich filters, as well as determine the driving forces around nutrient and pesticide removal for each layer in the filter.

Batch isotherm experiments will investigate the influence of different carbon types and water matrices on the adsorption of pesticides in TDW as well as investigate the sorption of phosphate onto IOCS. A following lab scale column study with sandwich filters will be operated for 14 weeks to investigate the influence of the different GAC types in an actual filter setup. A separate, third sandwich filter will be augmented with an IOCS layer to investigate the influence of the material as a top-up layer. The filters will be sampled weekly from each layer to determine the contribution of each separate layer to the overall filter performance. The sampling of each individual layer has not been done before and has been named as a recommendation from previous research to gain insight into the exact workings of the filters (Li, Campos, Zhang, & Xie, 2022). The results from the isotherm experiments will be used in an attempt to predict the breakthrough for the column experiments using homogeneous surface diffusion models (HSDM) and linear driving force (LDF) models from existing software (Burkhardt, 2025; FAST, 2024). The results of the column tests can, at a later stage, be compared with operational data from the pilot plant in Texel to investigate the differences between lab-scale and pilot-scale testing.

Literature Review

Water treatment with sand dates back to as far as 2000 BC, from which Greek and Sanskrit writings recommended methods for water treatment, including sand and gravel treatment. Over time, these treatment methods evolved, with the first known slow sand filtration units dating back to 1804.

The use of AC for water treatment followed much later, during the 70's, when the rapid rise in concentrations of OMPs in surface waters became a problem for conventional drinking water treatment. The high adsorption capacity made GAC a natural choice to remove OMPs and has since been actively used worldwide. Around this time, Thames Water combined the two technologies in what it first called its "super filter", creating a layered sandwich of a SSF and an activated carbon layer, followed by a sand gravel drainage layer (Bauer, et al., 1996). This was done as Thames Water required the adsorption capacity that GAC provided, but noticed that a standalone GAC column was too brittle to operate under heavy loading conditions and would be subjected to regular scraping from the buildup of material on top of the filter deck, similar to conventional SSFs. As GAC was too expensive to be disposed of with scraping, a sacrificial SSF layer was added on top.

With the rise of both the number and concentration of (measurable) OMPs over time, this filter combination has recently received renewed attention as a low-cost, resilient, advanced water treatment method. The following chapters will focus on the treatment mechanisms and state-of-the-art knowledge of SSF and GAC filters, with a concluding chapter that will examine the synergies of combining the two materials. In Chapter 3: Multimedia Filters, the SSF-GAC sandwich will be linked to the physiochemical and biological removal mechanisms in SSF and GAC filters to predict their removal rate in the column studies of this research. Additionally, the use of non-conventional filter layers, so-called "top-up layers", will be discussed as a theoretical expansion to SSF-GAC sandwich filters to increase the removal of nutrients and NOM, thereby prolonging filter life.

Chapter 1: Slow Sand Filtration

Slow sand filtration (SSF) is a treatment method most commonly used in the production of drinking water, but has due to its versatility and easy off implementation recently been employed in the secondary treatment of wastewaters and agricultural waters (Langenbach, Kusch, Horn, & Kästner, 2009). The filtration method utilized a combination of physical and biological aspects to treat water and is effective in the removal of organic matter (color and odor), turbidity, viruses, and bacteria, whilst requiring little maintenance and oversight, making it a popular method of water treatment even for modern plants.

1.1.1 Slow Sand Filter Design

SSFs can be subdivided into two different types: gravity and pressure filters. As this research focusses on gravity filters, pressure filters will not be taken into further account. Gravity filters are essentially a large open box (usually made of concrete filled with sand and a drainage system on the bottom). The SSF setup consists of 5 main components: the supernatant water, schmutzdecke, filter medium, flow control, and filter underdrain (Figure 3).

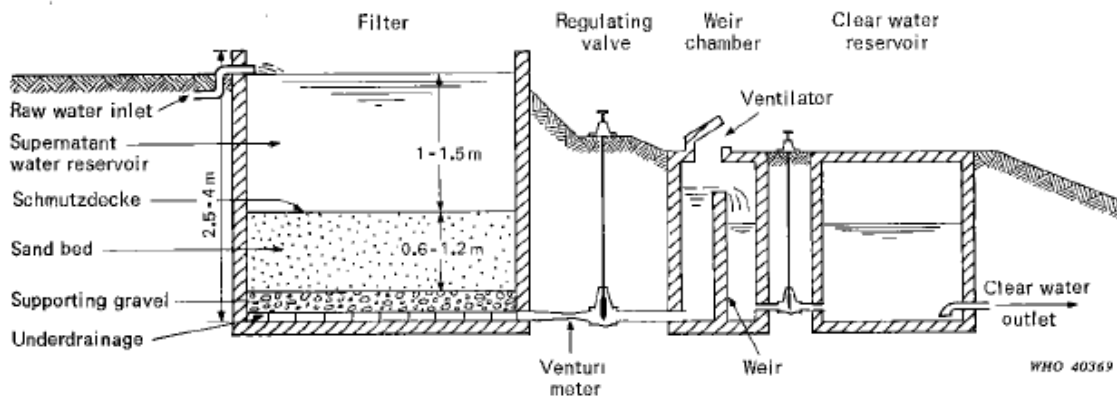


Figure 3 General overview of a slow sand filter, along with component indications. From (Huisman, 1974)

As the filter is operated over time, nutrients, NOM, bacteria, and other suspended matter will accumulate on top of the filter bed where a biologically active layer is formed that is commonly referred to as the schmutzdecke. This consists of a slimy layer of bacteria, algae, and other higher lifeforms that feed on the material in the influent (biodegradation) and on the biomass itself (predation), providing the biologically active treatment that SSFs are known for. The schmutzdecke and biological degradation of material will be elaborated further on in this chapter.

1.1.4 Slow Sand Filter Ripening

The development of biomass in a newly sanded SSF takes some time to develop, during which the filtrate is commonly discarded as it does not always adhere to treatment standards. This period of development is also called the “ripening period”. The exact duration of ripening is dependent on several factors; most notable are the nutrient load, water temperature, and flow rate. Covering a SSF can decrease the rate of biomass development at the surface by a factor 5 and deeper in a filter (>8 cm depth) by up to a factor 10 (Campos, Su, Graham, & Smith, 2002). A similar decrease in biomass accumulation occurs at higher flow rates and decreasing contact times, which have a detrimental effect on nutrient retention. In a

measurement campaign by Thames Water it was found that DOC and TOC concentrations decreased by 40 % and 50 % respectively in the first 20 days of SSF ripening, from an influent concentration of 3 mg/L at 15 °C water (Campos, Su, Graham, & Smith, 2002). A 2015 study on sand filters with 15 mins EBCT and an acclimation time of 4 months found only 5 % DOC removal at water temperatures of 2 °C from an influent concentration ranging between 5.14 and 7.16 mg/L (Halle, Huck, & Peldszus, 2015). This indicates that biomass development is temperature-dependent in filter ripening, even at high nutrient loads. Results from other studies suggest that the development of biomass in a SSF is highly dependent on the influent water conditions and, therefore difficult to predict exactly (Campos, Su, Graham, & Smith, 2002). Increasing the nutrient concentration, decreasing the flow rate and inoculation with bacteria of a mature SSF have all led to decreased ripening periods (Arora, 2017).

1.1.5 Removal mechanisms for slow sand filtration

The removal of contaminants in a SSF occurs through a multitude of forces that the particles are subjected to while entering and travelling through the filter, often acting in parallel to, and influencing each other. As mentioned before, a SSF treats water through physical, chemical, and biological removal processes (Huisman, 1974). The mechanisms involved in physical treatment can be referred to as transport and attachment mechanisms, while biological treatment is referred to as the purification mechanisms. Whereas transport mechanisms are responsible for bringing suspended matter into contact with the filter surfaces, it is the attachment mechanisms that ultimately ensure particles are retained within the filter and the biological processes that contribute to the eventual removal of particles (Weber-Shirk & I. Dick, 1997).

1.2 Physical treatment

1.2.1 Transport Mechanisms

Screening or straining is the removal of particles by retaining them at the top of the bed when they are too large to pass through the pore channels and are thus retained. With uniform grain sizes of 0.15 to 0.35 mm, the pore channels between the grains can retain particles up to 15 µm, trapping larger particles at the surface. As particles travel through the sand filter, they agglomerate and aggregate to a point where they eventually will be retained. Additionally, the screening of particles at the surface creates a layer of sediment that is finer than the initial pore channels. The maturation of the *schmutzdecke* aids the straining of material as it enters the filter both due to attachment mechanisms and due to the entrapment of increasingly smaller particles, thereby narrowing the pore channels and increasing filtration capacity. Over time, the pore spaces in this layer will decrease in size as the filter retains ever smaller particles. This increases the screening efficiency of the filter but comes with the cost of decreased permeability as a result of increased bed resistance (Arora, 2017; Weber-Shirk & I. Dick, 1997).

Sedimentation occurs in the filter bed where suspended matter is precipitated onto the sand grains. In contrast to a regular settling tank where grains are only deposited on the bottom, sedimentation in a SSF occurs throughout the whole bed, as each layer of sand particles allows for a surface area where suspended matter can be deposited, although most particles are retained at the top of the filter layer.

Other transport mechanisms that occur deeper in the filter and play a minor role in particle removal include interception, collision due to inertia, diffusion/attachment as a result of Brownian motion and hydrodynamic actions. As most particles are retained at the top of the filter, these forces contribute little to the overall removal and only affect the smaller particles that were able to pass through the schmutzdecke in the first place (Huisman, 1974).

1.2.2 Detachment Mechanisms

Detachment of particles is also possible due to differences in the strength of links between grain surfaces and varying particles. As a result, selective displacement can take place. In this scenario, particles that have adhered to grain surfaces with weaker links are released from said grain surface when particles that are subjected to a stronger adherence force are encountered. This process can continue for as long as new particles are being supplied to the filter that are subjected to stronger adherence forces than the particles currently in the filter. Experimental studies concluded that detachment of filter bed deposits is a major source of particles found in the filter effluent (Ginn, Amirtharajah, & Karr, 1992). This indicates that even in a well-operated filter, particles can be found in the effluent due to selective detachment well before the adsorption capacity is achieved (Jegatheesan & Vigneswaran, 2009).

1.3 Degradation mechanisms

Entrapped particles in a SSF can be removed through various biological processes. The two main mechanisms are biodegradation (through assimilation, oxidization, and degradation) of incoming particles and predation of organisms on the existing biomass in the filter (Huisman, 1974). According to literature, large hydrophobic humic organic molecules are predominantly removed by adsorption, while the smaller organic molecules are removed by both adsorption and biodegradation (Collins, Eighmy, & Fenstermacher, 1992). The schmutzdecke can be divided into two sections: a slimy layer, or filter cake on top of the sand packet and a biologically active region in the upper part of the sand bed, up to 10 cm deep (Chen, et al., 2021). How well a SSF can biodegrade NOM and OMPs, as well as the active depth of the biomass present in a SSF has been linked to the availability and concentration of nutrients, which are needed to sustain the biomass required for purification (Logsdon G. , 1987; Chen, et al., 2021; Campos, Su, Graham, & Smith, 2002).

In a SSF study between nutrient poor raw water from the Rocky Mountains that had an initial turbidity of 6-8 NTU, and nutrient rich surface water with an initial turbidity of 0.4-4.6 NTU, it was found that the turbidity of nutrient poor water could not be reduced down to the required level below 1 NTU, while this was attained with the nutrient rich water. This was attributed to the growth in biomass in the nutrient-rich filter that allowed the removal of unwanted components (Bellamy., Hendricks, & Logsdon, 1985b; Bellamy, Silverman, Hendricks, & Logsdon, 1985a). Similar studies found that the percentage of NOM removal in SSF increases with higher organic influent concentrations or increased loading rate, indicating an increased performance of the biomass present at increased nutrient inflow (Collins, Eighmy, & Fenstermacher, 1992).

The removal of OMPs in a SSF has been studied extensively over time, but due to the large variations between OMP groups and differences in operating parameters, it is difficult to predict exact removal rates for OMPs, both as a collective group and individual components. Among the factors that influence

biodegradation are number of OMPs present in the influent water, OMP concentration, molecular structure, pH, filter age, temperature, bacterial biomass present and duration of exposure (Aislabie & Lloyd-Jones, 1995). One factor that most OMPs share is that biodegradation generally only occurs under aerobic conditions, indicating that this is only possible in the schmutzdecke (Aislabie & Lloyd-Jones, 1995). While some pesticides can be biodegraded by SSF, the (initial) presence and toxicity of others negatively affect the biomass in a SSF, both by selectively killing off bacterial species and impacting removal rates (D'Alessio, Yoneyama, Kirs, Kisand, & Ray, 2015). Atrazine is a herbicide commonly found in The Netherlands, including the Texel, and is well documented as a biodegradable pesticide at room temperature in filters with prolonged exposure to the herbicide, but bio-degradation quickly drops at lower temperatures (Chowdhury, et al., 2021).

Prolonged exposure of the biomass to OMPs increases the formation of bacterial cultures that are resistant to and even can selectively degrade OMPs (D'Alessio, Yoneyama, Kirs, Kisand, & Ray, 2015). Studies in river bank filtration found that the presence of ethers and carbonyl groups in OMPs will increase their biodegradability, while the presence of amines, ring structures, aliphatic ethers, and sulfur will decrease biodegradability (Bertelkamp, et al., 2014). To the author's knowledge, only one published study has attempted to quantify the effects of adsorption versus biodegradation of OMPs onto SSFs, but failed to gain conclusive results as the concentration of NOM and nutrients was too low to form sufficient biomass needed for biodegradation (Bertelkamp, et al., 2014).

The presence of algae in the supernatant water can significantly influence SSF performance. In spring and summer, the growth of algae in the filter usually outpaces its death rate (net addition of algae). As a result concentration of DO will increase, whilst simultaneously decreasing the CO_2 concentrations. The former is beneficial for filtration as it increases biomass and nutrient uptake. The latter can be detrimental, as it can cause bicarbonates to dissociate and disrupt the bicarbonate buffer, causing calcium carbonate to precipitate, which can cause filter clogging. A large increase in algae content hinders the downward movement of water through the filter, requiring periodic removal.

The presence of algae in the filter is beneficial as long as their growth has reached a steady state, where the production of oxygen aids the filter biomass, both directly and by reacting with organic matter in the influent, making it more easily biodegradable. Algae can therefore aid in converting organic matter that is not biodegradable by filter biomass into biodegradable biomass, increasing NOM/TOC reduction. The high DO production by algae further increases the oxidative activity of the water and thus the conversion of unassailable organic matter into biodegradable organic matter. In the absence of daylight, the oxygen content can rapidly decrease, in extreme cases leading to anaerobic conditions in the filter, diminishing its purification capacity. During autumn and winter, algae death will outpace growth due to lower temperatures and decreasing amounts of sunlight. This results in an increase in organic matter but a decrease in oxygen concentrations in the filter, creating the possibility for anaerobic conditions. The same can happen at sudden temperature drops during warmer periods, which causes mass algae death and can take the filter out of commission for a while (Huisman, 1974).

As such, it is recommended to periodically remove algae from the filter, thus managing their concentration to prevent unwanted fluctuations in DO, CO_2 or dying biomass. The type of algae growing in the filter also

influence performance, filamentous algae can be beneficial as they act as floating filters, whereas diatomaceous algae grow on the schmutzdecke and can rapidly clog the filter. Different studies have investigated the effects of covering the SSF during operation. It was found that covering the filters decreased the rate and mass of total biomass formed during filter ripening but did not result in a reduction in the effluent quantity of the TOC and DOC (Campos, Su, Graham, & Smith, 2002). Other experiments found different results, which showed that covering did reduce both the rate of development and total biomass and found that covering impeded the removal efficiency of TOC and DOC (Barrett, Bryck, Collins, Janonis, & Logsdon, 1991). One key difference in both experiments is the fact that the influent water in the study of Campos had advanced water treatments such as reservoirs, pre-ozonation, floatation, rapid filtration, intermediate ozonation, and AC as preceding treatment steps, while the study by Collins used the SSF as first-in-line treatment. This makes it significantly more likely that a larger amount of bio-available organic material was present in the first study, resulting in more pronounced results in the effluent. In climates with highly fluctuating temperatures, covering a SSF is recommended as it ensures more regular filter runs and prevents excessive maintenance.

Excluding algae, up to 80 % of the total biomass concentration in the SSF is formed in the schmutzdecke and the top 2 cm of the sand packet (Chen, et al., 2021). The majority of the remaining 20 % of the biomass can be found in the top 10 cm of the sand packet, with only minor amounts that accumulate deeper in the filter as nutrients and oxygen become scarce and competition becomes greater (Chan, et al., 2018). Mature biofilters that are in operation for several years may have developed substantial biofilms in their deeper layers, hosting a microbial community essential for maintaining consistent water quality even after schmutzdecke removal resulting from maintenance (Chan, et al., 2018). A recent study proved the removal of E.coli WR1 by an active biofilm on all depths of a sand filter bed that was 19 years old, thereby highlighting the effect of deep layer biodegradation in mature sand filters (Trikannad, van Halem, Foppen, & van der Hoek, 2023). This is in contrast to older research, where it is mostly assumed that biological activity is constrained to the top few centimeters (Huisman, 1974). The total depth an active biomass can reach in a SSF increases with increasing flow rates and nutrient loading as it allows nutrients to penetrate deeper into the filter before they are consumed. The bulk of SSFs in the world operate without pre-treatment and receive higher loads of nutrients, particulate matter, and organics that could lead to an even more pronounced deep-layer microbial community and contribution to overall water treatment (Trikannad, van Halem, Foppen, & van der Hoek, 2023).

1.4 Slow Sand filter maintenance

The duration that a single SSF run can operate before terminal head loss is reached lasts until bed maintenance is required to restore hydraulic conductivity and depends on the composition of the influent water, hydraulic loading rate, and environmental conditions (mainly temperature). Due to large variations of influent waters, filter runs have been reported to last between several months up to 15 years (Arora, 2017). The accumulation of material on top of the filter bed and biomass growth in the schmutzdecke is responsible for the majority of head loss in a SSF. Restoring head loss is traditionally done by scraping, a process in which the water level is dropped to just above the sand packet and the top 2 - 3 cm of the sand packet is removed to restore permeability in the filter. Although the scraping process removes the majority of the biomass and temporarily diminishes the purification capacity of the filter, the biomass is

able to regenerate significantly faster than during its first development due to the remainder of residual matter deeper in the sand layers (Huisman, 1974). The recovery period can take anywhere between hours to several weeks depending on the filters age, its sand characteristics and biomass depth and influent water quality (Cullen & Letterman, 1985). The scraping process can be repeated until the minimum height of the sand in the SSF that is needed to properly function is reached, at which points the entire bed has to be lifted from the filter, cleaned and replaced by a new, full bed.

A second method, harrowing, was developed later in an attempt to restore hydraulic conductivity without significant loss of biomass that comes from scraping. Here the top layer is disturbed but not removed, instead the loosened material is flushed out through backwashing. In studies with SSF fed by secondary effluent of wastewater, harrowing of the *schmutzdecke* did not result in a decreased effluent quality or negatively affected the removal of BOD, which was as high as 30% over the filter run, on par with removal rates from conventional drinking water SSF (Langenbach, Kuschik, Horn, & Kästner, 2009).

1.5 Advantages and limitations of SSF treatment

SSFs have conventionally been designed for the treatment of drinking water (Huisman, 1974). The filters are simple to install and cheap to operate, whilst being excellent at the removal of DOM and TSS over prolonged periods of time with little to no maintenance. While there is some adsorption capacity in SSFs, most of the contaminant removal occurs through biodegradation, sedimentation and filtration (Li, Zhuo, & Campos, 2018). Several researchers mentioned that SSFs only have a limited capability to remove inorganic contaminants and synthetic organic chemicals (Logsdon G. , 1987; Lambert & Graham, 1995). As such, SSFs are unable to remove pollutants that are not readily biodegradable. Although there are certain compounds that are known to be biodegradable in soils that can also be biodegraded in SSFs, much of this is still unknown and the current focus of research (Cycoń & Piotrowska-Seget, 2006). The downside of OMP degradation is that the metabolites produced are often not further biodegradable and pass through the filter, which limits the water matrices that a standalone SSF can effectively treat.

Chapter 2: Water treatment by activated carbon

Activated carbon (AC) has historically been used to remove odor and color from drinking water, but with the onset and detection of heavy metals and OMPs in water has been employed as its high adsorption capacity is effective in removing a wide range of modern pollutants that are otherwise difficult to treat with conventional treatment methods (Bansal & Goyal, 2005). It is often chosen as a final treatment step, following regular filtration, prior to post-disinfection, to prevent high loading from substances that can be removed more easily with other treatment methods, such as NOM.

2.1 Properties of Granular Activated Carbon

AC is produced from organic carbon-based materials, including plant-based precursors such as wood, coconut shells, and large stone seeds or from metamorphosed material such as peat, lignite or coal (Table 1). The precursor material and activation method used to produce AC determine their eventual surface chemistry properties and their effectiveness in removing targeted compounds (Crittenden, Rhodes Trussell, Hand, Howe, & Tchobanoglous, 2022).

Table 1 General properties of selected GAC's (Calgon Carbon Corporation, 2024; EVERS GmbH & Co. KG, 2024)

Adsorbent	Manufacturer	Precursor	Activation process	Surface Area (BET) m^2/g	Packed bed density (g/cm)	Pore volume (cm^3/g)	Grain size distribution (mm)
Filtrisorb 300	Calgon	Bituminous coal	steam	950-1050	0.48	0.851	0.8-1
Filtrisorb 400	Calgon	Bituminous coal	steam	1075	0.4	1.071	0.55-0.75
Norit PK1-3	Norit	Wood	steam	875	0.25	0.55	0.71-3.55
Eversorb 520	Evers	Coconut shells	steam	1100	500	0.42	0.5-2.5

Production takes place either via chemical activation, which includes chemical treatment and pyrolysis, or from physical/thermal activation. The final surface functional groups and material properties such as density, porosity, pore size distribution, and adsorption preferences are determined by both the activation process and by the nature of the precursor material used (Bansal & Goyal, 2005). Thermal or physical activation is a two-step process in which the precursor material is first carbonized in a high-temperature pyrolysis process at 300 - 900 °C, in which moisture, volatiles, and most of the non-carbon elements in biomass, such as oxygen, hydrogen, nitrogen, and sulfur, are removed. The second step is the activation process, in which mild oxidizing agents such as steam or carbon dioxide are used to slowly oxidize the charr material at a temperature between 600 and 900 °C. Chemical activation involves carbonization and activation in a single step, in which the raw material is first impregnated with a chemical agent and subsequently thermally decomposed (Gao, Yue, Gao, & Li, 2020). The chemicals are added in a concentrated solution to the raw material, after which it is mixed and kneaded to break down the lignocellulosic biomass. The slow oxidation process intends to remove lignocellulosic biomass such as cellulose, hemicellulose and lignin, thereby creating new porosity and enlarging existing pore space (Bansal & Goyal, 2005).

The use of different gasses and temperatures impacts the total mass burn off and final porosity and surface area of the GAC, as well as the composition and amount of functional groups on the GAC surface (Crittenden, Rhodes Trussell, Hand, Howe, & Tchobanoglous, 2022). The final products porosity is

dependent on the lignin-to-cellulose ratio in the precursor material. Initially, the surface pore area can be increased by burning away more material, but if the process progresses too far, it will destroy pore walls and negatively impact the total pore structure. As such, there is a limit to the maximum porosity and internal surface area. The Norit PK1-3 GAC used in this study is an outlier from the theoretical values presented, with its extremely low density and high surface area.

The internal pore structure of GAC is commonly divided into three classifications;

- micropores (<2 nm)
- mesopores (20-500 nm)
- macropores (>50 nm)

The distribution of pore sizes between different types of carbon are mainly related to, and characteristic for, their precursor materials and are one of the main distinguishing factors for adsorption capabilities and preferences. The volume of micropores generally ranges between 40 - 60 %, but their surface area accounts for up to 95 % of the total surface area of the GAC. As such, the micropores determine a considerable extent of the adsorption capacity of the GAC. Mesopores account for most of the rest of the total surface area and contribute mainly to the adsorption capacity whilst also facilitating intraparticle transport for adsorbates (Piai, et al., 2019). Macropores are not considered of importance for the adsorption and only act as transport pathways towards the meso- and micropores.

While the pore structure of GAC governs intra-particle transport, attraction by van der Waals forces, and total sorption capacity, the adsorption of particles itself is strongly influenced by the functional groups of the pore surface. During carbonization, hereto-atoms such as sulfur, nitrogen, hydrogen, and halogens present in the precursor material that are not burnt off react with the structure of the GAC surface to form surface groups or surface complexes. As these compounds can only bind to the outer edges of the adsorbing surface, the presence of hetero-atoms modifies both the surface characteristics and surface properties of GAC (Bansal & Goyal, 2005).

The most important of these surface complexes are the carbon-oxygen functional surface groups (Tran, et al., 2019). These influence the surface characteristics such as wettability, polarity, acidity, and physio-chemical properties such as catalytic, electrical, and chemical reactivity of the material. The two types of carbon-oxygen functional surface groups that can be distinguished are acidic and basic surface groups. The state of these groups on the carbon surface depends on the pH of the water matrix it is in. At a low pH, there can be protonation of the GAC surface, providing it with a positive charge. The opposite happens at a high pH, when deprotonation of the surface gives it a negative charge. The point of zero charge, pH_{PZC} , indicates at which pH the GAC surface has a neutral charge. If the pH of the water matrix is lower, the GAC surface is positively charged, if the pH is higher, the surface will be negatively charged. The precursor material and activation method both heavily influence a carbons pH_{PZC} , with thermally ACs from coconut shells having reported $pH_{PZC} > 9$ while wood-based chemically ACs can have $3 < pH_{PZC} < 4.5$ (Piai, et al., 2019). Carbons with a lower pH_{PZC} therefore have more negatively charged surface groups at neutral pH, which translates to a higher affinity for cationic compounds compared with neutral or anionic compounds.

2.2 Design and operation of GAC filters

The design parameters of GAC filters depend on both the water matrix and targeted pollutants, but filters are commonly installed as fixed beds, similar to SSFs. GAC filters are used as a final treatment step in order to prevent heavy loading of the carbon due to its relatively high costs. As such, pre-treatment to remove organic matter and other competing elements is preferred to extend the filters' lifetime (Bauer, et al., 1996).

GAC is a relatively brittle material that suffers from losses due to attrition during handling, leading to the formation of carbon fines. As a result, it requires pre-treatment in the form of washing before it can be loaded into the filter housing. Failure to do so could lead to clogging of the beds or lead to fines ending up in the effluent. Additionally, fresh GAC can contain chemical residue from the activation process, such as acid residue or precipitated calcium carbonate that was formed during the washing phase after activation. These need to be washed out as they can impair adsorption capacity due to pore blockage or could otherwise precipitate further down the filter grains, causing clogging.

The design of GAC reactors is based on modelled data from isotherm and batch kinetic tests or from small-scale pilot studies. The isotherm and kinetics parameters can be found in literature for most pollutants but are tied to the specific conditions, GAC, and water matrices used. Alternatively, these parameters can be obtained from laboratory experiments. These small-scale, relatively quick tests in comparison to column studies provide an insight into the theoretical adsorption capacity of the GAC bed, affinity of the pollutants to the GAC used, and influence of the water matrix on competition. The downside of using only Freundlich and kinetic parameters is that competing elements in the water matrix make it difficult to predict accurately filter performance over its lifetime. As a result, it is often not possible to pinpoint the timeline of pollutant breakthrough and filter exhaustion. This is more difficult in waters with large fluctuations in NOM content between the seasons, as variations in loading are difficult to model accurately. This can be resolved with small-scale column tests using actual feedwater over a prolonged period that more accurately reflects the impact of seasonal fluctuations in NOM concentration. This can be done on a lab scale, which requires understanding of the scaling effects, or with pilot studies on site. The downside of the larger-scale pilot studies is that breakthrough can take an excessive amount of time (Crittenden, Rhodes Trussell, Hand, Howe, & Tchobanoglous, 2022).

When the mass transfer zone of the targeted pollutant through unsaturated carbon has become too short to allow sufficient uptake, then the pollutants will end up in the effluent. This is commonly called “filter breakthrough” and will lead to the replacement of the GAC filter bed. At this point, the bed still has residual adsorption capacity, but not enough to completely remove the targeted pollutants from the influent. When the concentration of the pollutant in the effluent equals that of the influent, the bed is called exhausted and is no longer able to remove any adsorbate (Crittenden, Rhodes Trussell, Hand, Howe, & Tchobanoglous, 2022).

GAC beds are operated continuously, whereby it was traditionally assumed that they cannot be backwashed as it increases stratification, thereby influencing filter resistance while also negatively impacting the removal of pollutants due to reshuffling of spent carbon through the filter. This would prevent making accurate predictions about the total filter loading and breakthrough estimations (Frank,

Ruhl, & Jekel, 2015). Other studies have shown that backwashing is possible under certain conditions, but outside the scope of this research (Frank, Ruhl, & Jekel, 2015; Clements & Haarhoff, 2004).

By tracking the compound with the least affinity for adsorption, the filter breakthrough can be monitored over time. The filters empty bed contact time (EBCT), which determines the flow rate, is based on the compounds with the least affinity for adsorption and lowest kinetics. The EBCT is defined as the ratio between the volume of the filter bed and the influent flow (Fundneider, et al., 2021).

Equation 1 EBCT formula

$$EBCT = \frac{V_F}{Q} = \frac{A_f L}{v * A_f} = \frac{L}{v}$$

in which

- $EBCT$ = empty bed contact time (hours)
- V_f = volume occupied by adsorber media including porosity volume (m^3)
- Q = flow rate to adsorber ($\frac{m^3}{h}$)
- A_f = adsorber area available for flow (m^2)
- L = adsorber or media depth (m)
- v = superficial flow velocity ($\frac{Q}{A_f}$) ($\frac{m}{h}$)

The EBCT can vary in fixed bed reactors depending on the targeted pollutants to treat. A collection of data from studies targeting the removal of OMPs over the last few years shows EBCT ranging from 10 -75 minutes and found that a range between 10 - 55 minutes should be maintained for OMP removal depending on the targeted pollutant affinity for adsorption (Pöpel, Schmidt-Bregas, & Wagner, 1988; Benstöm, et al., 2017). Increasing the EBCT generally leads to higher OMP uptake but also increases NOM adsorption on the carbon, thereby leading to a faster exhaustion of the bed and its need for renewal, which results in higher operating costs (Fundneider, et al., 2021).

Experiments were performed to test the influence of both longer contact times as a result of varying flow velocities as well as increasing the contact time by increasing the GAC bed depth (Li, Zhuo, & Campos, 2018). The variation in flow velocity with EBCT ranging from 120 - 30 minutes led to a less than 1 % increase in removal rate (97.7 - 98.4 %) of selected OMPs, while increasing the bed length led to a less than 2 % increase in removal rate (95.6 - 97.1 %). The lack of increase in filter performance, combined with higher NOM uptake at lower flow rates makes increasing the EBCT an uneconomic solution.

A later study performed on the secondary treatment of wastewater effluent with GAC bioreactors aimed at optimizing the use of the GAC bed adsorption capacity by tracking the adsorbed DOC removed during filter runs, in addition to the removal of OMPs (Fundneider, et al., 2021). It was found that an EBCT of 20-30 minutes yielded the highest carbon usage, while further increasing the EBCT did not significantly increase the utilization capacity of the GAC in terms of C/C_0 versus adsorbed DOC. The reduction in contact time led to faster breakthrough, where the reduction of 24 to 12 minutes showed the largest jump in breakthrough. Shorter contact times affected OMPs with higher adsorption affinity most prominently, with a similar trend occurring for selected OMPs that were poorly adsorbed but readily biodegradable.

These were removed 2 - 3 times better at an EBCT of 24 minutes compared to 6 minutes, indicating that the kinetics for biodegradation are slower than those for adsorption (Fundneider, et al., 2021). Apart from adjusting the flow rate, the EBCT can be adjusted by varying the carbon bed height. Increasing the GAC layer to extend the filters' lifetime is possible, but it increases the risk of deep filter carbon pre-loading by NOM present in the feedwaters, thereby diminishing its overall sorption capacity (Weber, 2004).

The performance of GAC filter bed can be calculated in several ways, one of which is the carbon usage rate (CUR), which is defined as the mass of GAC in the bed over the volume of water through the bed. As the densities of GAC vary significantly between the products available, similar volume reactors can have very different results. Another method of quantifying the performance is by determining the bed volumes (BV) treated, which quantifies the amount of water treated by the carbon volume before its exhausted whilst ignoring the carbon mass.

The downside of using CUR or BV treated is that it mostly focuses on EBCT while leaving the influent DOC concentrations out of the equations. Literature dictates that an increase in EBCT leads to better utilization of the GAC and thus longer filter lifetimes due to slower breakthrough (Fundneider, et al., 2021). However, it is known that high NOM influent concentrations decrease the GAC lifetime due to filter loading, pore blockage and competition with OMPs, thereby leading to faster exhaustion and a decrease in real breakthrough times. A new way of quantifying carbon utilizations was proposed where OMP removal ($\frac{c}{c_0}$) was compared to the adsorbed DOC (Q_{doc}) for each EBCT (Fundneider, et al., 2021). This allowed a more accurate distinction between different contact times for varying DOC influent concentrations.

2.3 GAC Removal Mechanisms

2.3.1 Adsorption

Adsorption of pollutants from water onto the AC occurs in two stages: the transport of the pollutants toward an available adsorption site and the subsequent binding of said pollutants onto the AC. The transport of pollutants occurs from the bulk solution to particle boundary followed by intraparticle diffusion, where the particle travels inside the adsorbents pore structure. Between these two steps, the pollutants have to diffuse through the liquid phase towards the adsorbent particle, which is often referred to as a thin film diffusion. The difference between the liquid phase concentration near the particle surface and the adsorbed concentration on the carbon surface serves as the driving force of adsorption and is considered the rate-determining step (Pia, et al., 2019).

Inside the carbon particle, further transport can occur through surface and pore diffusion. With surface diffusion, the particle is sorbed onto the AC and transported along the carbon's internal surface to a deeper adsorption site. In pore diffusion, the particle is transported in the liquid phase within the carbon's pore structure until it reaches an adsorption space. In practice it is often difficult to distinguish between both diffusion transport mechanisms (Pia, et al., 2019). While the adsorption kinetics are determined by both the thin film- and intraparticle diffusion, the relative contribution of both are dependent on parameters such as mixing regime, adsorbent type and adsorbate properties as described at the end of chapter 2.1. The surface diffusion coefficients and surface diffusion coefficients can be determined using

this information, which are needed to model breakthrough curves in fixed bed reactors using the HSDM and LDF numerical models (Sperlich, et al., 2008; Sontheimer, 1988).

The pore size distribution between macro- meso- and micropores plays an important role in the adsorption characteristics of different carbon types. It is hypothesized that the adsorption rate is limited by intraparticle diffusion and that it is the mesopores that facilitate the adsorbate diffusion into the granule, acting as pathways for the adsorbates to travel through (Valderrama, Gamisans, de las Heras, Farran, & Cortina, 2008). A higher degree of mesopores can facilitate diffusion, resulting in higher adsorption rates (Piai, et al., 2019). The adsorption rate is also dependent on the molecular sizes of targeted OMPs, as mesoporous GAC has been reported to be more suitable for the adsorption of larger (bulky) molecules, which do not suffer from size exclusion compared to microporous GAC (Piai, et al., 2019; Fundneider, et al., 2021). In contrast, other research found that pyrazole was difficult to remove due to its small molecular size in relation to the pore size distribution of mesoporous GAC, reducing the strength of the (van der Waals) interactions between the compound and GAC pore walls, where removal rates of pyrazole in a microporous GAC were significantly higher (Piai, et al., 2019). The micropores exhibit stronger adsorption interactions between the adsorbate and the pore walls, thus showing higher affinity and removal rates for smaller molecules (Li L. Q., 2002). In terms of carbon loading capacity, experiments between GAC types with different microporous volumes showed higher adsorption (loading) onto microporous GAC compared to carbons with more evenly distributed micro/mesopores (Masson, et al., 2016).

The surface of AC is hydrophobic and has a strong attraction to organic compounds and other non-polar pollutants. Adsorption itself occurs through similar forces as described for SSF adsorption. This includes sites, π - π dispersion, donor-acceptor electrostatic interaction, repulsive electrostatic interaction, formation of strong inner-sphere surface complexes, formation of hydrogen bonds with neighboring solutes or surface functional groups, van der Waal's forces and dipole-dipole forces (Huisman, 1974).

In AC adsorption, there is a distinction between physical adsorption (physisorption) and chemical adsorption (chemisorption). Physisorption occurs through relatively weak interaction forces such as ionic, electrostatic, hydrogen bonding and dipole interactions between the adsorbent and adsorbate. In chemisorption, pollutants and charged components form chemical bonds with the functional groups at the surface of the carbon. This type of bonding is highly dependent on the precursor material and the water matrix pH due to the carbons point of zero charge pH_{PZC} . A change in pH can significantly change the affinity of GAC towards charged (Salomón-Negrete, Reynel-Ávila, Mendoza-Castillo, Bonilla-Petriciolet, & Duran-Valle, 2018; Tran, et al., 2019). For instance, carbons that have been chemically activated usually have a high pH_{PZC} . If the pH_{PZC} of a carbon is 8. A solution with $pH < 8$ will favor the adsorption of anionic contaminants, while at a $pH > 8$ the adsorption of cationic contaminants is preferred (Bansal & Goyal, 2005). Moreover, an increase or decrease in solution pH will increase the amount of positively or negatively charged sites at the cost of the other one, respectively. This not only increases sorption sites for one charge, it simultaneously decreases sorption capacity for the opposite charge (Baccar, Blánquez, Bouzid, Feki, & Sarrà, 2010; Hejazifar, Azizian, Sarikhani, Li, & Zhao, 2011; Dong, et al., 2018). While most OMPs have a neutral charge and are relatively unaffected by this, it will still influence the sorption of NOM, which is negatively charged in water at neutral pH (Nguyen, et al., 2020).

Due to the change in the charge of the carbon surface at different pH, the ionic composition and strength of the water matrix affect the adsorption capacity of compounds. When the electrostatic forces between the adsorbent surface and adsorbate ions are attractive, an increase in ionic strength will decrease the adsorption capacity of targeted pollutants. The opposite also holds true: when the electrostatic attraction is repulsive, an increase in ionic strength will increase adsorption (Newcombe & Drikas, 1997; Alberghina, Bianchini, Fichera, & Fisichella, 2000; Germán-Heins & Flury, 2000). As GAC treatment is generally employed as a finishing step, it is normally not subjected to waters with high ionic strength. As such, little research is available on the effects of waters with high ionic strength, like TDW (Table 6), on adsorption capacity and kinetics of OMPs onto GAC. Studies on nitrate and phosphate, two commonly used fertilizers, adsorption onto GAC show both compounds readily sorb to GAC and can be modelled with Langmuir and Freundlich isotherms. While the adsorption capacity of both compounds is high, their kinetics are low, taking 2-3 hours to reach maximum removal rates (Youcef & Abdelkader, 2017; Abdelkader & Youcef, 2016). Nevertheless, with high ionic strength, the concentration gradient will push sorption even at lower contact times. The sorption of these charged compounds onto the GAC surface is reversible but will impact the affinity for other compounds to sorb, as there is a limited total adsorption capacity in GAC. As both compounds are negatively charged, they will be more readily sorbed at lower pH, where the GAC's surface groups obtain a positive charge, similar to the sorption of NOM. Ligand (ion) exchange and electrostatic attraction are the two principle mechanisms to fix phosphate to AC, which is reversible as the compounds can be displaced by adsorbates with higher affinity (Qi Zhou, 2012).

Apart from regular monolayer adsorption of pollutants to the carbon surface, it is also possible for multiple layers to stack on each other; in this case, not all adsorbed molecules are in contact with the carbon surface but rather with the previously sorbed particles. This process is called multilayer adsorption and is sometimes referred to as pore-filling. Under the assumption of pore filling, GAC can have a higher adsorption capacity than its surface area would indicate. Multilayer adsorption also increases the adsorption affinity for charged compounds that are otherwise repelled by the carbon surface. If the carbon surface is initially positively charged, it will repel positively charged pollutants and hold higher sorption affinity towards negatively charged particles. Over time, this forms a monolayer of negatively charged particles on top of the carbon surface, to which the positively charged particles can bind. This can lead to unexpected increased sorption of otherwise rejected particles (Li, et al., 2020b).

Stronger electrostatic attraction of pharmaceuticals on GAC preloaded with NOM was reported compared to fresh GAC, which could be attributed to the negative charge of previously sorbed NOM (De Ridder, et al., 2011). The process is difficult to examine using BET methods, as a decrease in surface area due to pore-filling can also be justified by pore blockage of other particles.

While GAC is excellent at removing NOM from water and has long been employed for taste and odor control, the presence and competition of NOM in feedwater is problematic for targeted compounds like OMPs. Due to the larger molecules and negative charge of NOM, it has a higher adsorption affinity than most OMPs as a result of stronger van der Waals interactions that are size dependent. Compared to OMPs, NOM has very slow adsorption kinetics, which requires a long mass transfer zone to allow for sufficient contact time to facilitate removal. The presence of dissolved NOM in concentrations as low as 1.5 mg/L

can reduce the adsorption of selected OMPs to GAC by a factor of 7 compared to similar experiments in demineralized water (Ahn, 2015.).

At the sandwich filter pilot on Texel, influent NOM concentrations up to 26 mg/L were observed in combination with high ionic water concentrations (Table 6). These concentrations can quickly deplete the adsorption capacity of the GAC filter beds, thereby preventing the removal of OMPs. The addition of the sand layer on top aids in the capture and degradation of NOM, which saw 10% removal rates in the first months of the filter operating in cold weather.

While OMPs build up a well-defined mass transfer zone in fixed GAC bed reactors, the adsorption of NOM over the bed length does not occur in such a well-defined zone at similar EBCT due to its lower adsorption kinetics. Instead, it quickly migrates downward through the filter, without completely saturating the zone above first, leading to a faster breakthrough and more irregular loading across the mass transfer zone. While the OMPs are being removed in the top section of the GAC filter, NOM loading at the bottom section is already occurring in a phenomenon called “preloading”. This diminishes the loading capacity of the bottom section of the filter. As a result, the bed has a greater exposure to NOM before the micropollutant arrives at a given bed depth. This process continues over the lifetime of the filter and not only reduces total adsorption capacity for targets OMPs but also impacts OMP adsorption kinetics. The filter performance will diminish faster than expected from modelling as time progresses (Crittenden, Rhodes Trussell, Hand, Howe, & Tchobanoglous, 2022). Additionally, the large molecular sizes of NOM can lead to pore blockage in GAC. This occurs when NOM adsorbs in mesopores, thereby blocking off the micropore channels. This is especially problematic in GACs with a high micropore content, as pore blockage completely removes the sorption capacity of the pore structure behind it. Combined with competition and preloading, these phenomena are the main problems regarding the exhaustion of sorption capacity for GAC filters. Full-scale observations of sandwich filters at Thames Water showed an initial TOC (influent 4-8 mg/L) removal of 60 % after 6 months (5000 BV), which stabilized at 30 - 40 % after 1 year (10000 BV), indicating a breakthrough. The residual removal of TOC can be attributed to biological degradation (Bauer, et al., 1996).

2.3.2 Biodegradation

Studies that focused on biologically active carbon filters (BAC) found that BAC systems can degrade both adsorbed organic matter and (partially) degrade OMPs. The GACs large internal surface area and affinity for NOM make it a suitable media for microbiological growth. The combination of adsorption/biodegradation allows for the degradation of otherwise difficult-to-degrade organic matter, as residence time in the filter is significantly increased due to sorption on the carbon biofilm (Carlson & Silverstein, 1998). In BAC, a slimy biofilm grows around the GAC grains, in contrast to SSF where a solid layer forms on top of the filter bed (Simpson, 2008). The nutrient levels (NOM, phosphorus, and nitrogen), DO and pH are considered to be the main growth requirements of biofilm (Korotta-Gamage & Shashika Madushi Sathasivan, 2017). As a result, the majority of biomass is present in the top part (0-10 cm) of the filter, where all are abundantly present.

Contrary to biological activity in SSF, there is no conclusive verdict on the influence of temperature on the biodegradation of AOC/DOC in BAC filters. While some research has shown that low water temperatures

(<9 °C) are detrimental for both biomass growth and removal of biodegradable organics (Brown & Lauderdale, 2006; Moll & Summers, 1999). Other research found that low temperatures do not affect the total biomass or substrate removal (Koffskey & Lykins, 1999).

Infiltration at the pilot on Texel takes place during the autumn and winter periods, when temperatures in the Netherlands are generally <10 °C and where little biomass development is expected. While the filters can be operated at low flow rates during warmer periods to keep the biomass active, it is unclear which percentage of biomass will remain active at lower temperatures.

Biodegradation of OMPs is mostly an aerobic process, which occurs through hydrolysis, fermentation or methanogenesis, with each method targeting different chemical structures (Gangola, et al., 2022; Guo, Askari, Smets, & Appels, 2024; Aislabie & Lloyd-Jones, 1995). OMP biodegradation shows only very low removal rates in conventional sand filters due to their low residence time, as OMP are not adsorbed to the substrate and the filters lack the bio cultures to degrade OMPs. While most OMPs are recalcitrant to direct biodegradation, co-metabolism of OMPs is more favorable and often the dominant degradation pathway (Guo, Askari, Smets, & Appels, 2024). In BAC filters, the OMPs sorb to the carbon and remain trapped, allowing the biomass present higher HRT to co-metabolize the OMPs. The degradation of pesticides in studies with high soil retention times has shown promising results, which is similar to the long retention times found in GAC filters. Atrazine is one compound that shows mixed removal in RSF or SSF, but shows excellent removal when retained in soils where bacterial cultures are present. Studies show that the removal of OMPs works significantly better when inoculating the columns with selected OMP-degrading biomass (Goux, et al., 2000; Dimitrios G. Karpouzas, 2005). In one study with aerobic conditions, RSFs were inoculated with selected bacteria that showed >75% removal of Bentazone and Glyphosate, two pesticides commonly found in the Netherlands (Hedegaard & Albrechtsen, 2014). A study where pyrazole-degrading bacteria were inoculated to a GAC filter showed 90% removal rates. Furthermore, after a 30-day starvation period, the biomass successfully switched back to pyrazole degradation once it was spiked into the influent once again (Piai, Dykstra, van der Wal, & Langenhoff, 2022). While these studies cannot be compared 1 - 1 with a natural adaptation of biomass on BAC filters, it does indicate that bacteria can evolve to metabolize OMPs and that OMP (co-)metabolism is possible by selected bacteria. However, under natural conditions, it will take time for such communities to develop and evolve in fresh BAC filters. Overall, the biodegradation of OMPs in BAC systems remains understudied as it is difficult to make the distinction between adsorption and biodegradation inside the filter bed.

Both aerobic and anaerobic conditions significantly contribute to the degradation of different OMPs when used in series as it allows for a more diverse microbial community to develop, demonstrating synergies in systems that harbor biomass in both settings (Xue, et al., 2010). Recent studies have proven the concept of co-metabolism of OMPs under nitrifying conditions, where in a bio-augmented RSF, nitrifying bacteria were able to co-metabolize caffeine and Bentazone (Wang, et al., 2022).

Another advantage of BAC filters is their ability to degrade NOM. Biodegradation of adsorbed NOM frees up used adsorption sites, thus increasing the sorption capacity and bed life of a carbon filter. BAC has mostly been targeted to remove NOM, as it is the main cause of the reduction in adsorption capacity of GAC filters, but has been reported to remove organic chemicals (i.e. Atrazine, PCB's and Simazine),

inorganics like ammonia, disinfection byproducts pre-cursors and total organic halogen (Takeuchi, et al., 1997; Dussert & Van Stone, 1994; Scholz & Martin, 1997).

The lifetime of a BAC filter can be described in 3 phases (Korotta-Gamage & Shashika Madushi Sathasivan, 2017). In the initial phase, the adsorption rate significantly surpasses the biodegradation rate as biomass accumulates in the filter. As the filter matures and biomass accumulates, the sorption sites are slowly becoming saturated, DOC removal from adsorption gradually decreases and is taken over by biodegradation. In the third phase, the DOC removal from the influent has reached a steady state, where biological degradation is the main driver of DOC removal, as the GAC adsorption capacity has become exhausted (Figure 4).

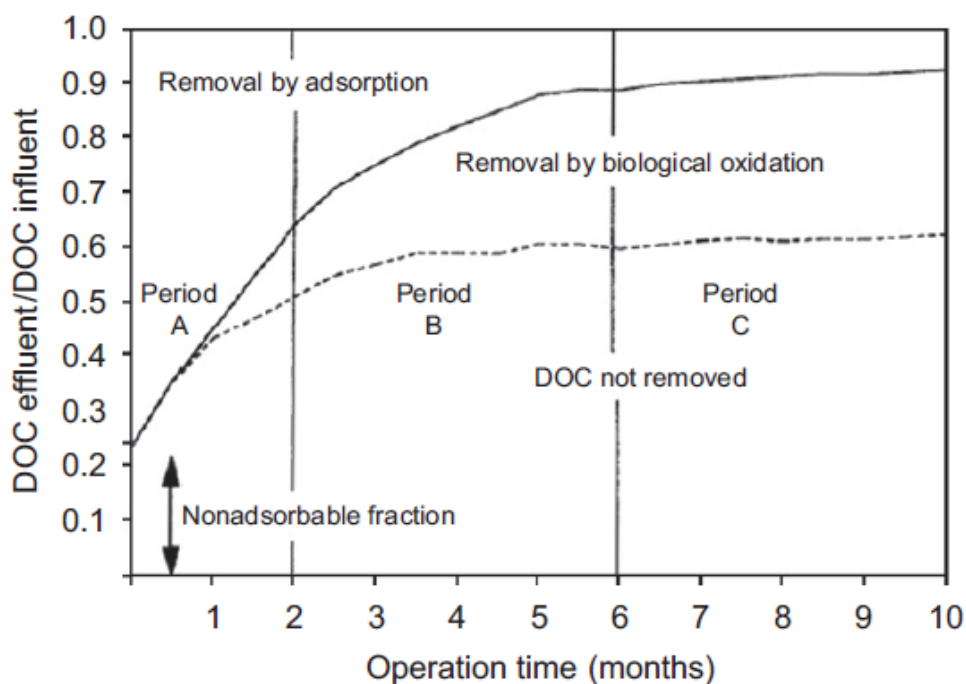


Figure 4 Conceptualized representation of ozonated DOC removal by adsorption and biological degradation over time (Dussert & Van Stone, 1994)

2.4 GAC Adsorption Models

The performance of full-scale GAC reactors can be predicted with reasonable accuracy by collecting data from small-scale lab experiments when full-size column studies are not an option. The two most common types of experiments performed for this are batch kinetics and adsorption isotherm experiments. Batch kinetic tests provide information on the speed of adsorption and can be used to determine the EBCT required to remove the targeted pollutants. For this, the concentration of OMP in a single reactor is measured over time to get an adsorption profile, which provides information on the speed and total adsorption capacity of the GAC for a specific pollutant. Adsorption isotherms describe the amount of adsorbate that is adsorbed for a change either in adsorbate or adsorbent concentration. By varying the concentration of GAC over different reactors with a similar concentration pollutant, the carbon loading in equilibrium vs equilibrium loading capacity can be plotted. There are several different theories regarding the speed of and quantity possible for adsorption of pollutants onto GAC. The models of Freundlich and Langmuir are commonly used to describe the adsorption isotherms and will be used for this research (Kalam, Abu-Khamsin, Kamal, & Patil, 2021). Graphs are plotted assuming carbon loading in equilibrium, according to the carbon equilibrium loading (Equation 2).

Equation 2 Carbon equilibrium loading

$$q_e = \frac{C_0 - C_e}{Dose_{AC}} \left(\frac{\frac{\mu g}{L}}{\frac{mg}{L}} \right)$$

in which

- q_e equals the equilibrium loading capacity ($\mu g/mg$)
- C_0 equals the initial concentration ($\mu g/L$)
- C_e equals the final or equilibrium concentrations ($\mu g/L$)
- $Dose_{AC}$ equals the dose of carbon in the reactor (mg/L)

The Langmuir model assumes that the carbon surface is homogeneous with respect to the energy of adsorption, there is no interaction between the adsorbed species, there is no competition between the adsorbed species and that adsorption sites are available for all. Finally it assumed that adsorption onto GAC occurs through a monolayer, sorbed species cannot stack on top of each other.

Equation 3 Langmuir equation

$$q_e = \frac{q_{max} * K_L * C_e}{1 + K_L * C_e}$$

Linearized this becomes

$$\frac{C_e}{q_e} = \frac{1}{q_{max}} * C_e + \frac{1}{K_L * q_{max}}$$

In which

- q_e equals the equilibrium loading capacity ($\mu\text{g}/\text{mg}$)
- K_L equals the Langmuir constant (L/mmol)
- C_e equals the final or equilibrium concentrations ($\mu\text{g}/\text{L}$)
- q_{max} equals the maximum monolayer adsorption capacity (mmol/g)
- The linearized form of the Langmuir equation can be used to derive q_{max} , K_L

The Freundlich model is an empirical equation that does account for surface heterogeneity of the carbon and assumes different affinities over both the surface and towards the pollutants. The model assumes that multilayer adsorption is possible. As it doesn't have a maximum adsorption capacity, it can only be used for low to medium concentration ranges of pollutants as it otherwise overestimates the total adsorption capacity.

Equation 4 Freundlich equation

$$\log(q_e) = \log(K_f) + \frac{1}{n} * \log(C_e)$$

Linearized this becomes

$$Q_e = K_f * C_e^n$$

In which

- q_e equals the equilibrium loading capacity ($\mu\text{g}/\text{mg}$).
- K_f equals the Freundlich constant $\left(\frac{\mu\text{g}}{\text{g}}\right) * \left(\frac{\text{L}}{\mu\text{g}}\right)^n$. This can be calculated with the intercept of $C_e = 0$. K_f is an indicator of the adsorption capacity, the higher the value for K_f the higher the maximum adsorption capacity.
- C_e equals the final or equilibrium concentrations ($\mu\text{g}/\text{L}$).
- N is a Freundlich constant as a function of the adsorbent heterogeneity. This indicates if adsorption is favorable and can be calculated by taken the gradient of the slope ($1/n$). The higher the value for $1/n$, the more favorable the adsorption.
- The linearized form of the Langmuir equation can be used to derive $\frac{1}{n}$ and k_f .

2.5 Advantages and limitations of GAC filters

GAC filters are mainly used for the adsorption of NOM (to remove color and odor), OMPs, and heavy metals from influent water and are often used as a final treatment step, thereby subjected to relatively clean water. The filters can operate in a large range of water matrices, are resilient to changing conditions, and require little to no maintenance during their operational period. With the proper selection of carbon type, the removal rate and loading capacity can be optimized to maximize the filter's lifetime. The addition of biologically active layers can extend filter life by regenerating the filters in-situ as a result of NOM degradation, whilst also reducing the nutrient load of the effluent.

The downside of GAC filters is that they come with high initial costs (CAPEX) and often require pretreatment of the source water to prevent overloading of the (brittle) carbon (Bauer, et al., 1996). In situations where OMPs are targeted, the presence of NOM is considered problematic due to its competition with the targeted OMPs, which negatively impacts the removal of OMPs from the water matrix. Preloading and pore blockage of the carbon filter with NOM will cause a reduction in adsorption capacity and will lead to a decrease in filter performance and capacity over time (Collins, Eighmy, & Fenstermacher, 1992). Due to the slower adsorption kinetics of NOM, it will break through faster, causing potential taste and odor problems in drinking water. High concentrations of NOM can quickly saturate a GAC filter, exhausting its adsorption capacity long before that would occur purely through OMP uptake. Once the adsorption capacity has been exhausted, the entire bed must be lifted from the filter to be thermally regenerated or replaced. As such, it is important to keep the NOM concentration of the influent as low as possible, thereby extending bed life and removal efficiency of targeted pollutants and decreasing total costs.

Chapter 3: Multimedia Filters

3.1 Design and operation

With the rise of OMP concentrations in the Thames river in the 1970s, the Thames drinking water company started looking into GAC filters to add to their existing operations. It was found that a standalone GAC filter would not suffice due to the brittle nature of the carbon and the quick buildup of material on top of the bed (similar to a *schmutzdecke* in a SSF) that would require regular carbon scraping in order to retain a desired throughput. This resulted in the SSF/GAC sandwich filter concept (Figure 2), in which the SSF would act as a sacrificial layer, as filter sand is significantly cheaper than GAC, allowing it to be scraped away over time while the GAC filter is left undisturbed so that its adsorption capacity can be fully utilized. The *schmutzdecke* on top of the SSF filters out particles and biodegrades part of the NOM, nutrients, and even a small fraction of biodegradable OMPs, thus lowering the loading and competition on the GAC bed whilst also removing nutrients (Li, Campos, Zhang, & Xie, 2022; Li, Zhuo, & Campos, 2018).

The sandwich filters are large due to their low hydraulic filtration rate, with the ones at Thames Water measuring 80 - 120 m long by 20 - 35 m wide. The first sand layer, consisting of well sorted 0.3 mm effective size, is usually 0.7 - 1 m in height, which allows for regular scraping and restoration of the hydraulic flow rate similar to SSFs, up to a minimum operational height of 0.3 m. Usual flow rates are targeted at around 0.1 - 0.3 m/h, which is determined by the fine sand layer as it has the lowest permeability of all layers. The thickness of the underlying GAC-layer can range from 7.5 - 20 cm, depending on the expected OMPs to be treated and NOM loading. As a rule of thumb, the carbon layer height is calculated around an empty bed contact time (EBCT) of 10 - 20 minutes (Pöpel, Schmidt-Bregas, & Wagner, 1988; Benstöm, et al., 2017). The bottom sand and gravel layers serve as a support and drainage, whereas it additionally captures any fines released from the carbon. These layers are usually 15 - 30 cm deep (Bauer, et al., 1996; Logsdon, Kohne, Abel, & LaBonde, 2002).

After the 1990's the sandwich filter method fell out of grace with researchers as advanced treatment methods as oxidation, ozonation, and powdered activated carbon came to light. These were small, reliable, and effective. As a result of these modern treatment methods, little to no publications on sandwich filters have been submitted since the initial reports by Thames Water in the 90's until the beginning of the 2020's, when this filter method came under renewed attention due to the rapid rise and detection of OMPs in (drinking) water systems around the globe. The latest publications have attempted to investigate the influence of modifying the sand filter parameters and determine the influence of biodegradation on total OMP removal under normal NOM and nutrient conditions (Li, Zhuo, & Campos, 2018; Li, Campos, Zhang, & Xie, 2022; Xu, Campos, Li, Karu, & Ciric, 2021). They found that while filtration through biologically active sand in a 50 cm column can remove 30 - 50 % of certain OMPs, it needs a very low filtration rate to achieve this (0.05 m/hour), whereby removal rates rapidly decline when sped up to 0.1 and 0.2 m/hour, making it unfeasible for commercial filtration, which operates at rates of 0.1 - 0.3 m/hour. While biodegradation of OMPs was confirmed, the studies only focused on sampling the influent and effluent of each filter rather than between each filter layer, which, to the author's knowledge, has not been performed to date. As such, they were unable to pinpoint the location and contribution of each layer in the filter and did not highlight any synergy effects from the combination of a SSF with a GAC layer. The authors recommended looking at the influence of different operational conditions and

investigating different removal mechanisms, evaluating the effectiveness of combining SSF with other treatment methods and materials (Li, Campos, Zhang, & Xie, 2022).

This combination of filtration/biodegradation and subsequent adsorption has proven highly effective, often surpassing results from standalone (larger) GAC-filters. In previous lab scale experiments, the average removal of 4 pharmaceuticals and personal care products (PPCP's) at a flow rate of 5 cm/h was higher for a sandwich filter compared to a pure GAC filter with a 4x thicker GAC bed height over 10 weeks of operation (Li, Zhuo, & Campos, 2018). This coincided with higher COD and TOC removal rates in the sandwich filter compared to the pure GAC column. The higher removal rates of OMPs can be attributed to a multitude of factors, including the removal of NOM by the sand layer, lowering competition in the GAC bed. By bio-sorption of OMPs onto the sand layer or by (selective) biodegradation in the schmutzdecke (Li, Zhuo, & Campos, 2018). Additionally, some adsorption and biodegradation of moderate and easy-to-degrade OMPs occurs in SSFs, this further decreases the loading on GAC and increases filter bed life (Paredes, Fernandez-Fontaina, Lema, Omil, & Carballa, 2016).

At Thames Water, they found that as a result of lower DO concentrations in the GAC layer, anaerobic reduction of nitrate occurred. As mentioned earlier, the co-metabolism of selected OMPs is possible under nitrifying conditions (Wang, et al., 2022). The sandwich filters had a higher DO demand compared to sand-only-SSF, indicating increased bacterial activity in the deep GAC layers of the filter. Microbial communities were found to be present along the full GAC layer and not limited to the top section, allowing for both aerobic and anaerobic communities to co-exist over the length of the GAC layer (Gimbel, Graham, & Collins, 2006). In mature sandwich filters, where the NOM adsorption capacity of the bed had been spent, the microbial communities were able to achieve 30-40 % TOC removal, compared to 15-20 % for standalone mature SSFs (Bauer, et al., 1996). While DO concentrations in the influent were significantly lower in the winter months, there remained a steady consumption of DO across the GAC layer, indicating continued biodegradation even in colder conditions (Gimbel, Graham, & Collins, 2006).

While the exact contribution of each factor mentioned above is still unknown, the sandwich filters have been proven to work effectively in a multitude of water matrices, ranging from drinking water treatment to the secondary treatment of wastewater effluent (Fu, et al., 2019). These results underline the sandwich filters strong performance at significantly reduced total capital and operational costs versus a GAC-only filter or other modern advanced treatment systems.

3.2 Additional filter materials and top-up layers

With renewed interest in the sandwich filters originally designed by Thames Water has come additional interest in using a variety of materials as substitution of the sand/carbon layers, or even the addition of additional top up layers. The focus so far has been on finding materials that are either more attractive financially than GAC or can attain higher removal rates. Studies with anthracite and SSF as a replacement for GAC attained similar results as a conventional SSF but well underperformed the SSF-GAC sandwich filter in a similar study, attaining 20 % OMP removal rate vs 60 % removal rate for sandwich filters (Xu, Campos, Li, Karu, & Ciric, 2021).

The pilot study in Texel deals with exceptionally high nutrient and NOM loads (Table 6), which can quickly diminish the adsorption capacity of the GAC, as the SSF is not expected to degrade such high concentrations, which would quickly lead to overloading the GAC filters. Due to the strict maximum concentrations of nutrients set for underground infiltration (Bijlage XIX Besluit kwaliteit leefomgeving, 2024), a top-up layer targeting the removal of nitrate and phosphate would be necessary to adhere to water quality standards. The additional removal of NOM by a top-up layer would further reduce loading on the GAC bed and is, hence, highly desirable.

Iron oxide coated media (IOCM) could act as one such top-up layer, as it has high adsorption affinities towards both NOM and phosphate (Abdelkader & Youcef, 2016; McMeen & Benjamin, 1997). This layer can act as pre-treatment, reducing NOM loading and ionic strength of the water.

The hydrophobic fractions of NOM that sorbs to IOCM are the same fractions of NOM that are removed by GAC adsorption, indicating that removal through IOCM before exposure to GAC could decrease carbon loading and increase GAC filter life (Korshin, Benjamin, & Sletten, 1997; Dinga, Yana, Liu, Chang, & Shang, 2010). Additionally, hydrophobic NOM generally has a larger molecular size than hydrophilic NOM, meaning that increased removal would theoretically lead to a decrease in pore blockage in GAC adsorption (Dinga, Yana, Liu, Chang, & Shang, 2010). To date, this has not been tested with field experiments to the author's knowledge.

The adsorption of NOM on IOCM follows pseudo second-order rate models (Langmuir, Freundlich), with rapid initial adsorption followed by a slowdown and a plateau after 20 - 30 hours for fresh, unloaded IOCM. The initial adsorption has been attributed to physical adsorption mechanisms such as electrostatic interactions. The second, slower phase occurs through the ligand (ion) exchange, which becomes more effective at lower pH, due to the hydroxylated oxide surface sites of the IOCM (Dinga, Yana, Liu, Chang, & Shang, 2010). The pH of the solution is the limiting factor, as the -OH surface groups needed for adsorption are only present at $pH \leq P_{pzc}$. If the pH increases above this point, electrostatic repulsion between the IOCM surface and the NOM occurs, hindering sorption.

One option to increase adsorption at higher pH has been to modify the surface of IOCM by surfactants, which resulted in increased removal rates at a wide pH range and a higher affinity for the (larger) hydrophobic NOM molecules (Dinga, Yana, Liu, Chang, & Shang, 2010). As the scope of this study is to use low-effort materials that can be employed straight out of the bag due to the remote location and lack of operators, this will not be investigated further.

So far, only one long-term pilot study using IOCM as a standalone material to remove NOM has been performed to the author's knowledge (McMeen & Benjamin, 1997). A 16-month pilot using Iron Oxide Coated Olivine (IOCO) and SSF showed a 32% removal rate versus regular SSFs at 9-12% removal rate. In rapid IOCO filters, adsorption was the main removal method, while low filtration rates showed the accumulation of biomass and higher levels of bacterial activity with increased removal due to biodegradation over time, like seen in SSFs. The biomass growth and removal of NOM was similar to the ripening process of BAC/ SSFs, where, initially, adsorption was the dominant removal method and the influence of biodegradation became apparent after several months, when sufficient biomass had

accumulated (Figure 4). This is supported by the rapid decrease in DO in the top 4 - 5 mm of the IOCO filter cake in the mature filter. As the NOM is sorbed to the IOCO its retention time in the filter drastically increases, providing the biomass with ample time to degrade (less biodegradable) material that would otherwise pass through SSF. This was coupled with a slightly higher head loss, but it was unclear whether this resulted from the increasing biomass or differences in material properties between filter setups. Near the end of the 16-month pilot study, the influent/effluent DO concentration became similar during winter weather, indicating that at colder temperatures, the biomass becomes inactive. Despite this, NOM removal maintained elevated versus commercial sand filters, indicating that after 16 months of filter operation, there was still net sorption onto the IOCO, and the filter had not yet arrived at a sorptive steady state (McMeen & Benjamin, 1997).

In separate studies with IOCM the successful removal of phosphate from the influent water has been reported through electrostatic attraction, pH-dependent ligand (ion) exchange, adsorption onto amorphous oxides, van der Waals forces, and precipitation onto the IOCM, where chemisorption (ion exchange and electrostatic attraction) are the prevalent sorption mechanisms (Edgar, Hamdan, Morales, & Boyer, 2022; Mengxue, Jianyong, Yunfeng, & Guangren, 2016). Ion exchange and electrostatic attraction occur through binding and attraction between the phosphate and -OH surface active sites, which show similar sorption as in GAC and occur only when $pH \leq P_{pzc}$. Ion exchange occurs when the PO_4^{3-} Anions create covalent bonds with the IOCM cations on the surface of the metal hydroxides. This can lead to the liberation of other anions that were previously attached to the IOCM ions, like the displacement of NOM (Mengxue, Jianyong, Yunfeng, & Guangren, 2016). Precipitation occurs when the solubility of a precipitate is exceeded, leading to fast precipitation onto the IOCM surface as phosphate complexes. This can occur for both Calcium and Magnesium when present in high concentrations in waters that suffer a sudden drop in pH. This can lead to fouling/clogging of the IOCM surface and can quickly lead to exhaustion of the adsorption capacity (Edgar, Hamdan, Morales, & Boyer, 2022). Isotherm experiments testing the influence of pH on sorption saw an increase from 4.6 mgP/g to 8.6 mgP/g over a pH range from 10-3 (Zenga, Lia, & Liub, 2004).

The materials used vary from Iron Oxide Coated Sand (IOCS), Iron oxide mining tailings (IOMT) to iron oxide steel slag (IOSS) and IOCO. Previous isotherm and column experiments with IOCT found high levels of phosphate adsorption (6 mgP/g IOCT at pH 6 - 7) and rapid adsorption kinetics, with the majority of the adsorption occurring within 20 - 30 minutes in isotherm experiments with little influence from temperature variations (Edgar, Hamdan, Morales, & Boyer, 2022; Zenga, Lia, & Liub, 2004). Later column studies showed that the capacity more than doubled with regards to batch testing, to over 13 mgP/g (Zhang, Wang, Lakho, Yang, & Depuydt, 2022). Further large scale testing in an integrated system with wastewater influent that had phosphate concentrations at >20 mgP/L showed increased phosphate removal from 34 % to 99 % over 400 days or 1000 BV with the implementation of IOCM into a conventional filter setup (Zhang, Wang, Lakho, Yang, & Depuydt, 2022). Moreover, no desorption of heavy metals nor arsenic was detected in all experiments with IOCM (Edgar, Hamdan, Morales, & Boyer, 2022; Zenga, Lia, & Liub, 2004). The presence of other ions in a water matrix can induce competition with phosphate for adsorption onto IOCM. Ions with the highest ionic potential are removed first, as are ions that are stronger electronegatively charged. Higher valence ions show stronger competition than

monovalent ions, with SO_4^{2-} – and CO_3^{2-} inducing the largest competition with phosphate for adsorption (Mengxue, Jianyong, Yunfeng, & Guangren, 2016). To date, no research has been performed where IOCM has been employed as dual or multi filter media in combination with GAC in NOM/phosphate rich waters.

3.3 Advantages and limitations of multimedia filters

The SSF-GAC sandwich filters display improved performance versus similar-sized GAC standalone systems at significantly lower initial and operational costs. In systems with enhanced biodegradation, they achieve longer lifetimes than regular GAC filters due to increased total adsorption capacity and biodegradation (Bauer, et al., 1996). The combined sandwich filter is compact, requires little operator knowledge or maintenance, and can operate with flexibility against changes in the water matrix. The potential addition of a IOCM top layer could further extend the bed life by removing NOM and nutrients from the feedwater. IOCS is produced as a waste product by drinking water companies in both The Netherlands and Belgium, which makes it a readily available, cheap-to-use product. The downside of this is that the material is pre-loaded with NOM at these drinking water plants, leading to initial leaching of NOM during use and diminishing initial sorption capacity.

The sandwich filters do come with several drawbacks; once the material has been placed, it is difficult to implement changes to the GAC layer, as the carbon is covered by a layer of sand. The sand bed height needs to be chosen so that it can be scraped until the carbon is spent, or risk that the filters GAC bed can foul and clog up. As the sandwich filter is a biological active system, is it temperature dependent and operates best during warmer seasons, both for the present biomass as for the adsorption interactions. The pilot on Texel is active during the wet season in late summer and fall, when temperatures are dropping. If the temperatures become too low, the benefits of biodegradation could become negligible as the biomass becomes inactive.

Chapter 4: Materials and Methods

4.1 Materials and Methods

4.1.1 Granular Activated Carbon

Two types of GAC are used in the pilot installation of Acacia Water on Texel from which material was sampled as used in this research, NORIT PK1-3M (GAC-N) and Eversorb 520 (GAC-E) (Table 2). During the preparation of the GAC, it became apparent that GAC-N contains 2 different precursor materials, as the density differences between individual grains deviated up to 100 %. Additionally, visual observations of the carbon showed two distinct types of grain structures in the GAC-N.

Table 2 GAC types and properties used

	NORIT PK1-3M	Eversorb 520
Abbreviation	GAC-N	GAC-E
Source material	Coconut	Coconut//Bituminous coal
Activation method	Steam	Steam
Density (kg/m ³)	250	500
Specific total surface area m ² /g	875	1100

GAC is produced in batches from heterogeneous precursor materials, and as such, the parameters of the final product can often deviate between batches and the generalized manufacturer provided MSDS (Appendix 1 MSDS GAC). Both carbon types were tested to verify their pore size distribution and internal surface area as stated by the manufacturer. This was done with a TriStart II 3020 utilizing N₂ gas and the Harkins and Jura method (Micromeritics, 2016).

The particle size distribution was analyzed using a wsTyler RX-29 tap test sieve shaker. The top sieve was loaded with around 150 - 300 grams of carbon and sieved for 10 minutes. The loading mass was constrained by the volume the top sieve would hold without the possibility of clogging or overloading on the underlying sieves. Before the analysis, all sieves were cleaned with a plastic brush to ensure no other material was trapped on or between the sieves and subsequently washed and dried in an oven at 105 °C. The GAC was likewise dried in an oven at 105 °C before sieving as the stock material contained up to 4 % water. The removal of water ensures the grains won't stick together during sieving.

At the end of each sieving cycle, the shaker was left to rest for several minutes to let the majority of the fine carbon dust settle before the sieves were opened. As both carbon types are marketed as a coarse material with no particles smaller than 0.5 mm and 0.71 mm, respectively, the finest sieve was set at 0.5 mm, with little to no fines expected.

The fine content of both GACs had to be completely removed to provide accurate data for GAC adsorption on both the batch and column experiments and to prevent clogging of the column experiments. Fine removal by sieving was ruled out as it generates more fines due to abrasion of the grains and might accidentally sort the material due to improper re-mixing afterwards. It was, therefore, opted to use a wet fine removal method for which fresh carbon was loaded into a column with 0.2 mm screens at the top and bottom, after which a demi water up-flow was forced through the bottom of the column. By adjusting the flow rate, the material was brought into a state of suspension. The presence of fines was regularly checked in the effluent of the column, which turns into a distinctive black color as long as fines are present in the water. The removal of fines using this method took approximately 20 minutes for both carbon types. While this method was successful in removing the fines from both GACs, there remained a small fraction of fine fibrous carbon material with the GAC-N that did not get washed out. It is theorized that these are activated wood fibers. After washing, the carbon was placed in a glass jar and dried in an oven at 105 °C for 4 hours before being placed in a desiccator to cool down and prevent the attraction of moisture.

4.1.2 Iron Oxide Coated Sand

The IOCS used for this research was provided by the drinking water company Pidpa from their drinking water production plant in Mol (Belgium). The material was too brittle to create a PSD in-house, but one was provided by Pidpa (Figure 5). The IOCS arrived with a significant amount of fines, which originated from transport due to the brittle nature of the material. The same method employed for washing GAC fines was used for the IOCS, after which the IOCS was dried and left to cool in an identical way as described with the GAC earlier.

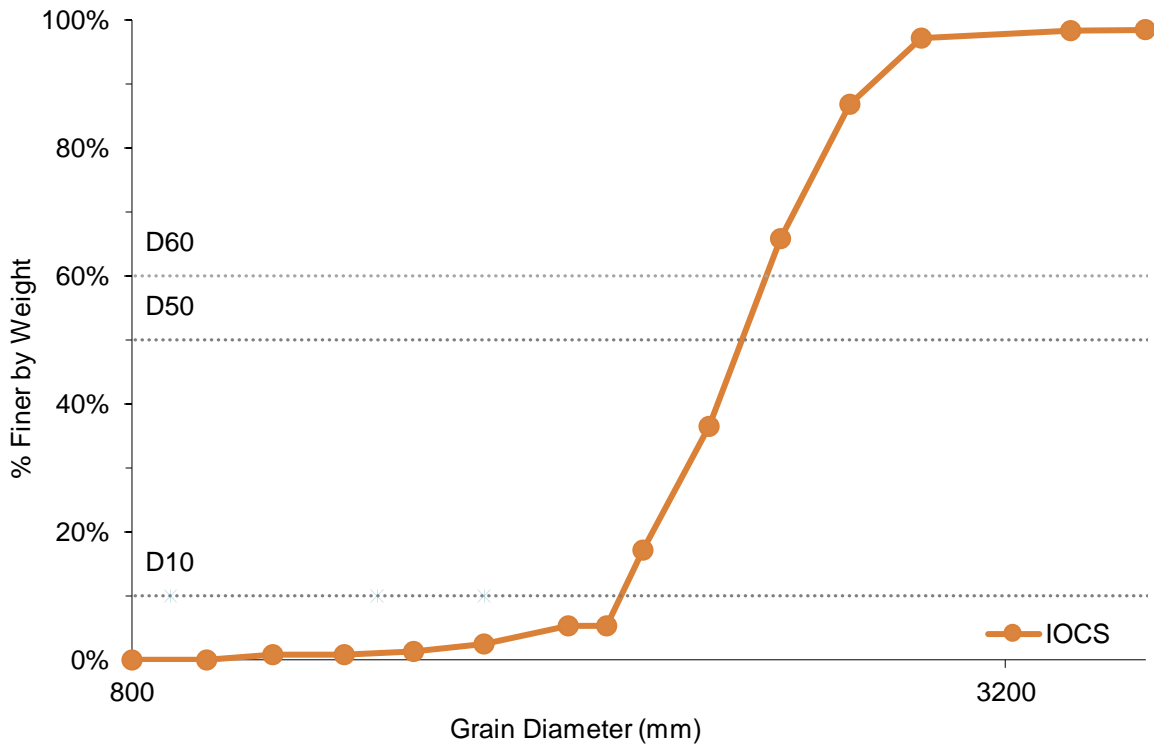


Figure 5 Particle size distribution IOCS. Shaker parameters: $T=10\text{mins}$. Amplitude= 0.5mm/g . Interval 10 seconds

4.1.3 OMP Selection

The selection of OMPs for the project is based on their occurrence in Dutch surface waters from a study by Delphi in the waters around Zuid-Holland, which identified a total of 72 substances of interest for research in various concentrations. As it is not feasible to dose 72 components into a column study, a cluster analysis was performed with internal software from Acacia Waters (Figure 6) to create a subset of 10 OMPs to be used for this research (Table 3). The parameters used for the cluster analysis were solubility, molecular weight, density, LogP, soil degradation constant DT50, linear isotherms and groundwater ubiquity score.

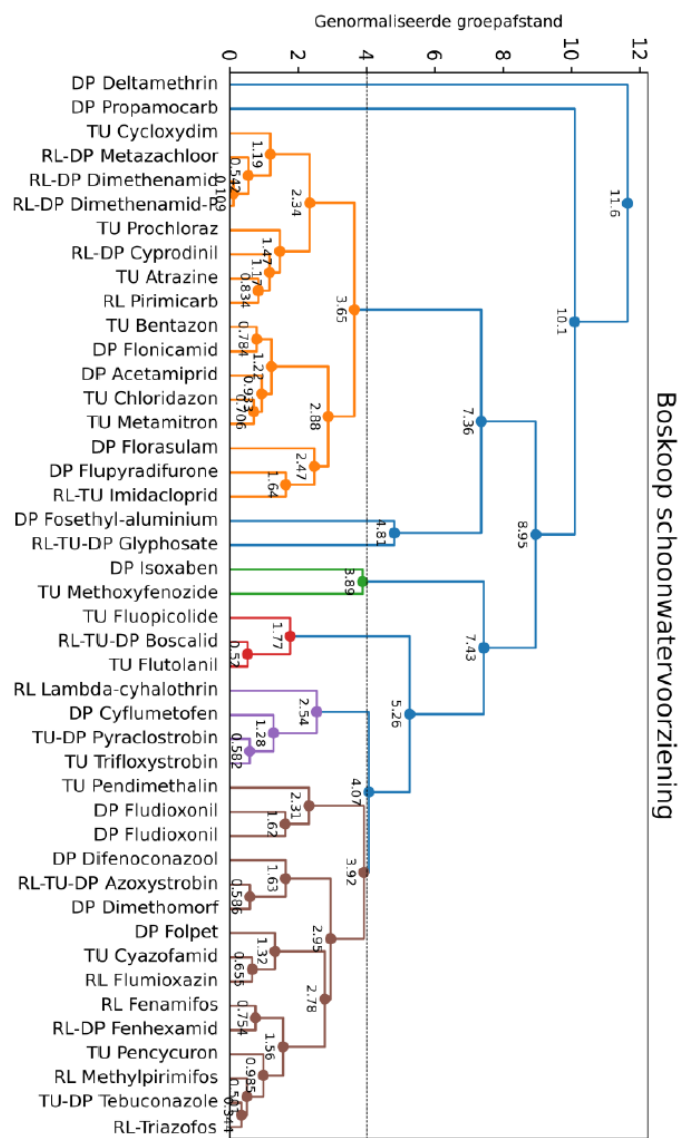


Figure 6 Cluster analysis of OMPs present in Zuid-Holland surface waters

Table 3 selection of OMP's proposed by Acasia. From: (University of Hertfordshire, 2023)

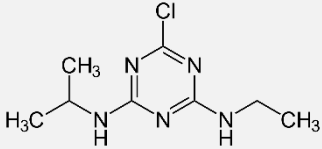
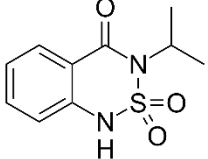
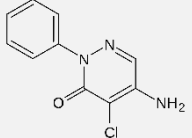
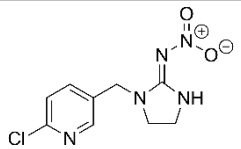
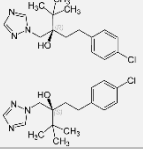
Organic Micropollutants	Type	Mol. Weight	Density	LogP	Soil Degradation (DT50)	ubiquity score	Solubility water at 20 degC (mg/l)
Atrazine	Herbicide	215.68	1.23	2.7	75	2.6	35
Chloridazon	Herbicide	221.6	1.51	1.2	3	2.2	422
Imidacloprid	Insecticide	255.66	1.54	0.6	191	3.7	610
Glyphosate	Herbicide	169.1	1.71	-6.3	16.11	0.2	100000
Methoxyfenozide	Insecticide	368.47	0.634	3.7	456	3	3.3
Boscalid	Fungicide	343.21	1.381	3	484.4	2.7	4.6
Pendimethalin	Herbicide	281.31	1.17	5.4	182.3	0.59	0.33
Pyraclostrobin	Fungicide	387.82	1.37	3.9	41.9	0.1	1.9
Tebuconazole	Fungicide	307.82	1.25	3.7	63	1.9	36

Initial calibration measurements on the Waters LC-MS for the isotherm studies with the set chosen by Acasia (Table 3) revealed that Glyphosate, Methoxyfenozide, Pendimethalin, Boscalid and Pyraclostrobin could not be accurately measured on equipment both at Tu-Delft nor externally in The Netherlands, resulting in the removal of these compounds from the OMP matrix. Bentazone was added as a substitute compound in the column experiments due to its reliability of measurements in previous pesticide research (Krijn, 2021). Both the column and isotherm studies were performed with a pesticide matrix consisting of Atrazine, Bentazone, Chloridazon, Imidacloprid and Tebuconazole (Table 4). The chemical structures and molecular properties for the 5 compounds used are summarized below to provide an overview of the factors contributing to adsorption onto GAC during the experiments (Table 5).

Table 4 Selection of OMP's used in this research. From: (University of Hertfordshire, 2023)

Organic Micropollutants	Type	Mol. Weight	Density	LogP	Soil Degradation (DT50)	ubiquity score	Solubility water at 20 °C (mg/l)
Atrazine	Herbicide	215.68	1.23	2.7	75	2.6	35
Bentazone	Herbicide	240.28	1.5	-0.46	20	1.95	7112
Chloridazon	Herbicide	221.6	1.51	1.2	3	2.2	422
Imidacloprid	Insecticide	255.66	1.54	0.6	191	3.7	610
Tebuconazole	Fungicide	307.82	1.25	3.7	63	1.9	36

Table 5 Molecular structures influencing adsorption of OMPs used in this research

Organic Micropollutants	Type	Mol. Structure	Key Structural Features	Hydrophilicity/phobicity	Adsorption Mechanism
Atrazine	Herbicide		Triazine ring, Chlorine, Amine groups	Hydrophobic	Van der Waals interactions
Bentazone	Herbicide		Benzoic acid, Sulfonyl group, Chlorine	Hydrophilic (acidic)	Electrostatic, polar interactions
Chloridazon	Herbicide		Pyridazinone ring, Chlorine, Ketone	Moderately polar	Polar and nonpolar interactions
Imidacloprid	Insecticide		Imidazole ring, Nitroguanidine, Chlorine	Amphiphilic (polar/nonpolar)	Hydrogen bonding and van der Waals interactions
Tebuconazole	Fungicide		Triazole ring, Chlorinated aromatic	Hydrophobic	Nonpolar interactions, Van der Waals interactions

The pesticide dose for the isotherm and column experiment was set to 10 µg/L, based on oral discussions relating to research by Prof. Heijman and as it is comparable to the upper concentration ranges observed in the field feedwaters. Higher concentrations would lead to unrealistic dosing and possible unrealistic ratios between competing elements such as NOM and free ions with the OMPs for adsorption spaces onto the GAC that do not occur in field operations.

The stock solution was made by dissolving 2 mg of each pesticide in a 2 L volumetric BlauBrand borosilicate flask in ultrapure water, starting with the lowest solubility pesticide and working up from there. As not all OMPs dissolved initially due to clumping of material, the volumetric flask was left in a 15 L DK-Sonic sonicator for 1 hour to aid dissolution. As the sonicator warms up during use, it was completely filled with water to prevent excessive heating of the stock solution, which reached a maximum of 30 °C during operation. Following sonication, the flask was placed on a stirrer plate for a minimum of 72 hours to ensure complete dissolution of the pesticides. To ensure no microscopic hydrophobic flocks remained, the solution was filtered over a Advantec GF-75 glass fiber filter. Three control samples were measured of each stock solution on the LC-MS to verify the pesticide concentrations.

4.1.4 Water Matrix

Due to volume and transport constraints, it was not possible to directly use water from the Texel or Boskoop pilots in Delft for the column experiments. A readily available source of surface water from a Delft canal (Schiewater) was chosen as a substitution as it has similar high NOM contents to the other two water sources of interest. Table 6 shows the characteristics of all water types, including those of Thames Water, from which most GAC-SSF sandwich filter research data is available. The isotherm required significantly smaller water volumes and, as such, could be performed with both Boskoop and Schiewater. This was done to compare the differences in sorption between the two different water matrices. Phosphorous was dosed during the column experiments in a dose of 10 mg/L by adding 0.358 g of K_2PO_4 to 25 L of Schiewater. Both water matrices were pre-filtered over a 1 μ m cartridge filter (Pentek P1) before to prevent excessive bio growth from influencing the isotherm experiments and clogging of the tubing and columns during operation.

Table 6 Comparison between tile drainage water from Texel (sampled March 2023), Thames feedwater (Data from (Bauer, et al., 1996) for their sandwich filters, Schiewater (sampled June 2023) and Boskoop water (sampled July 2023). Data labelled N/A was either not available (Thames Water) or below the detection limit (rest)

	Unit	TDW Texel		Thames Water	Schiewater	Boskoop
Location		Postweg	Hoofdweg	N/A	Waterlab	Lavafeld
pH	(-)	7.4	7.33	N/A	7.8	6.7
DOC	(mg/L)	15.83	18.38	4-8	20.46	23.05
NTU	(-)	N/A	N/A	1.19	3.96	1.4
UV254	(cm ⁻¹)	0.57	0.559	0.12-0.08	0.42	0.71
Cl ⁻	(mg/L)	268.45	150.24	N/A	136.00	85.33
NO ₂ ⁻	(mg/L)	N/A	N/A	N/A	N/A	N/A
NO ₃ ²⁻	(mg/L)	38.24	43.02	N/A	N/A	541.82
PO ₄ ³⁻	(mg/L)	2.47	4.502	N/A	1.3	14.01
SO ₄ ²⁻	(mg/L)	77.67	62.67	N/A	78.36	208.56
Na ⁺	(mg/L)	150.47	89.82	N/A	98.06	61.72
NH ₄ ⁺	(mg/L)	N/A	N/A	N/A	0.38	N/A
K ⁺	(mg/L)	18.25	23.44	N/A	12.73	147.00
Mg ⁺	(mg/L)	24.38	19.59	N/A	20.96	58.10
Ca ⁺	(mg/L)	137.26	131.32	N/A	97.24	175.74

4.1.5 Sampling and analysis

Sampling for both the isotherm and column experiments focused on tracking the adsorption of OMPs and NOM to the AC, and NOM and phosphate adsorption to the IOCS. Additionally, general water parameters are checked from time to time to ensure the water matrix does not fluctuate dramatically over time. To achieve this, the following sampling methods are used:

- UV254 Absorbance
 - With a Thermo Scientific Genesys 10S UV-Vis photo spectrometer at a wavelength of 254 nm an indication of the concentration of organic matter in water can be given. The wavelength is specifically sorbed by the carbon molecules containing aromatic rings or unsaturated bonds. By measuring the concentrations at the beginning and during experiments, it can be determined how much organic matter of this faction is removed during each step. This in term indicates the competition with the OMPs, as the concentration of organic matter is tracked over time (Ridder, Verliefde, Mcconville, & Heijman, 2009).

The UV254 samples are extracted using a 30 mL plastic syringe with a Chromafil Xtra PES45/25 Filter. The syringe is prerinsed once after which the filter was loaded with 10 mL of solution before the 10 mL sample was taken.

- TOC-Meter
 - The TOC-meter provides a measurement of the total organic carbon in the water. By looking at the TOC values, insight can be provided into how the carbon content in the water varies over time for the isotherm experiments and between different layers for the column experiments.

The TOC samples are extracted using a 30 mL plastic syringe with a Chromafil Xtra PES45/25 Filter. The syringe was prerinsed once, and the filter was loaded with 15 mL of solution before the 30 mL sample was taken.

- LC-MS
 - The LC-MS measures the concentrations of the OMPs in the water. These measurements provide insight into how well the adsorption onto the GAC has been during each time interval.

The LCMS samples are extracted using a 30 mL plastic syringe with a Swinnex filter capsule containing a 0.3 µm Advantec GF7525MM Glass Fiber Filters. The syringe is prerinsed once with sample water and the filter was loaded with 5 mL of sample solution before the 1 mL sample was taken.

The Swinnex filters used to take samples for the LC-MS consisted of 3 parts, the housing, filter, and an O-ring, which had to be cleaned and re-assembled after each use. This was done by first disassembling a used filter before rinsing them with demi water. The filter capsules and O-rings were then washed in methanol to remove any organic matter before finally being thoroughly washed with ultrapure water and left to dry overnight. The clean filters were then reassembled with new filter paper.

- IC
 - Using IC, the phosphate concentration and general water quality parameters could be measured. This gives insight into the adsorption of phosphate onto the IOCS over time and the change in water quality during the experiments. A total of 5 anions and 5 cations can be tracked, which notably include nitrite/nitrate, phosphate, sodium, calcium, and potassium.

The IC samples are extracted using a 30 mL plastic syringe with a Chromafil Xtra PES45/25 Filter. The syringe was prerinsed once, and the filter was loaded with 10 mL of solution before the 15 mL sample was taken.

4.2 Isotherm experiments

4.2.1 GAC Isotherms

The isotherm experiments were performed in order to get insight into the adsorption capacity and affinity of the subset of pesticides on both carbons (Table 2) in both water types (Table 6). While general information is present on the competition of NOM and free ions with OMPs, the concentrations found here were significantly higher than literature values (Bauer, et al., 1996). These generally do not exceed 5 - 8 mg/L for NOM and 2 - 50 mg/L for free ions in GAC treatment for drinking water production, assuming GAC is used as a final treatment (Bedrijfstechische parameters, 2024). Additionally, it was of interest to see what the effects of pore blockage would be as a result of the high NOM concentrations on the predominantly microporous GAC-N (Table 10). The first 2 isotherm sets (Table 7) were run with Schiewater to make accurate comparisons with the follow-up column experiments. A third isotherm (Table 7) was run with Boskoop water.

Initial isotherm experiments, which followed a similar protocol as the experiments run by the author in 2021 (Krijn, 2021) and 1 μm pre-filtered water failed due to excessive bio growth visible during the 2-month equilibrium period. This was likely the result of the high nutrient concentrations in the feedwaters present and relatively high temperatures in the laboratory during the summer months, averaging around 26 °C. Bio growth became visually present after 2 weeks during three different trials, which were subsequently aborted. The experiments performed in 2021 were conducted in the winter months, when temperatures in the laboratory were below 20 °C on a groundwater matrix that had received pre-treatment and, as such, contained little nutrients for bio growth.

To reduce the equilibrium time needed for the isotherms, the GAC was reduced to powdered activated carbon (PAC) with the use of steel bearings and the wsTyler RX-29 tap test sieve shaker. The carbon was loaded with steel bearings placed over a range of 3 sieves and left to shake for 1 hour, thereby pulverizing it to a fine fraction <0.1 mm. By using PAC, the equilibrium time needed for isotherm experiments could be reduced from 2 months to 3 days. This timeframe is too short for biomass to form and influence experimental results, eliminating the initial problems. To further reduce the chance of bio growth, the 1 μm pre-filtered water was filtered over a second Whatmann (GF/F1825-0.47) glass fiber filter of 0.7 μm . Both the Boskoop and Schiewater were spiked with 1 mg/L of each pesticide (Table 4) stock solution to obtain 10 $\mu\text{g/L}$ of each pesticide spiked water that was left to mix for 72 hours on a stirrer before the 0.5 L BlauBrand reactors were filled with 500 mL spiked water and PAC. The experimental duration was chosen

based on the literature, where PAC equilibriums for OMPs are usually reached between 1 - 24 hours (Agboeze & Chime, 2022). To ensure equilibrium would be reached, samples were taken after only 72 hours, as the material was slightly coarser than conventional PAC.

The carbon powder was prepared in a 5 g/L, 50 mL bottle (GAC-E, 249 mg, GAC-N 251.7 mg) using ultrapure water stirred on a vortex (Snijders 34524) to create a carbon slurry. As it is difficult to maintain the carbon in suspension, a set protocol was used to ensure an equal concentration of PAC was present in the slurry during transferring from the stock slurry solution to the spiked reactors using pipetting. To prevent straining of the powdered particles by the pipette tips, they were partially cut to increase their opening. The slurry was transferred to the reactors by turning upside down 3 times, placing it on a vortex for 10 seconds, and again turning upside down 3 times before the required volumetric sample was taken using the pipettes. This procedure was repeated for each separate reactor.

Each isotherm set contains 2 carbon types and 4 control bottles (Table 7).

- Bottle I_0 verifying the composition of the water matrix and initial concentrations spiked.
- Bottle I_0 -control to determine pesticide adherence to glass, breakdown or volatilization under controlled (no GAC added) conditions.
- Bottles $I_x - 4$ and $I_x - 5$ are duplicates to ensure accurate measurements can be made.

Table 7 GAC isotherm reactor set

Water type	GAC type	bottle #	Sample ID	Reactor Volume (mL)	GAC dose (mg/L)	OMP dose (each) (µg/L)	Contact time (days)
Boskoop water	n/a	3	I0-0	500	0	10	0
	n/a (negative control)	4	I0-control	500	0	10	3
Schie water	n/a	5	I1-0	500	0	10	0
	n/a (negative control)	6	I1-control	500	0	10	3
Schie water	Norit	7	I1-1	500	0.5	10	3
		8	I1-2	500	1	10	3
		9	I1-3	500	2	10	3
		10	I1-4	500	5	10	3
		11	I1-5	500	5	10	3
		12	I1-6	500	10	10	3
		13	I1-7	500	20	10	3
		14	I1-8	500	50	10	3
Schie water	Eversorb	15	I2-1	500	0.5	10	3
		16	I2-2	500	1	10	3
		17	I2-3	500	2	10	3
		18	I2-4	500	5	10	3
		19	I2-5	500	5	10	3
		20	I2-6	500	10	10	3
		21	I2-7	500	20	10	3
		22	I1-8	500	50	10	3
Boskoop water	Norit	23	I3-1	500	0.5	10	3
		24	I3-2	500	1	10	3
		25	I3-3	500	2	10	3
		26	I3-4	500	5	10	3
		27	I3-5	500	5	10	3
		28	I3-6	500	10	10	3
		29	I3-7	500	20	10	3
		30	I3-8	500	50	10	3

4.2.2 IOCS Isotherms

The IOCS isotherm (Table 8) was set up using phosphate spiked Schiewater (Table 6). From previous isotherm experiments with iron oxide tailings dosed with KH_2PO_4 , it was determined that the material they used had a maximum PO_4^{3-} adsorption capacity of around 8 mg P/mg tailings, with equilibrium attained after 1 week (Zenga, Lia, & Liub, 2004). The phosphate dose for the IOCS isotherms was set at 50 mg/L PO_4^{3-} with the use of KH_2PO_4 and a range of IOCS from 100 - 16000 mg/L. 5 L, 1 μm filtered Schiewater which contained 1.3 mg/L PO_4^{3-} was spiked with 348.7 mg KH_2PO_4 to bring the total phosphate content up to 50 mg/L. The IOCS was added to each empty reactor with 10 mL of ultrapure water and degassed for 15 minutes to ensure the grains were fully wetted, as per the protocol used by the author for GAC isotherms in previous research (Krijn, 2021). The stock solution was left to stir for 24 hours before the IOCS reactors were filled. For the IOCS isotherms, the bio growth was not taken into account as it had a small influence on PO_4^{3-} consumption. Previous studies used fresh IOCM, while this study used pre-loaded IOCS, which can influence the time it takes to reach equilibrium (Zenga, Lia, & Liub, 2004). To ensure equilibrium would be reached for this material, a contact time of 3 weeks was maintained.

Similar to the GAC isotherm set, control bottles were used to identify measurement errors ($P_1 - 1$ & $P_2 - 2$). Additionally, 1 bottle filled with 16 g/L IOCS was loaded with the pesticide stock solution to investigate the adsorption of pesticides onto IOCS.

Table 8 IOCS Isotherm reactor set

Water type	Sample ID	IOCS	Reactor Volume (mL)	Phosphate dose	Contact time
		mg/L	500	mgP/L	days
Raw water	P1-0	0	500	50	0
Raw water spiked	P0-control	0	500	50	21
IOCS	P1-1	100	500	50	21
	P1-2	100	500	50	21
	P1-3	200	500	50	21
	P1-4	600	500	50	21
	P1-5	1000	500	50	21
	P1-6	2000	500	50	21
	P1-7	4000	500	50	21
	P1-8	8000	500	50	21
	P1-9	16000	500	50	21
	p1-10-OMP	16000	500	1.3	21

4.3 Column experiments

Following the isotherm experiments, a scale lab column study was set up to investigate the breakthrough of the pesticides through the sandwich filters for both carbon types. Additionally, a third column set was augmented with an IOCS filter to investigate the influence on phosphate and NOM removal. The main goal of the setup was to record a breakthrough of the pesticides over a period of 2 - 3 months. As such, it was opted to use small glass columns of 1.89 cm diameter with a length of 21 cm each. The upper element of each column set consists of a 4 cm GAC layer, with the bottom element consisting of SSF sand. The column setup consists of 3 sets of columns to evaluate the difference in performance between the GAC types and to evaluate the use of a top-up layer (Table 9). The first column (C#1) contains GAC-N, with the other two columns (C#2 & C#3) containing GAC-E. The GAC layer is supported by coarser sand to provide support and drainage. The third column set (#3) contains an additional column element containing IOCS as pre-treatment but is otherwise identical to column set 1 (Table 9). To ensure full wetting of each column and prevent gas from getting trapped in the system, as mentioned in Chapter 1: Slow, the columns were operated in an up-flow method, contrary to normal down flow for field sandwich filters. One column set consists of two connected elements, allowing for sampling in between the upper media and the GAC, as well as a sampling port after the GAC to investigate the contribution of each separate layer to the removal of pesticides or NOM (Figure 7).

Table 9 Content of each column in the column study, including weight and size of column units.

Column	Layer 1	Layer 2	Water matrix	GAC weight (g)	GAC length (cm)	SSF weight (g)	SSF length (cm)	IOCS weight (g)	IOCS length (cm)
1	Sand	GAC-N	Schiewater	3,17	5	87,02	21	N/A	N/A
2	Sand	GAC-E	Schiewater	5,84	5	86,43	21	N/A	N/A
3	IOCS+SSF	GAC-E	Schiewater	5,5	5	73,4	21	84,4	23

The glass columns are fabricated by the Tu-Delft inhouse workshop (DEMO), with the connections and tubing from Festo. As the glue connecting the glass columns to the plastic caps was prone to failure, the columns were additionally glued with Liqui Moly liquid sealant.

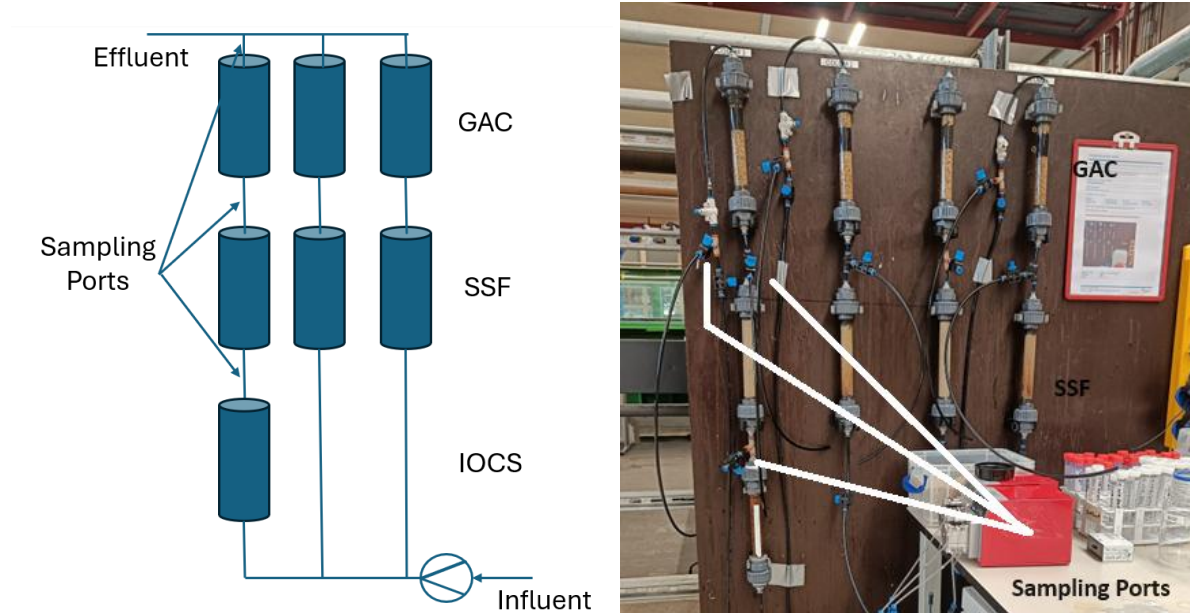


Figure 7 Schematic overview of column setup (A) and full column setup (B)

All columns received Schiewater, which is comparable in NOM concentrations to Boskoop or Texel TDW (Table 6), from 2 interconnected 25 L jerry cans. To simulate the nutrient content of Boskoop and Texel water, 10 mg/L phosphate (PO_4^{3-}) was added to the water in addition to the 10 $\mu\text{g/L}$ of each of the 5 pesticides used (Table 4). The flow rate, controlled by 2 peristaltic pumps type Watson Marlow WM120, of each column was measured on a weekly basis by weighing the effluent samples after 90 minutes. To prevent bio growth in the feedwater tank and clogging of the tubing due to bio growth, the feedwater was placed in a fridge at 7 °C. From temperature measurements, it was concluded that by the time the water reached the first column elements, it had warmed back up to room temperature, allowing for normal operating conditions in the columns. To simulate commercial SSFs, the flow rate was set to 0.27 m/h or 1.25 mL/min, which corresponded to an EBCT of 11.2 minutes. The column effluent is pumped through a 2 kg GAC filter to prevent any pesticide from ending up in the drains.

Before the column infiltration, a salt tracer test was performed to determine the pore volume of each column as supplementary information for the reader, as some fields of water research prefer pore volumes (PV) over bed volumes (BV). For this, a 1 g/L NaCl solution was pumped through the column at 0.3 m/h (1.8 mL/min) with 3-minute samples taken every 5 minutes for 90 minutes following the first flow. The results are added in the Appendix 6 Column studies.

Chapter 5 Results and Discussion

5.1 Physical characteristics of GAC

5.1.1 Surface Area

The Tristart measurements showed that GAC-N has a much higher micropore volume and micropore surface area than the GAC-E, even though it showed a lower total surface area (Table 10). While this information seems conflicting, the most likely conclusion of this is that the GAC-N has a high percentage of micropores with regard to its meso- and macropores, while the GAC-E has a more even distribution of pore sizes. The TriStart had a measuring range between 1.7 nm and 300 nm, which could indicate that there is additional pore space available below 1.7 nm that could not be measured using this method. Apart from this, the Harkins and Jura method does not produce a perfect fit in the lower regions of pore sizes. This would simultaneously explain the extremely low density of the GAC-N.

Table 10 Pore volume and density parameters of both carbon types

TriStart II results	Unit	Norit PK1-3M	Eversorb 520
Micropore volume	cm ³ /g	0.29	0.21
Micropore area	m ² /g	741.78	503.00
External surface area	m ² /g	151.15	505.9
Total surface area (BET)	m ² /g	892.94	1008.91
Percentage micropores of total surface area	%	83.1	49.9
Density	Kg/m ³	250	500

5.1.2 Grain size distribution

The particle size distribution (Figure 8) shows that the already coarse grained GAC-E (D_{10} 840. D_{50} 1290. D_{60} 1310) is still considerably finer than the GAC-N (D_{10} 1300. D_{50} 1710. D_{60} 1720). While the MSDS of both GAC-E and GAC-N mention size fractions as small as 0.7 and 0.5 mm, respectively, there were barely any particles below 1 mm for both carbon types, even though the MSDS of the materials mentions.

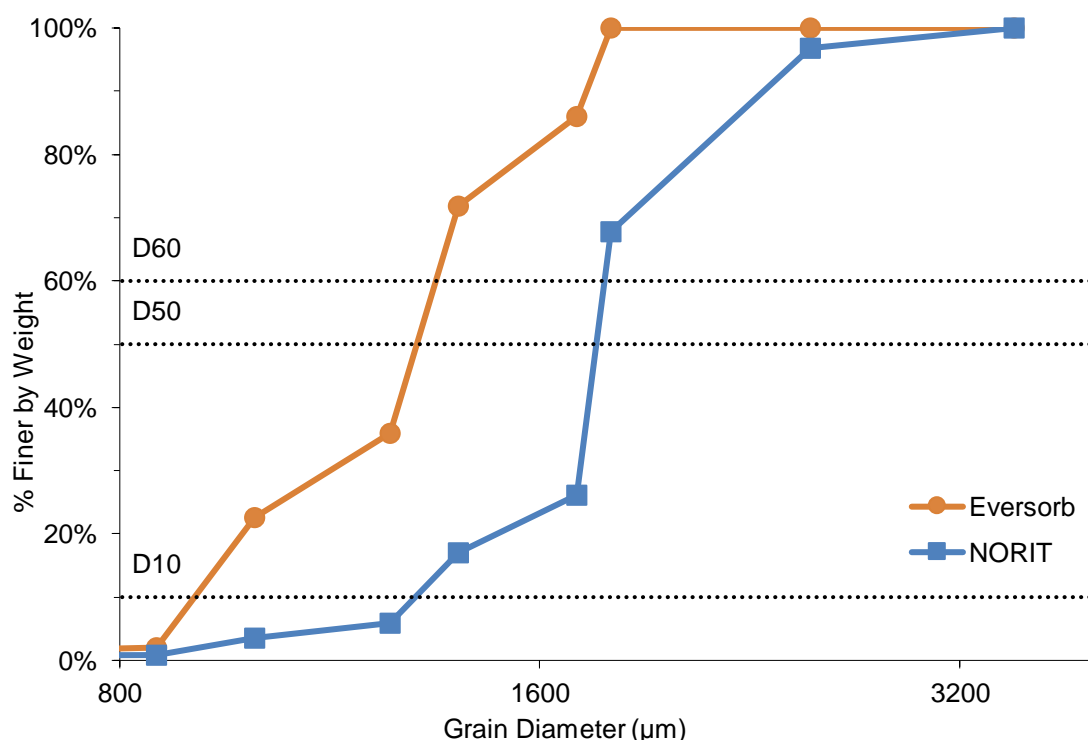


Figure 8 Particle size distribution for Norit PK1-3M and Eversorb 520

5.1.3 Observations during washing

The glass bottle containing the GAC-N had a distinctive white film resulting from drying in the oven. To determine the origin of this, both bottles were filled with fresh carbon and demineralized water and left to shake for 10 minutes. pH measurements performed afterwards noted a pH of 10.3 in the bottle containing GAC-N, whereas GAC-E had a pH of 8.6. IC measurements with ultrapure water containing 100 g/L unwashed GAC soaked for 2 weeks showed high concentrations of selected ions for both carbon types (Table 11). As the carbon is washed at least 20 minutes before the column or isotherm studies to remove fines, it is expected that it does not leach significant amounts of free ions.

Table 11 Ions leached from the washed GAC, soaked for 2 weeks in ultrapure water.

	Cl ⁻	Br ⁻	NO ₃ ²⁻	PO ₄ ²⁻	SO ₄ ²⁻	Na ⁺	K ⁺	Mg ²⁺	Ca ²⁺
Eversorb	0.23	N/A	0.42	0.43	0.99	2.22	0.28	5.92	26.73
Norit	54.27	0.51	0.44	4.90	85.08	42.32	936.22	2.41	3.85

5.2 GAC Isotherm results

5.2.1 Quality Control

The standard deviation and measurement error for TOC, UV, and LC-MS measurements were calculated with the use of duplicates and control bottles in the isotherm sets. Both water matrices contained a set of control bottles I_0 – control & I_1 – control, which did not contain GAC, to determine measurement errors, verify initial concentrations, and ensure that no adherence to glass or volatilization of compounds occurred for the duration of the experiments. Furthermore, duplicate bottles (I_{1-3} – 4 & 5), which contained equal amounts of GAC for each isotherm set were used for all isotherm sets to determine the variability in adsorption between reactors with equal concentrations of GAC.

For the duration of this research, the LC-MS measurements returned values of $\sim 1/5^{\text{th}}$ of the expected concentrations. This was most likely due either to a problem with the internal stock solutions of the LC-MS or related to LC-MS data processing, as calculation errors in the samples and stock solutions have been ruled out. As such, a correction factor has been used to convert the data back to its correct values by comparing the theoretical concentrations of the 2 stock solutions used for this research (on both isotherm and column experiments) against the measured triplicates (Appendix 3 correction factor).

The stock solution was diluted with ultrapure water for the isotherm experiments and measured in triplicate on the LC-MS. The measurements showed low variance for all pesticides (Table 12). Similarly, the control bottles with pesticides spiked in Boskoop and Schiewater also show low variance between measurements, indicating that the water matrix composition does not significantly influence LC-MS results.

The duplicate and control LC-MS measurements showed standard deviations (as a percentage of the mean) of up to 23% for the duplicates I_{1-3} – 4 & 5. The differences were highest between the two carbon types; GAC-E showed the highest measurement error, notably for Chloridazon and Imidacloprid (Table 12).

The high variability between the duplicate bottles (I_{1-3} – 4 & 5) can be attributed to differences in uptake by the GAC. GAC is a natural, heterogeneous product that can consist of a blend of precursor materials that are not all equally transformed by the activation process, which can cause variations in the uptake between individual (powdered) grains. As these isotherms were performed with low concentrations of GAC, it is possible that the heterogeneity of the material can affect the uptake. Additionally, Eversorb is manufactured from two distinct precursor materials, as stated by the manufacturer. This was confirmed visually during carbon weighing, where it also became apparent that different grains of GAC-E had shown large variations in density. The large differences in pesticide uptake between the duplicate bottles indicate that the materials have differing affinities or capacities for adsorption, which could influence isotherm results where individual grains are used. As the total duration of the experiment was capped at 72 hours, it is assumed that there is little to no pesticide degradation or adherence to reactor glass over this period influencing variability.

Table 12 Variability in duplicate reactor uptake

	Water Type	GAC Type	Atrazine	Bentazone	Chloridazon	Imidacloprid	Tebuconazole
LC-MS triplicate							
T1,2,3	MiliQ	-	2%	2%	3%	2%	3%
Control bottles							
I0-0,Control	Schie	-	1.3%	0.6%	0.1%	1.5%	1.5%
I1-1,Control	Boskoop	-	0.8%	3.2%	1.0%	1.9%	5.0%
Duplicate bottles							
I1-4.5	Schie	Norit	5.3%	0.9%	9.1%	5.6%	17.8%
I2-4.5	Schie	Eversorb	6.9%	0.2%	22.9%	20.5%	19.5%
I3-4.5	Boskoop	Norit	3.3%	4.4%	6.6%	6.4%	4.4%

To verify that the pesticides used did not adhere to the plastic tubing in the column setup, a separate sample of 10ppm stock solution was made in which Watson Marlow PVC manifold pump tubing was submerged. This sample was left to sit for 3 weeks, after which it was sampled. None of the compounds used in this experiment showed adherence to the PVC during this period.

The TOC measurements of control bottles (I_0 & I_1 – control) returned nearly identical values in both sets, while the duplicate bottle sets (I_{1-3} – 4 & 5) showed a variance of 0.36 % and 1.44 % for Schiewater and 0.04 % for Boskoop water.

Several bottles with low concentrations of GAC returned higher TOC values than the control bottles, deviating by up to 2.1 % (Table 13). While no conclusion could be drawn from the available data, several hypothesis include leaching of carbon from the filters used and TOC measurement errors. The latter is supported when looking at the concentrations of the TOC standards used, which showed measurement errors of up to 5 % on a standard stock solutions of 10 mg/L.

Table 13 Selective bottles from TOC measurements. Low concentration GAC reactors often returned higher TOC values than control bottles.

	GAC concentration	TOC	Deviation from control
	mg/L	mg/L	%
I0-0	0	13.85	-
I0-CONTROL	0	13.85	-
I1-1	0.5	13.79	0.43%
I1-2	1	14.14	2.09%
I2-1	0.5	13.89	0.29%
I2-2	1	13.95	0.72%
I2-3	2	13.96	0.79%

The UV254 duplicates (I_{1-3} – 4 & 5) showed low variance, which was 0.02 % and 0.04 %, respectively. In the control bottles (I_0 & I_1 – *control*), the variance was 4.7% for the Schiewater water (I_0) and 4.4 % for the Boskoop water (I_1).

The variance in the IC control sample did not exceed 0.04 % for either the control or duplicate bottles.

5.2.2 Ion adsorption

The Boskoop water had a higher ionic concentration and ionic strength compared to Schiewater, which resulted in a higher uptake of ions driven by higher concentration gradients. The ionic strength was calculated from the ionic concentrations measured by the IC (Table 14, Equation 5)

Equation 5 molar ionic strength formula

$$I = \frac{1}{2} * \sum_{i=1}^n c_i * z_i^2$$

In which

- c_i = the molar concentration of ion i
- z_i = the charge number of ion i

While the percentages of each ion removed do not differ between the two water types, the total mass removed increased by a factor of 17 when comparing GAC-N in Boskoop water versus Schiewater. It is assumed that the decrease in ion concentration is due to adsorption onto the GAC through ligand (ion) exchange, electrostatic attraction, and van der Waals forces and not due to the development of biomass, as the water was prefiltered at 0.7 μm and the experimental duration was capped at 72 hours. As mentioned earlier in 2.3 GAC Removal Mechanisms, the sorption of ions onto GAC has previously been proven and studied for nitrate and phosphate, with high concentrations of phosphate removed at a relative low ionic concentration compared to other ions in the water matrix (Youcef & Abdelkader, 2017; Abdelkader & Youcef, 2016). The high adsorption of phosphate, even at lower concentration compared to other ions in Boskoop water, highlights its affinity for GAC, though it remains to be proven whether this influences the adsorption of OMPs (Abdelkader & Youcef, 2016).

Table 14 Ionic water composition and ion adsorption by GAC for each isotherm

Compound	Schiewater	Boskoop	I1- GAC- N Schiewater	I2- GAC- E Schiewater	I3- GAC-N Boskoop
	Initial Concentration (mg/L)		$\Delta C I_x - 1 \text{ to } I_x - 8$		
Cl ⁻	68	34.8	-0.8%	-1.2%	-1.50%
NO ₂	0.5	4.9	0.2%	-1.0%	-1.70%
NO ₃ ⁻	2.9	852.8	-0.7%	-0.8%	-2.10%
PO ₄ ³⁻	0.9	9.8	-0.7%	0.8%	-6.00%
SO ₄ ²⁻	56.6	166.1	-0.5%	-0.4%	-1.80%
Na ⁺	48	45.4	-0.8%	-1.0%	-1.20%
K ⁺	9.7	135.4	4.1%	0.3%	-2.20%
Mg ²⁺	14.4	53.4	0.2%	0.0%	-2.10%
Ca ²⁺	96.9	185.0	0.0%	-1.2%	-4.10%
Ionic Strength (mmol/L)	9.38	27.46	-0,11%	-0,86%	-2,81%
Sum of ions removed from water matrix (mg/L)			1.67	1.59	26.74

5.2.3 NOM adsorption

The removal of NOM from the water matrix was analyzed by measuring both TOC and UV254 adsorption. It was attempted to model both TOC and UV254 adsorption as Q_e over C_e as is custom with GAC isotherm experiments, but this did not yield any usable plots. As such, the data in this subchapter is presented as normalized removal rates with the initial concentrations present in each graph. Additionally, the error bars show the measurement error for each method as derived in the previous subchapter.

The TOC adsorption on GAC-N was in relative terms roughly equal for both water matrices (9.1 % vs 12.2 % for Schiewater and Boskoop water, respectively (Figure 9). Boskoop water contained significantly higher TOC concentration than the Schiewater (23.5 mg/L vs 13.85 mg/L), which resulted in a 124% higher total TOC adsorption in terms of mass. This indicates that the total adsorption of NOM is driven by the concentration gradient, highlighting its need for removal from the TDW influent waters before reaching the GAC layers to prevent preloading or pore blockage of the carbon.

The UV254 adsorption, which measures unsaturated carbon bonds and aromatic carbon rings, often referred to as humic substances, showed an opposite correlation, with lower relative (12.3 % vs 22.6 % respectively) but higher absolute (0,14 cm⁻¹ vs 0,11 cm⁻¹) removal rates for the Boskoop compared to Schiewater, indicating that the NOM fractions and their sorption affinity differ significantly in both water matrices. As some pesticides have molecular structures that are also measured with UV254 adsorption, the 10 ppm stock solution was measured to determine the influence of pesticide uptake on UV254 adsorption. The 10 ppm stock solution showed 0.14 cm⁻¹ UV254 adsorption, indicating that a significant part of UV254 reduction originates from pesticide uptake. Accounting for pesticide influence, the difference in absolute values indicates that a higher fraction of UV254-NOM was adsorbed in the Boskoop water.

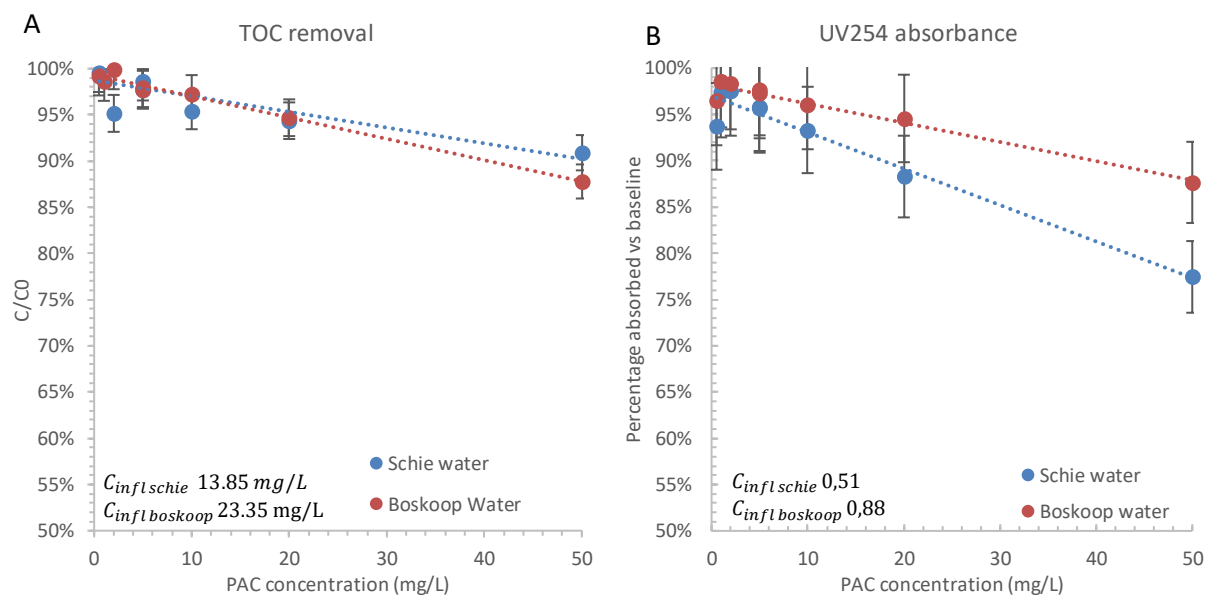


Figure 9A-B Difference in TOC (A) and UV254 adsorption (B) for the Boskoop and Schie waters on the same type of carbon (Norit PK-1). Error bars depict variance between control bottles.

When comparing the removal of NOM for the two GAC types in an identical water matrix, the GAC-N and GAC-E showed similar removal rates for both TOC and UV254 when tested on the Schiewater, differing only by 2-3 % on both measurements, indicating that the difference in pore structures between GAC-N and GAC-E has a negligible impact on NOM uptake. Both carbon types showed higher relative reduction in UV254 compared to TOC, which in part comes from the adsorption of pesticides but also indicates that a high fraction of NOM removed contains double bonds and aromatic rings.

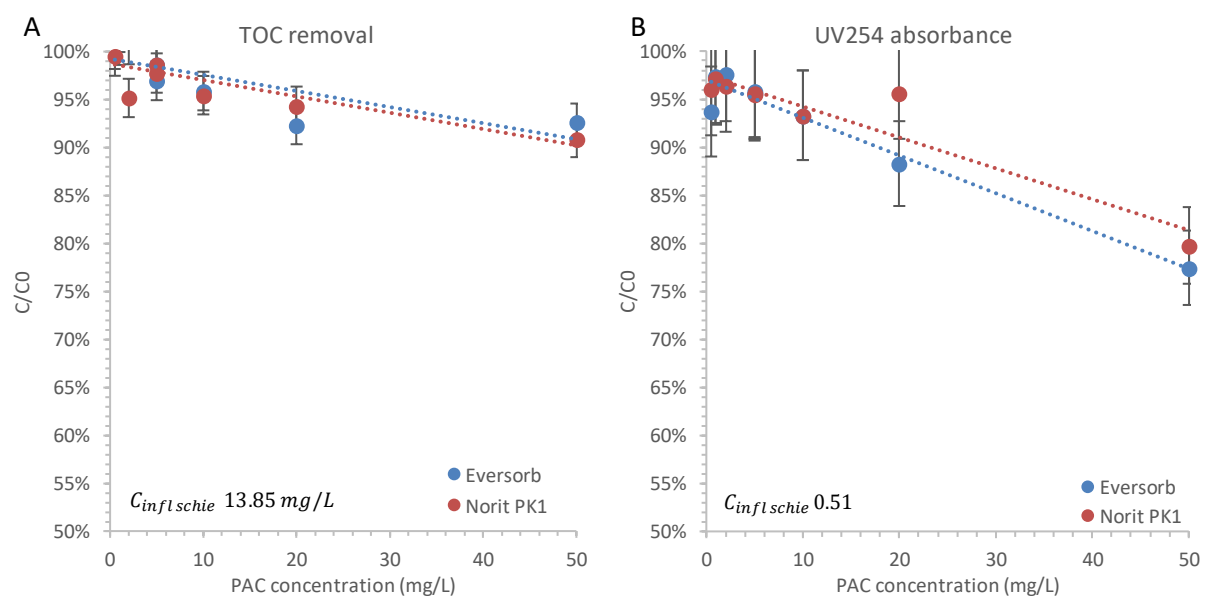


Figure 10A-B Difference in TOC (A) and UV254 (B) adsorption for the two different carbon types (Eversorb and Norit PK-1) in an identical water matrix (Schiewater). Error bars depict variance between control bottles.

5.2.4 Pesticide adsorption

The pesticide adsorption was modelled with Freundlich parameters as described in Chapter 2.4 GAC Adsorption Models. For all isotherms, $I_{1-3} = 1$ to $I_{1-3} = 3$ where often not suitable for modeling due to the low concentrations of GAC used in combination with the resulting low removal rate of pesticides compared to C_0 , leading to extreme outliers at low ΔC_e in the Freundlich equation. The datapoints not used in the models in this chapter are left as hollow datapoints on each graph for the reader's interpretation. The results of pesticide adsorption are presented as a comparison of adsorption between different water matrices (Schiewater and Boskoop water) for GAC-N and a comparison between adsorption of different carbon types (GAC-E and GAC-N) in an identical water matrix (Schiewater). Schiewater was chosen to compare both carbon types as the pilot would also be performed with Schiewater. GAC-N was chosen to compare both water matrices as it was expected that its micropore structure would be influenced most by the difference in NOM content.

The Bentazone measurements returned 2- 7 % higher concentrations on reactors $I_{1-3} = 1$ and $I_{1.2} = 2$ compared to the control bottles, making them unusable for interpretation. Setting C_0 equal to $I_{1-3} = 1$ did not result in usable data for isotherm modeling. The adsorption of Bentazone in all 3 isotherms was exceptionally low, with removal being only 10 – 20 % of what was achieved for all other compounds. Between the 3 isotherms, Bentazone showed the highest adsorption in $I_2 = \text{GAC} - \text{E}$, followed by an almost equal performance in $I_1 = \text{GAC} - \text{N}$. It had the lowest adsorption in $I_3 = \text{GAC} - \text{N}$, in line with the other compounds used in this study. It was not possible to model the remaining datapoints to Freundlich or Langmuir equations, leading to the omission of Bentazone in the following subchapters but added as supplementary data (Appendix 5 Pesticide Isotherms). Bentazone is a weak acid and was the only charged compound of the set of pesticides used, making its adsorption both pH dependent and dependent on the charge of functional groups on the GAC's surface, which could have influenced its removal rate. More research would be needed to conclude why Bentazone showed such weak adsorption for these GACs and water matrices used, as similar results might occur with the adsorption of other charged compounds found TDW in the Netherlands.

5.2.4.1 Comparison of carbon types

The performance of both carbon types in an identical water matrix differed significantly, as GAC-E attained higher adsorption for all pesticides compared to GAC-N (Figure 11). One likely factor attributing the difference in sorption between GAC-E versus GAC-N is the more evenly distributed pore area of the GAC-E, which contained a higher percentage of mesopores to facilitate transport to adsorption sites deeper into the carbon and can more easily facilitate transport of larger molecules, as compared to the GAC-N, which contains mostly micropores (Table 10). Both water matrices have high concentrations of NOM, where the dominant micropore structure of GAC-N makes it more susceptible to pore blockage at similar NOM loading, leading to lower sorption capacity and reduced pesticide uptake.

In addition to differences in pore distribution between the two carbon types, differences in their surface chemistry and functional groups likely play a large role in the adsorption capacity and affinity of different compounds, as mentioned in chapter 2.3 GAC Removal Mechanisms. Atrazine, which had the lowest sorption of all compounds, is a relatively non-polar substance. While its amine group allows for dipole interactions with the surface, the main factor contributing to its adsorption is the weaker van der Waals

forces through its triazine ring. The other compounds have one or more functional groups that allow for stronger binding with the carbon surface, resulting in more favorable adsorption, and as such, all show significantly higher sorption (Table 5). Of all compounds, Tebuconazole shows the least variation in sorption between the two carbon types, as in addition to its polar functional group, it can also sorb through $\pi - \pi$ interactions and van der Waals forces. The same holds for Imidacloprid, which holds both polar (through its nitro group) and non-polar (through its aromatic ring) regions in its molecular structure. Chloridazon lacks these aromatic rings and cannot bind through $\pi - \pi$ interactions, but can bind to the GAC surface with strong hydrogen bonding due to its carbonyl group.

Combining the bonding types from the functional groups with the Freundlich isotherm data indicates that, in addition to a more favorable pore structure, GAC-E has more (available) polar or oxygenated surface groups that allow for $\pi - \pi$ interactions and hydrogen bonding compared to GAC-N, allowing for higher sorption of all pesticides used here. Assuming that GAC-N does not contain significant polar surface regions, the sorption mechanisms for the compounds rely primarily on van der Waals forces and $\pi - \pi$ interactions. Tebuconazole and Imidacloprid, which in this case primarily sorb through (stronger) $\pi - \pi$ interactions, show higher sorption than Atrazine and Chloridazon to GAC-N, which are in this case dependent on (weaker) van der Waals forces. As Atrazine lacks the strong functional groups that facilitate polar interactions, it exhibits the lowest removal rate of the set of compounds used here as well as the lowest variance in removal between the two GACs.

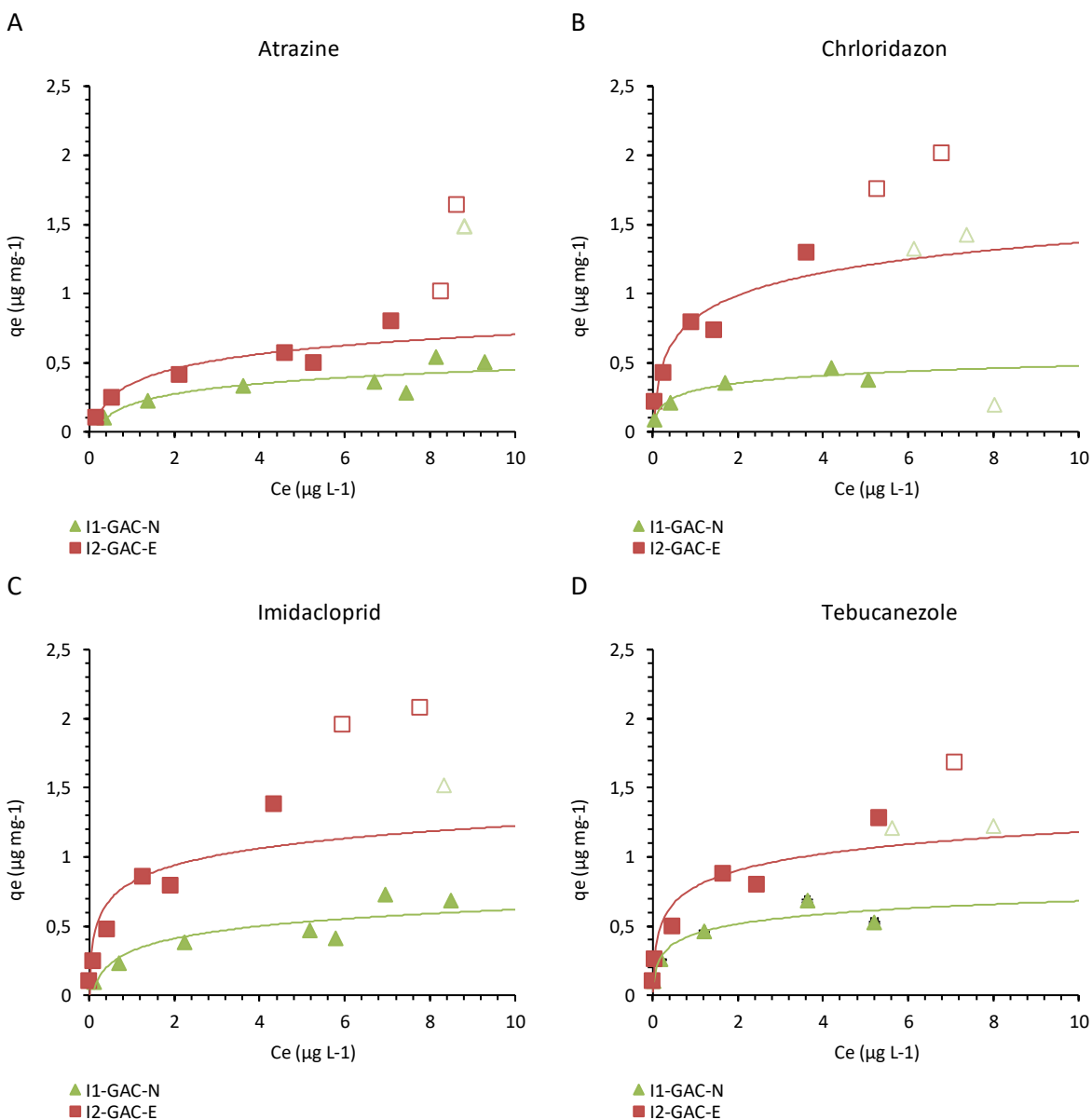


Figure 11A-D Comparison of adsorption of GAC-N and GAC-E in Schiewater for 4 pesticides. Error bars as variance in control bottles (too small to be observable)

5.2.4.2 Comparison of water matrices

When comparing the two different water matrices, it can be seen that the GAC-N attained higher adsorption in Schiewater (I_1) compared to Boskoop water (I_3) for all pesticides (Figure 12). This coincides with the lower concentration of NOM, which is known to impede the sorption of pesticides. In Boskoop water, the uptake of free ions in terms of mass was 17x as high as in Schiewater for GAC-N (Table 14), which could have further influenced the difference in pesticide removal, though this remains to be proven in further research. The effect seems most pronounced with Imidacloprid, followed by Atrazine, which both showed weaker sorption in the GAC comparison. Both Chloridazon and Tebuconazole are least

impacted by the increase in NOM and high ion concentration. No correlation could be derived between the type of bonding, molecular size, and increased competition of NOM and ions with the 4 compounds analyzed.

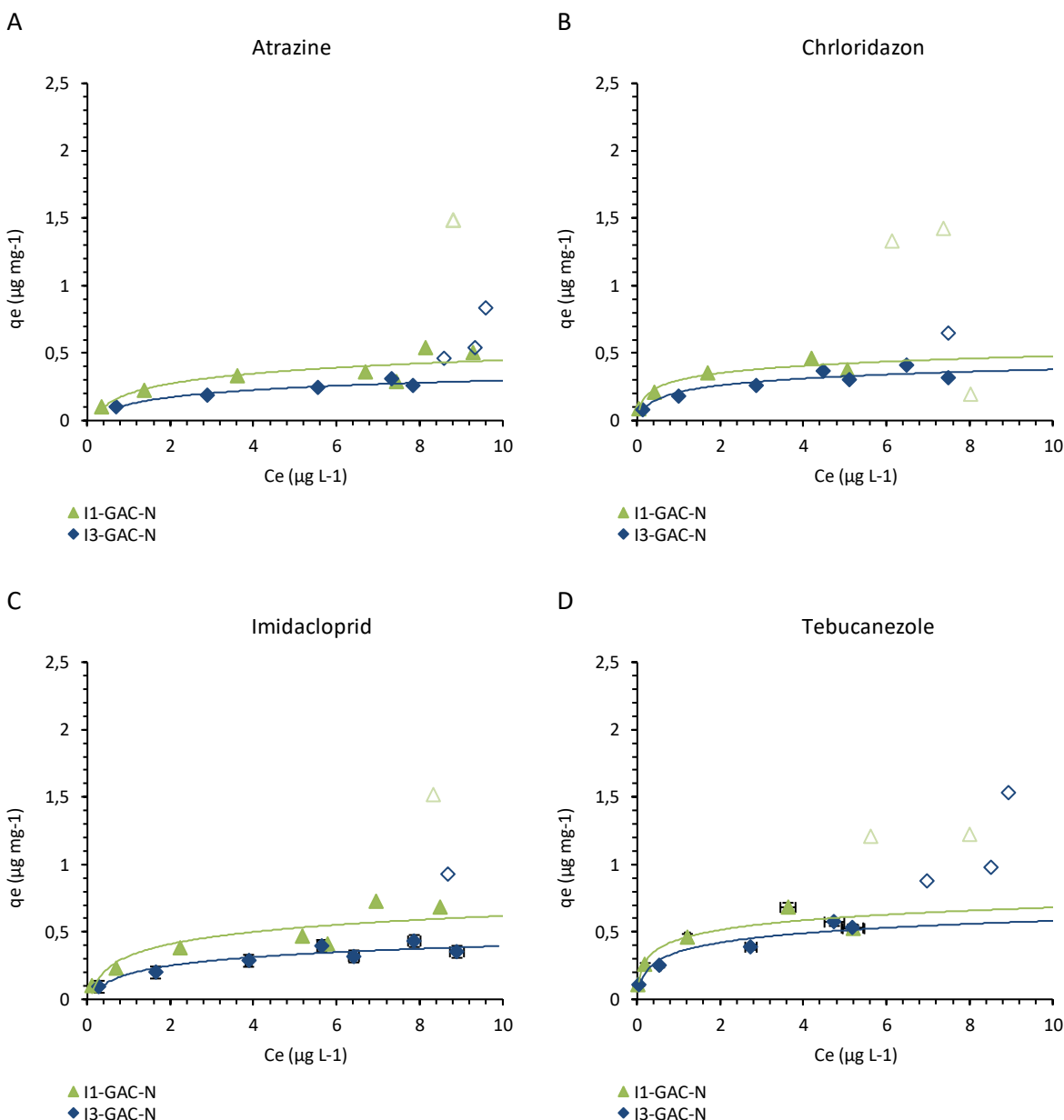


Figure 12A-D Comparison of adsorption of GAC-N on both Schie (I1) and Boskoop (I3) water for 4 pesticides. Error bars as variance in control bottles for each water type. Error bars as variance in control bottles (too small to be observable).

Control samples from each isotherm ($I_{1-3} - 6$) were taken after 7 days and showed that the isotherm equilibrium had not yet been attained (Table 15). This contrasts PAC isotherm procedures, where equilibrium is often attained within 1 - 24 hours for OMPs. The somewhat larger size of the material used in this experiment versus commercial grade PAC, 100 μm vs 25 μm , could partly explain this. The 72 hours was purposely chosen as previous biomass growth due to high nutrient content had rendered the

isotherms unusable in combination with the fact that PAC isotherms are known to desorb OMPs if their experimental duration becomes too long. While the 7 day samples were measured in a timely matter, the results of the control measurement came back long after the experiments had ended due to problems with the LC-MS calibration lines. As such, it was not possible to take a new batch of isotherm samples. The differences in concentration are relatively equal for each individual pesticide over all 3 isotherms (i.e. Pest A for isotherm 1,2,3), indicating that the differences in sorption affinity can be used to make predictions on breakthrough order, carbon affinity, and influence of competition. The difference between pesticides was largest for Bentazone, possibly as it has the lowest kinetics for the GACs tested and requires the longest EBCT to reach equilibrium concentrations in the column study, though this remains to be confirmed.

Table 15 7-day isotherm sample to check if equilibrium has been attained

	Atrazine	Bentazone	Chloridazon	Imidacloprid	Tebuconazole
	µg/l	µg/l	µg/l	µg/l	µg/l
72 hour sample					
I1-6 GAC-N	0,65	1,67	0,31	0,34	0,27
I2-6 GAC-E	0,38	1,78	0,05	0,06	0,11
I3-6 GAC-N	1,01	2,04	0,53	0,60	0,61
7 day sample					
I1-6 GAC-N	0,28	1,79	0,07	0,10	0,03
I2-6 GAC-E	0,13	1,42	0,01	0,02	0,01
I3-6 GAC-N	0,49	1,62	0,16	0,21	0,12
Difference					
I1-6 GAC-N	42%	107%	21%	30%	12%
I2-6 GAC-E	35%	80%	30%	30%	13%
I3-6 GAC-N	49%	79%	29%	35%	19%

The isotherms were drawn as log-log (Appendix 5 Pesticide Isotherms) to extract the Freundlich parameters (Table 16), which indicate the adsorption affinity and capacity of the compounds for both carbon types and water matrix. The breakthrough sequence is based on K_f , where the lowest value coincides with an earlier breakthrough. From the isotherm data, it is predicted that GAC-E will outperform GAC-N for all compounds. For the individual compounds it is estimated that Atrazine will break through first, while Tebuconazole will show high removal rates and breakthrough last.

Table 16 K_f and N values for pesticides used in the Isotherm experiments derived using Freundlich equation k_f in $(\frac{\mu g}{m} g)/(\frac{\mu g}{L})^n$.

		Water Matrix	Atrazine		Chloridazon		Imidacloprid		Tebuconazole	
			K_f	n	K_f	n	K_f	n	K_f	n
I-1	GAC-N	Schie	0.17	2.27	0.26	2.82	0.28	2.29	0.38	2.44
I-2	GAC-E	Schie	0.27	2.06	0.74	2.43	0.74	2.36	0.66	2.36
I-3	GAC-N	Boskoop	0.11	2.25	0.18	2.60	0.16	2.33	0.29	2.70

Modelling was attempted with fixed bed adsorption simulations tools using HSDM and LDF solvers through software such as FAST, AddesignS and MATLAB scripts (FAST, 2024; Burkhardt, 2025), but failed to generate usable data for the Freundlich values obtained & operating column parameters (Table 9). The diffusion coefficients for these experiments were unknown and while literature values were available and tested in wide ranges, they did not aid in obtaining usable models (Crittenden, Rhodes Trussell, Hand, Howe, & Tchobanoglous, 2022; Burkhardt, 2025). This even though they were useful in computing the breakthrough model for phosphate adsorption onto IOCS, which will be discussed in the next subchapter (Figure 15).

5.3 IOCS Isotherm results

The IOCS isotherms bottles were visually examined at the end of the run and measured for UV254, TOC, and IC (Appendix 4 IOCS isotherms). Of note is that reactor $P_1 - 6$ experienced grinding of the IOCS. This was the result of a loose reactor holder in the shaker, allowing the bottle to sway. Coincidentally, this was the only bottle in which the magnesium concentration had significantly decreased from an initial concentration of 14 mg/L down to 0.1 mg/L. No other reactor showed such a strong reduction in the magnesium concentration and as such, is treated as an outlier.

The IC and TOC analysis further showed increasing nitrate and TOC concentrations with increasing IOCS concentrations (Figure 31). The nitrate increase is theorized to occur from biomass growth. As the type of IOCS used in these experiments is being produced in a drinking water plant it comes pre-loaded with NOM, which both desorbed from the IOCS to the water matrix due to the concentration gradient and is selectively displaced by the adsorption of phosphate.

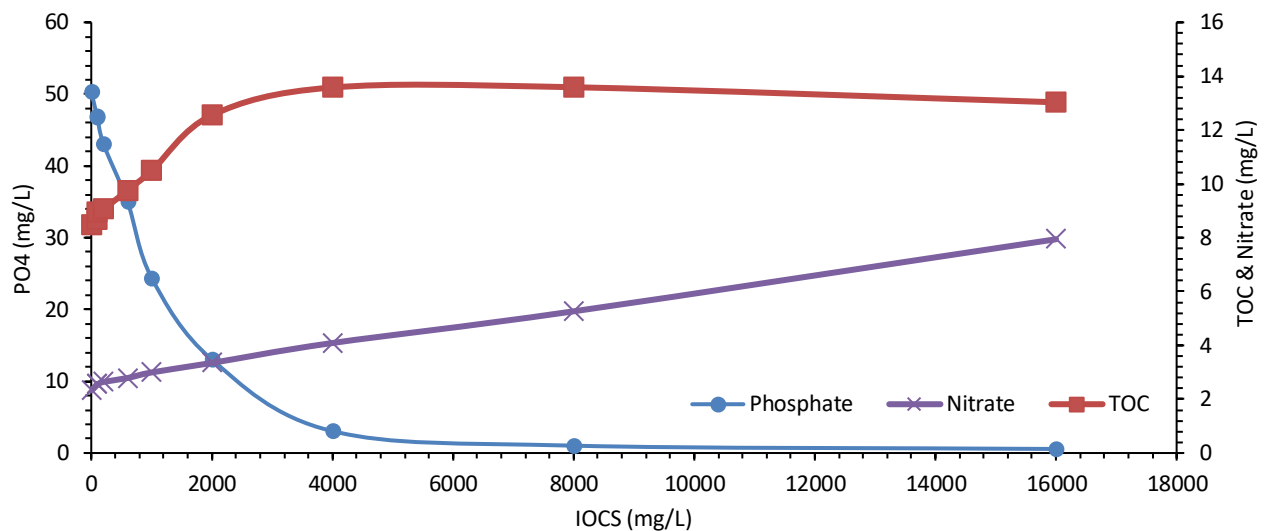


Figure 13 IOCS Isotherm results for the 3-week set. PO_4^{3-} (blue, left axis) TOC (Red, right axis) and Nitrate (Purple, right axis). Measurement error too small to depict.

The influence of NOM displacement as a result of phosphate adsorption was examined with a second set of IOCS reactors prepared in ultrapure water. Half of this set was spiked with phosphate to stimulate

uptake, while the other half reactors was used as a control to determine NOM as a result of the concentration gradient (Table 17).

Table 17 IOCS reactors in ultrapure water to determine NOM release due to selective displacement by phosphate.

Bottle	IOCS (mg/L)	Contact time	PO ₄ ³⁻ (mg/L) dosed	PO ₄ ³⁻ (mg/L) final	TOC (mg/L)	NO ₃ ⁻ (mg/L)	NH ₄ ⁺ (mg/L)
P2-0 Control	0	3 weeks	50	49.71	0.31	0	0
P2-1	8000	3 weeks	0	0	6.17	0	0.48
P2-2	16000	3 weeks	0	0	9.70	0	0.74
P2-3	8000	3 weeks	50	2.81	20.86	0	0.37
P2-4	16000	3 weeks	50	0.77	18.68	0	0.79

The results show that NOM desorbs in ultrapure water as a result of the concentration gradient. The addition of phosphate to the water matrix results in a strong increase in the desorption of NOM from the IOCS in ultrapure water, confirming that NOM is selectively displaced from IOCS by adsorbing phosphate. The increased desorption of NOM in ultrapure water (Table 17) compared to Schiewater (Figure 17) under similar phosphate loading rates can be attributed to a higher gradient in NOM between the two water matrices, thereby increasing NOM desorption.

No nitrate was formed during the ultrapure experiments, indicating that the biomass formed on the IOCS in the original isotherms with Schiewater stemmed from the water matrix itself rather than from the IOCS. The release of the cation NH₄⁺ can be attributed to similar desorption as seen from the TOC. This was not visible in the initial isotherms as the ammonium was most likely converted into nitrate by the biomass growth.

Reactor $P_1 - 10 - OMP$ was used to track the adsorption of pesticides onto the GAC over time, which found no adsorption of any pesticide onto the highest concentration IOCS used over the three week period.

Along with the removal of the negatively charged NOM and PO_4^{3-} , the positively charged cations in the water matrix showed increased removal with increasing concentrations of IOCS (Table 18), most likely because they can form precipitates with the free phosphate and with phosphate previously bound to the IOCS, as well as form complexes with the negatively charged surface hydroxyl groups (Mengxue, Jianyong, Yunfeng, & Guangren, 2016). The di-cations bind more strongly to these groups due to their higher charge, with monovalent ions showing lower sorption rates. While the uptake compared to phosphate was relatively weak, some influence and removal of these cations is expected during the column studies.

Table 18 Cation removal during IOCS isotherms. Note that P1-6 is marked as outlier

	Ca^{2+}	K^+	Mg^{2+}	Na^+
	C_0 (mg/L)			
P0 3W	69.05	28.89	14.23	52.75
	Percentage removed			
P1-1 3W	3%	3%	3%	2%
P1-2 3W	2%	2%	3%	2%
P1-3 3W	5%	2%	3%	2%
P1-4 3W	10%	2%	7%	3%
P1-5 3W	21%	3%	11%	2%
P1-6 3W	21%	4%	99%	3%
P1-7 3W	27%	3%	16%	3%
P1-8 3W	33%	8%	22%	3%
P1-9 3W	37%	10%	27%	4%

The adsorption of phosphate onto the IOCS could be modelled to Freundlich isotherms, from which the Freundlich isotherm parameters $k_f = 5.39$ & $n = 2.04$ could be obtained (Figure 14). The loading capacity for phosphate onto the IOCS with an influent dosage of 10 mg/L was determined to be 16.9 mg PO_4^{3-} /g IOCS.

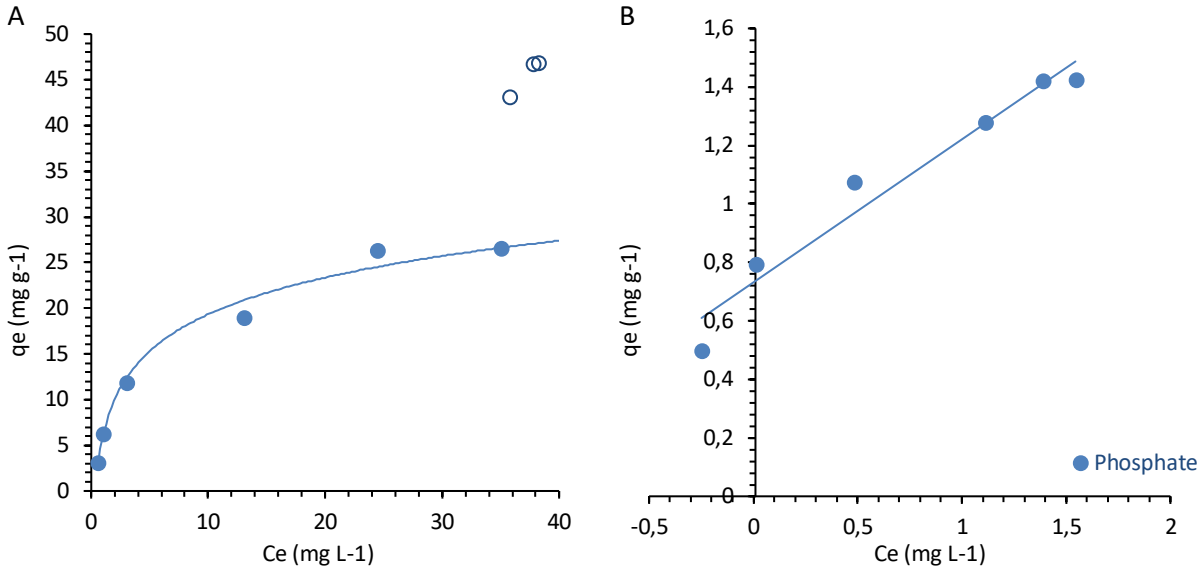


Figure 14A-B phosphate isotherm results for normal (A) and log (B) scales, derived with Freundlich equations. Measurement error too small to depict.

The Freundlich parameters from the Isotherm experiments were used to run simulations on the expected breakthrough curves for the columns using a fixed bed adsorption simulation tool with HSDM and LDF modelling (FAST, 2024). The film diffusion and surface diffusion coefficients are unknown but estimated from literature: the surface diffusion coefficients found in literature ranged from 10^{-10} to $10^{-9} \text{ m}^2/\text{s}$ for liquids (Crittenden, Rhodes Trussell, Hand, Howe, & Tchobanoglous, 2022). The choice between the two was found to have a negligible difference in the outcome of the simulations. As such, the latter was chosen for the simulations. The film diffusion coefficient came pre-loaded in another fixed bed adsorption simulation tool, for which the simulation was run with 10^{-7} and $10^{-6} \text{ m}^2/\text{s}$ (Burkhardt, 2025)). The rest of the parameters were set equal to the operating parameters of the column study (Table 19). Depending on the diffusion coefficients, phosphate breakthrough on the IOCS column is predicted to occur somewhere between week 4 and 10, and the IOCS will become exhausted between week 12 and 18 (Figure 15).

Table 19 Parameters set for modelling phosphate breakthrough on the column experiments.

Dimensions	Unit	
EBCT	h	0.92
Mass of IOC	g	84.00
Porosity	-	0.31
Bed Volume	cm ³	68.78
Q	mL/min	1.25
Particle diameter	mm	2
Material density	Kg/m ³	1500
mA/Q	g*d/L	46.78
C0	Mg PO ₄ ³⁻ /L	10
N - Freundlich	-	0.49
KF- Freundlich	(mg/g)(L/mg) ^{1/n}	5.39
kL	m/s	10 ⁻⁷ and 10 ⁻⁶
Ds	m ² /s	10 ⁻⁹

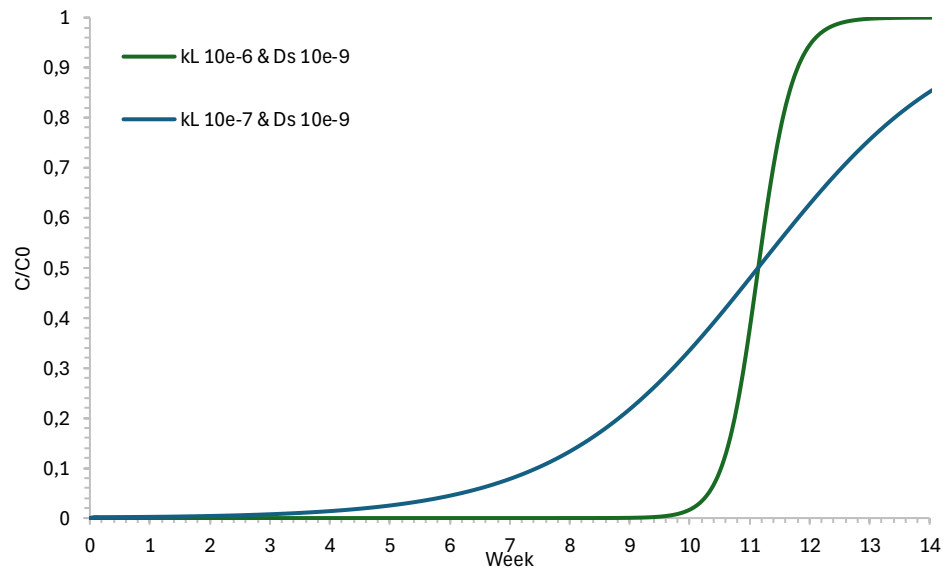


Figure 15 Modelled breakthrough curve for phosphate removal ($C_0 = 10\text{mg/L}$) from the IOCS column. Parameters can be found in table 19. Conversion of Weeks to BV in Appendix Column studies.

5.4 Column Results

The 14-week column study was performed to compare the difference in performance between two GAC types in a filter versus the isotherm experiments and to determine the influence of the additional IOCS top-up layer. Bio growth on the SSF columns became visible after 4 weeks, after which the columns were covered with aluminum foil to prevent excessive growth and clogging due to their small diameter, and the pump tubing was replaced. The delay in bio growth versus growth rates found in literature can be attributed to the pre-filtering of the water over 1 μm filters, which remove a large part of biologically active matter (Campos, Su, Graham, & Smith, 2002). The bio growth was accompanied by gas production, which became partly entrapped in the SSF column and predominantly in between the coarser GAC (Figure 16). This resulted in lower EBCT and mass transfer zone for the GAC, negatively impacting adsorption. The bio growth was not constrained to the top layers, such as observed in regular SSFs, but rather trended upwards throughout the columns, likely due to preferential flow paths and wall effects from the narrow columns (Figure 31).



Figure 16A-B Air entrapment in (A) column 1 (GAC-N) and (B) column 2 (SSF) observed during week 5.5

The columns were flushed after sampling in week 5 to remove the entrapped air by connecting the water to the sampling ports between the columns and closing off the SSF outlet, which successfully removed all air. After flushing the column, re-connected with flow resuming as normal. Entrapped gas again became visible in the following weeks, predominantly in the GAC column, after which the columns were flushed weekly from week 6 - 8. The columns were flushed post sampling each week, allowing the flow to normalize for close to a week before the next sampling period. Initial flushing greatly reduced the entrapped air in the SSF, which showed less accumulation in the following weeks. Flushing was terminated as the volume of air in the column did not decline after week 8. C#1-GAC-N suffered to most from the entrapped gas, most likely as it had the largest grain size, making it easy to retain gas in the free space between the pores (Figure 16). The other columns containing GAC-E likewise suffered from entrapped gas, but to a slightly lesser amount.

The flow rate through the columns was monitored weekly by weighing a 90-minute sample. During the first weeks, the flow rate declined steadily over all columns, after which it sharply rose following the initial flushing due re-arrangement of the particles in the fluidized beds (Figure 17). C#3-GAC-E-IOCS, which contained the additional IOCS column element, experienced the greatest head loss during the study. This coincided with literature, which states that additional head loss is expected in IOCM filters (McMeen & Benjamin, 1997).

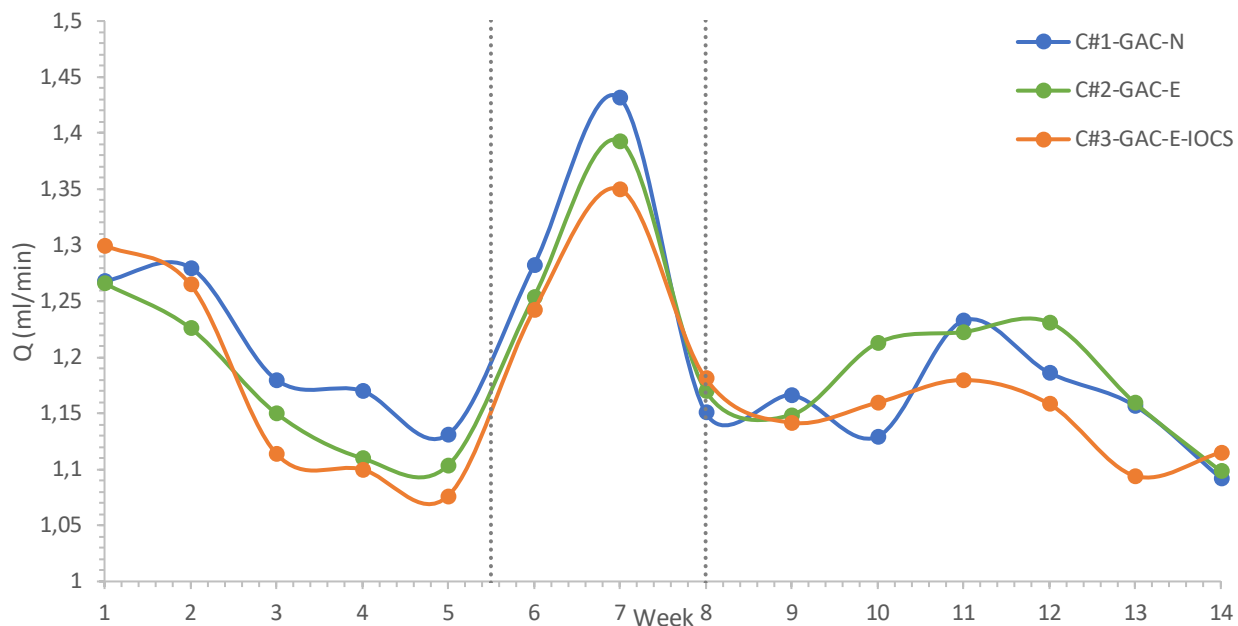


Figure 17 flow rate over time for each column. Dashed lines indicate start and end of weekly flushing

The IOCS layer has a longer bed length than the SSF layers (23 vs 21 cm), which would lead to mismatched scatter graphs as a result of slightly different BV. As such, the graphs in this subchapter are plotted with the x-axis as weeks. As the flow rates between the columns are nearly identical, there is a negligible difference in BV between the SSF layers each week (< 0.1 %). Appendix 6 Column studies contains the conversion of weeks to BV for the interested reader.

5.4.1 Water Matrix

The water matrix remained relatively stable for the duration of the column run (14 weeks) except nitrate and nitrite due to low initial concentrations in the feedwater, where small increases (1 - 2 mg/L) resulted in large outliers (Table 20). The UV254 absorbance of the influent varied more than the TOC influent concentrations over the study, indicating that the composition of different NOM fractions in the feedwater varies week to week.

Table 20 Average NOM and ion concentration of the influent water during the column experiments.

	pH	UV254	TOC	Cl ⁻	NO ₃ ⁻	PO ₄ ³⁻	SO ₄ ²⁻	Na ⁺	NH ₄ ⁺	K ⁺	Mg ²⁺	Ca ²⁺
Units	-	cm ⁻¹	mg/L	mg/L	mg/L	mg/L	mg/L	mg/L	mg/L	mg/L	mg/L	mg/L
Average	8,3	0,50	14,76	66,86	2,86	9,67	56,17	46,82	0,16	13,80	14,15	93,25
Std	0,26	0,07	1,95	6,03	0,53	0,50	4,97	3,34	0,34	1,38	0,69	2,99
Std %	3,1%	15.61%	13.24%	9,02%	18,60%	5,18%	8,84%	7,14%	208,21%	9,97%	4,90%	3,20%

The pesticide concentrations were measured weekly by sampling both interconnected jerrycans. This feedwater was re-filled roughly every 5 days from 25 L jerrycans to which 250 mL 1 mg/L stock solution was added, resulting in a 10 µg/L spiked Schiewater influent. In total, 2x2L stock solution was used during these experiments, for which the initial concentrations can be found in (Table 29). Despite adding equal concentrations of pesticides to the feedwater tanks every week and using a set sampling method, large variations between the influent tanks were measured (Figure 17). This could stem from the degradation of stock solutions, improper mixing of pesticides, differences in concentration between stock solutions, differences in LC-MS measurements due to internal standards or mixing errors, though no one reason was found to explain this difference.

Table 21 Average pesticide concentration of the influent water during the column experiments, in µg/L.

	Atrazine	Bentazone	Chloridazon	Imidacloprid	Tebuconazole
Average (µg/L)	9,67	10,16	9,18	8,47	9,85
Std	0,5	0,9	0,86	0,65	1,39
Std %	5,22%	8,92%	9,13%	7,87%	13,98%
Var %	3,26%	3,40%	2,23%	1,36%	8,70%

The effluent of the carbon sink, which was put in place to remove any pesticides in the column effluent, was measured several times throughout the column study and did not measure any pesticide concentration.

5.4.2 NOM adsorption

The change in NOM concentrations over each column element was measured by tracking the UV254 adsorption and TOC concentrations (4.1.5 Sampling and analysis). This chapter will present the results in order of the water flowing through the filters; initially, the NOM adsorption by the IOCS and SSF layers will be presented (Figure 19), followed by the GAC layers (Figure 20). Finally, the complete results are presented as NOM adsorption over the entire filters (Figure 24). All columns showed systematic TOC release that could not be explained and did not match with the UV254 measurements. The UV254 data showed results that could be explained and appeared more “in line” with expectations. As such, it is advised that the reader take the TOC results lighter than the UV254 measurements.

In all columns, there was consistent TOC release from the layers that were first in contact with the influent water, being the SSF in C#1-GAC-N & C#2-GAC-E and the IOCS layer in C#3-GAC-E-IOCS. There was a higher TOC release from the SSF of C#1 versus C#2 (Figure 18) despite the column elements being identical, indicating a high degree of variability in the TOC results. The TOC release from the IOCS could be explained from the isotherm results, which showed net displacement of pre-loaded NOM from the IOCS by adsorption of phosphate (Table 17). The SSF in C#3, which follows the IOCS layer is the only SSF layer that sorbs TOC, though in lower amounts than released from the IOCS, indicating that the material released in the IOCS is partially re-captured in the SSF column. It is unclear why the SSF in C#3 sorbs TOC while the other two SSFs release TOC, as all SSFs are identical in shape, size, and material. The SSF sand was investigated to see if it was the source of TOC release by soaking 100g of material in 500mL of water for 3 weeks, during which they released 0.0017 mgTOC/g/L for SSF. As such, it is not expected that the released TOC seen in the measurements originates from the sandy material. The material was, however, not tested for TOC release as a result of a shearing force, as in a column, the water flows along the grains, inducing a shear force, which could result in the release of TOC.

The UV254 measurements contradicted the TOC results, with results that were more “in line” with expectations and showed net sorption over the columns during the 14 weeks study. The SSF layers in C#1 and C#2 show 10% removal during the first weeks, and after briefly trending to zero contribution, the removal stabilizes around 5%. The IOCS layer in C#3 showed higher and more prolonged removal, which initially stabilized around 10%. It is suspected that the initial removal in all columns stems from physiochemical removal by the material through screening and straining as described in 1.2.1 Transport Mechanisms. This is supported by the initial 5% removal of the SSF layer in C#3 following the IOCS layer, which quickly diminishes to 0 for the duration of the study. The increased removal from the IOCS versus the SSF is thought to occur from NOM binding to the IOCS, as shown from earlier literature (McMeen & Benjamin, 1997). It is suspected that the increasing removal after 6 weeks stems from biodegradation, as it shows a contribution in the first layers in contact with the influent water (C#1&2 SSF and C#3 IOCS) but does not show any contribution from the SSF layer in C#3, where the DO in the water is expected to be consumed prior in the IOCS layer, preventing biomass from significantly contributing to NOM uptake. This is supported by the uptake of phosphate and production of nitrate, which indicate an increased presence of biomass over time (Figure 29). As there was little to no nitrite or ammonia present in the influent, it was not possible to derive consumption rates. While SSF biomass is expected to mature within 2 months in such a high temperature, high nutrient environment (Campos, Su, Graham, & Smith, 2002), pre-filtering

the influent could have caused a reduction in biomass growth rate, as no stabilization has been observed after 14 weeks. A prolonged study would be needed to further investigate the development of TOC release and removal of NOM over the SSF layers.

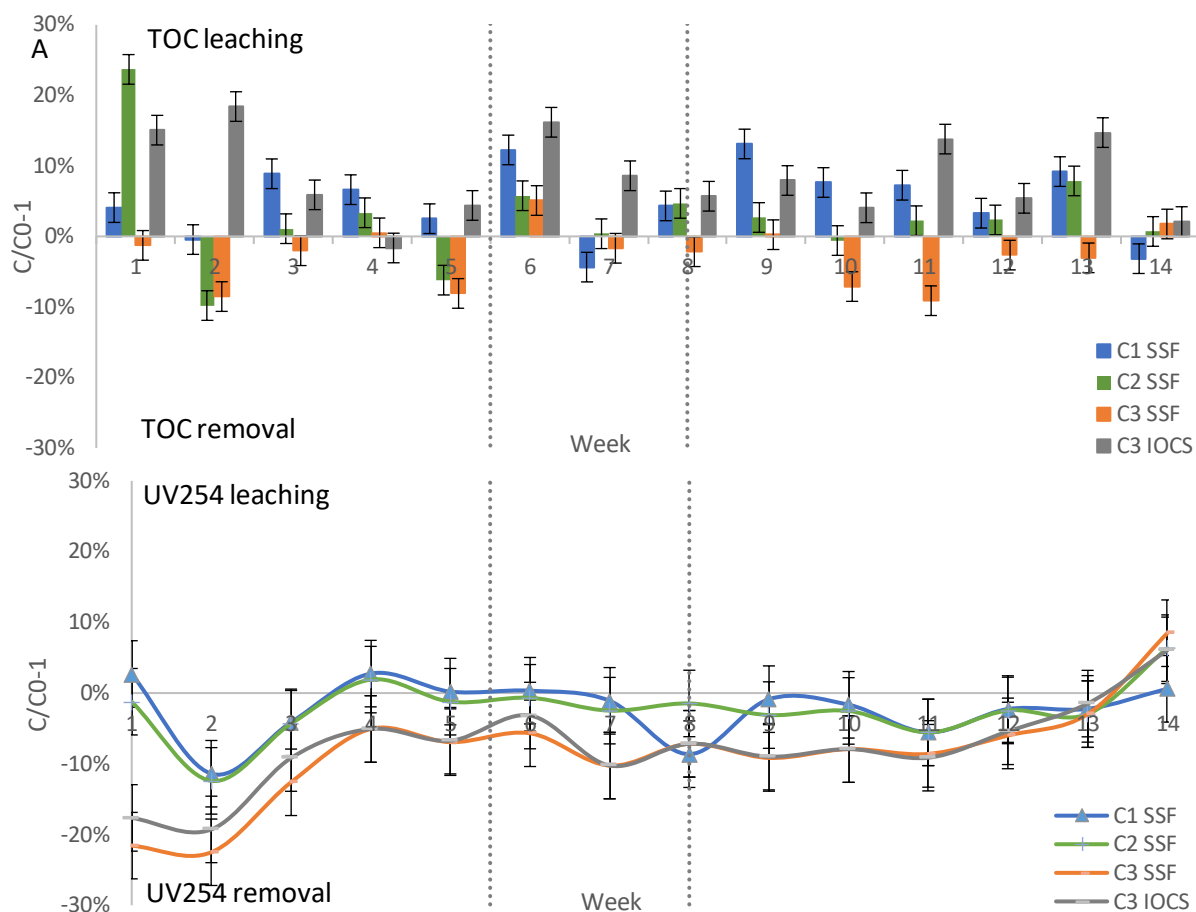


Figure 18 A-B UV254 absorbance, TOC influent and effluent concentrations for SSF and IOCS layer over each column layer versus influent concentrations during the 14-week study. Error bars indicate variance between control bottles.

While the TOC/UV254 measurements contradicted each other in terms of leaching/removal, the overall trends for NOM removal over the GAC layer between TOC/UV254 measurements line up. The GAC columns leached TOC during the initial stages of the study, which trended to net sorption towards the end of the study, while the UV254 showed net adsorption during the entire study (Figure 19). The abrupt net sorption of TOC by all columns during week 4 is an outlier in the dataset, as no operational or sampling difference occurred, and the UV254 data does not show a correlation supporting the net sorption during this week.

TOC leaching was lower over GAC-N (C#1) versus GAC-E (C#2), with C#1 showing net sorption from week 9 onwards, indicating that GAC-N had a higher loading of TOC/gGAC due to its significantly lower density vs GAC-E (Table 9), as the TOC influent concentrations for both column sets were comparable. Little difference between the UV254 uptake C#1-GAC-N and C#2-GAC-E was found, though GAC-E had a higher pesticide uptake over the entire column study, as will be shown in a later chapter (Figure 23). The

pesticides react to UV254 measurements, for which the NOM-UV254 needs to be corrected. As with the TOC measurements, the Norrit again showed higher UV254-NOM loading/g GAC versus the Eversorb.

C#3-GAC-E-IOCS showed lower TOC release versus C#2-GAC-E, despite both columns having on average equal influent concentrations of TOC. TOC leaching from the carbon was ruled out as no indications of this became visible from the isotherm experiments (Figure 9, Figure 10) The sand supporting the GAC was tested similarly to the SSF sand and did not contribute to TOC leaching (0.0022 mgTOC/g sand/L leached).

C#3-GAC-E-IOCS had higher initial removal of UV254 and better performance over the entire column study versus C#2-GAC-E, despite receiving lower NOM-UV254 influent concentrations. This could be due to the absorbance of other competing fractions of NOM onto the IOCS, or due to higher sorption of pesticides, which show up in the UV254 measurements, but a more detailed investigation into the absorbance of different NOM fractions in each layer would be needed to confirm this. The GAC columns did not show any significant uptake phosphate over the study in contrast to its high affinity during the isotherm experiments (Table 14). Furthermore, there was only minor nitrate consumption, indicating (in combination with the phosphate measurements) that no significant biomass had developed at the conclusion of the experiments.

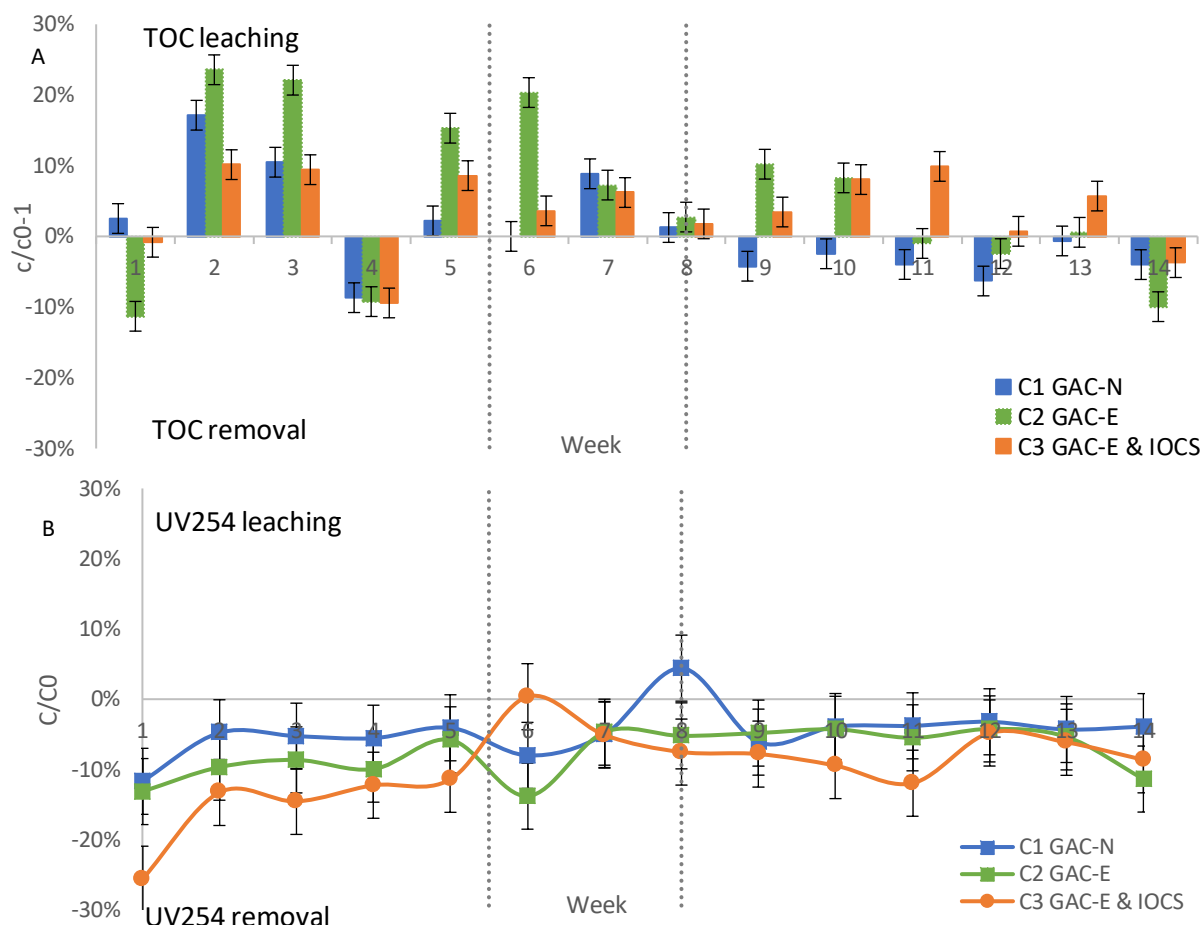


Figure 19A-B UV254 absorbance, TOC influent and effluent concentrations for the GAC layer over each column during the 14 week study. Error bars indicate variance between control bottles.

Combining the NOM removal over the IOCS/SSF and GAC layers provides an overview of removal over the whole filters (Figure 20). Between the two carbon types, C#1-GAC-N shows a higher loading of NOM for TOC and UV254, especially if the graphs are corrected for density differences. The addition of the IOCS column in C#3-GAC-E-IOCS shows elevated NOM removal compared to the other columns. This stems from both increased removal in the IOCS as well as increased removal in the GAC layers as shown earlier, despite having lower influent concentrations, hinting at a synergy between the two layers not seen in the other columns. More research into the composition of NOM fractions in the water, as well as NOM fraction sorption, is needed to determine what causes the increased removal in the GAC layer as a result of the IOCS layer. The removal of UV254 decreased to 0 for all columns during the end of the study, though it is unclear if this is temporary or due to exhaustion of the material, for which longer term studies would be needed.

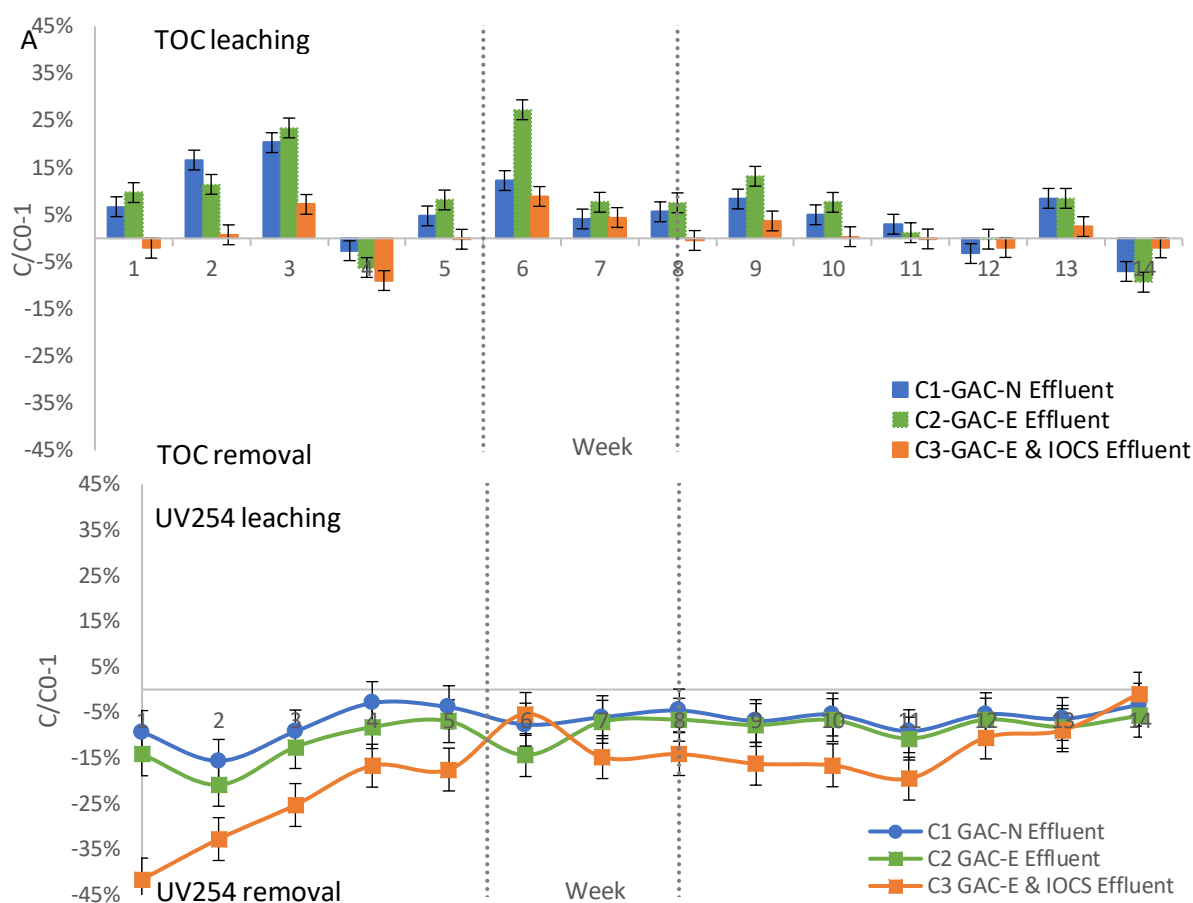


Figure 20A-B UV254 absorbance, TOC influent and effluent concentrations for all columns during the 14 week study. Vertical lines indicate start and end of weekly flushing Error bars indicate variance between control bottles.

5.4.3 Phosphate adsorption on IOCS

Phosphate was completely removed from the influent during the first week but showed breakthrough as early as week 2 with an EBCT of 55 minutes for the IOCS column (Figure 2). Despite faster than predicted breakthrough, the sorption capacity decreased slower than expected from modelling and appeared to round off at 50% in the last weeks of the experiments. Longer experiments would be needed to obtain a full breakthrough curve, but if the current trendline holds, the final sorption capacity of the material until full breakthrough is achieved would be higher than predicted from the model. The higher-than-predicted sorption capacity in columns versus isotherms has been similarly found in other studies but remains to be investigated. (Zhang, Wang, Lakho, Yang, & Depuydt, 2022). Key differences between the isotherm and column study are the concentration of calcium (69.5 mg/L vs 93.25 mg/L) and pH (7.3 vs 8.0), respectively. The increase in both parameters favors the precipitation of calcium phosphates, which could explain the slower breakthrough (Stumm & Morgan, 1981; Suresh Kumar, 2018). The pH of the water remained stable over the column and is not expected to have influenced the adsorption of phosphate. During the isotherm experiments, the IOCS showed a high affinity to calcium and magnesium removal (Table 18). While the removal of magnesium was low during the column study, calcium removal remained elevated (Table 22). The initial high removal of calcium is hypothesized to come from the precipitation of $\text{Ca}_3(\text{PO}_4)_2$, which appears to be responsible for the removal of a sizable amount of total calcium and phosphate removal during the study, as indicated by the ratio of $\text{Ca}:\text{PO}_4$ (Suresh Kumar, 2018). The theory remains unproven for this study but is supported by literature, which mentions that the chemical precipitation of various forms of calcium phosphates is favored above a pH of 7.5, as was the case during this study (Stumm & Morgan, 1981). The removal of calcium decreases significantly faster than the removal of phosphate throughout the 14-week study, indicating that over time, the role of calcium precipitation decreases while sorption of phosphate onto the IOCS as a result of ion exchange and electrostatic attraction with iron oxides becomes more dominant. The calcium precipitation index for these measurements was not available as the alkalinity of the samples was not measured.

Table 22 Phosphate vs calcium removal in the IOCS column

Week	Influent C ₀		Removal						
	mg/L		Percentage		mg/L		mmol/L		Ratio (mmol)
	PO ₄ ³⁻	Ca ²⁺	PO ₄ ³⁻	Ca ²⁺	PO ₄ ³⁻	Ca ²⁺	PO ₄ ³⁻	Ca ²⁺	
1	9,0	88,1	100%	12,3%	8,98	10,85	0,09	0,27	2,9
2	10,0	94,6	87,9%	10,3%	8,82	9,72	0,09	0,24	2,6
3	10,1	95,5	81,4%	6,4%	8,21	6,11	0,09	0,15	1,8
4	9,1	91,3	77,2%	7,0%	7,00	6,39	0,07	0,16	2,2
5	8,6	91,0	70,0%	4,9%	6,02	4,42	0,06	0,11	1,7
6	9,7	100,2	65,7%	4,1%	6,40	4,13	0,07	0,10	1,5
7	9,9	93,0	65,3%	7,4%	6,47	6,84	0,07	0,17	2,5
8	10,1	93,9	61,6%	0,7%	6,19	0,63	0,07	0,02	0,2
9	10,0	94,1	58,3%	1,5%	5,83	1,41	0,06	0,04	0,6
10	9,9	93,5	55,6%	0,9%	5,51	0,83	0,06	0,02	0,4
11	9,8	92,1	50,4%	2,6%	4,95	2,41	0,05	0,06	1,2
12	10,4	91,0	50,3%	2,0%	5,25	1,80	0,06	0,04	0,8
13	10,7	88,1	49,5%	-0,4%	5,31	-0,38	0,06	-0,01	-0,2
14	9,1	88,1	49,0%	1,7%	4,47	1,52	0,05	0,04	0,8

From literature, it was found that the IOCS had relatively fast kinetics that indicated a short EBCT would suffice (Nacéra Yeddou & Bensmaili, April 2009). In contrary to this, literature column experiments showed that prolonging the EBCT from 0.5 BV/H to 0.3 BV/H doubled the time to initial breakthrough, despite the fact that the material used exhibited fast kinetics during isotherm experiments (Zhang, Wang, Lakho, Yang, & Depuydt, 2022). This contradiction remains to be investigated but might explain why phosphate broke through faster than expected while maintaining sorption capacity longer then modeled.

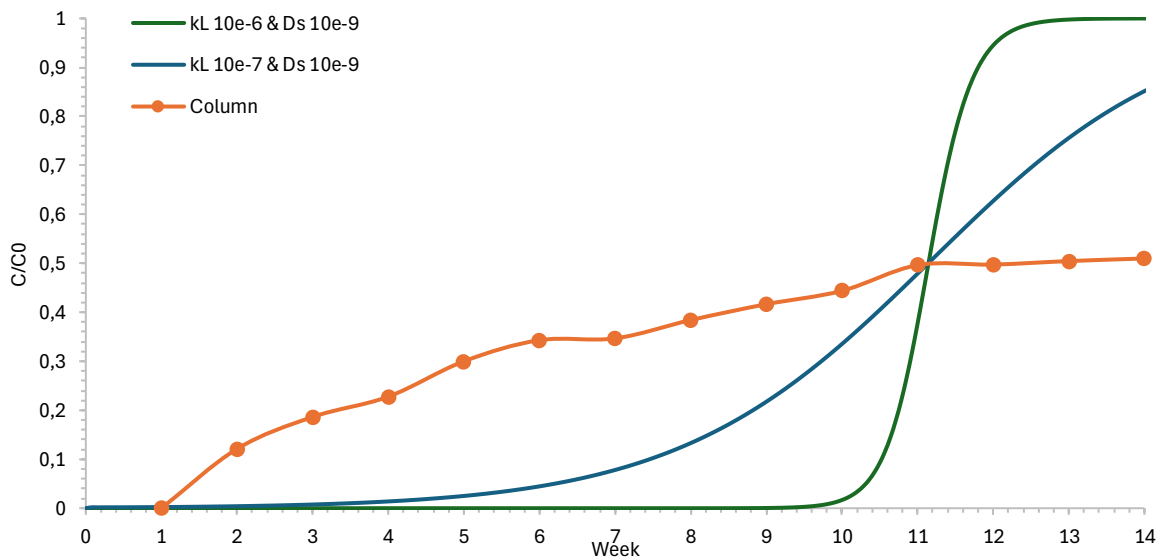


Figure 21 Breakthrough curve for phosphate on the IOCS column during the 14 week column study ($C_0 = 10\text{mg/L}$) together with the modelled breakthrough curve.

The Freundlich model assumed a sorption capacity of $16.9 \text{ mg PO}_4^{3-} / \text{g IOCS}$, with 90 % breakthrough occurring after 2000-3000 BV with $10 \text{ mg PO}_4^{3-} / \text{L}$ influent (Figure 28 Appendix 6 Column studies). At the conclusion of the experiments, the column had sorbed $1075 \text{ mg PO}_4^{3-}$ onto 84.5 mg IOCS , for a sorption capacity of $12.6 \text{ mg PO}_4^{3-} / \text{g}$ with ~50 % residual sorption capacity remaining. Should the current trendline hold, the sorption capacity of the IOCS based on the column study would be $43 \text{ mg PO}_4^{3-} / \text{g IOCS}$, with 90 % breakthrough occurring after 17700 BV. However, this most likely oversimplifies reality and overestimates the total sorption capacity. Longer term experiments (> 12 months) would be needed to investigate the contribution of biomass on phosphate degradation on the IOCS as it is currently unknown at what point biomass would mature. Bio growth on the IOCS column could result in further uptake of phosphate, freeing up sorption spaces, contributing to a longer bed lifetime similar to the theory of BAC as explained in the theory earlier (2.3.2 Biodegradation). This is supported by the production of nitrate in the IOCS column (Figure 29A) and visual observations of bio growth in the column throughout the study. In contrast to the SSF and GAC layers, the IOCS column did not show an accumulation of gas between grains and was not influenced by weekly flushing. The removal of phosphate by bio growth is hypothesized but not confirmed through biomass measurements.

To summarize, the IOCS column was successful in removing phosphate with influent concentrations at 2-4x of what was observed in the Boskoop and Texel pilots. While the initial breakthrough occurred faster than expected, the loss of sorption capacity progressed slower than modeled. Theory suggests that while IOCM have relatively fast kinetics, further increasing the EBCT from 55 minutes by either decreasing the flow rate or increasing the bed height would significantly postpone the time until breakthrough, making it an effective material at removing phosphate from the TDW influent, in addition to the NOM removal demonstrated earlier.

Using the modelling software (FAST, 2024), it is expected that the 10 ton IOCS could treat 23.500 m^3 of water assuming $10 \text{ m}^3 / \text{h}$ containing $5 \text{ mg PO}_4^{3-} / \text{L}$ at 55 minutes EBCT before 12% breakthrough would occur and the phosphate concentration would exceed the legal limit (Omgevingswet, 2024). However, the column experiments have shown that breakthrough occurs faster than expected, despite losing sorption capacity slower than expected. As such, further research would be advised into long-term experiments with IOCS to determine how fast it would take to reach a full breakthrough. In any case, a longer EBCT would be advised as literature has mentioned it can significantly delay breakthrough (Zhang, Wang, Lakho, Yang, & Depuydt, 2022). The material is easy to work with and can be set up as either a separate filter (making renewal of the material an easy option) or an additional layer on top of existing filters to be scraped off. Literature suggests that regeneration of the material is possible, further increasing its life of use, but this remains outside the scope of this research (Boeckert, 2023).

5.4.4 Pesticide adsorption

The adsorption of pesticides by the columns tracked the removal of 5 compounds over 14 weeks (Figure 24). This chapter will first present the pesticide adsorption by the SSF and IOCS layers, followed by the adsorption of the GAC layers. It will conclude by presenting the adsorption of pesticides through the combined IOCS-SSF-GAC filters.

The sorption of Bentazone was particularly weak compared in all likelihood as it is the only charged compound used, leading to rapid breakthrough, with 20 - 60 % breakthrough observed from week 1 onwards. This coincided with the isotherm results that saw particularly weak adsorption of Bentazone. As such, the results are again omitted from the chapter but added in the Appendix 6 Column studies. It is possible that the high pH of the water negatively influenced the weak-acid Bentazone, but further research should be needed to confirm this and to determine if the weak adsorption is constrained to one compound or indicative for all charged OMPs found in Dutch TDW.

When comparing pesticide removal over the SSF/IOCS layer(s), it can be seen that there are large differences between the compounds investigated (Figure 22). The graphs show the removal rate of the layer versus the influent concentration. Care should be taken to interpret the SSF layer in C#3, which shows C/C_0 where C_0 is the influent of the full column, not the effluent of the IOCS layer preceding it. The spike in Chloridazon concentration from week 6 is most likely due to the use of a new internal standard for the samples as well as the use of a new stock solution, which resulted in higher measurement values. The Chloridazon concentrations should be interpreted with an offset of 20% from week 6 onwards, but have been left as original data as the origin of the offset could not be proven.

Atrazine and Tebuconazole are initially removed in the first layer in contact with the influent water for all columns (Figure 7), being the IOCS layer in C#3 and the SSF in C#1 and C#2, with removal rates seen of 20 - 40 %, yet this removal quickly diminishes to near 0 after 5 - 7 weeks. During the isotherm experiments, the removal of pesticides by adsorption onto IOCS was ruled out, in contrast to what is observed here (5.3 IOCS Isotherm results). This, combined with the fact that the SSF in C#3 barely contributes to the physiochemical removal in the initial stages indicates that the pesticides in the first layer in contact with the water are retained along with or by material that is strained on top of the filter layers instead of physiochemically retained by the substrate. This remains a theory and should be proven in further research. The total mass removed was approximately 82 μg for Atrazine and 180 μg for Tebuconazole in each column.

The removal of all compounds increases from week 6 onwards in the first contact in the influent water, irrelevant of the substrate material (IOCS or SSF). The delayed removal and increase over time in the first layers, which is rich in (biodegradable) NOM and DO, suggest biological capture or (co-metabolism) by the developing biomass. The growth of biomass was supported by visual observations of the columns showing increasing bio growth over the entire duration of the column operation. The contribution of suspected biodegradation in the SSF in C#3-GAC-E-IOCS is smaller, most likely due to (assumed) lower DO concentrations, but becomes active after 6 weeks with increasing removal of Tebuconazole and, notably, Imidacloprid. Biodegradation of OMPs had earlier been proven in SSF-GAC sandwich filters by other researchers, yet they required EBCT of 10 hours with rapid decline in degradation if this was reduced to 5

hours (Li, Zhuo, & Campos, 2018; Li, Campos, Zhang, & Xie, 2022; Xu, Campos, Li, Karu, & Ciric, 2021). This is the first research that has obtained such high removal by suspected biodegradation with SSF-GAC filters. The high removal of OMPs by slow or rapid sand filters has been proven for selected compounds (Wang, de Ridder, van der Wal, & Sutton, 2023). Additionally, the high removal by biodegradation for Tebuconazole and Chloridazon has been shown in small-scale laboratory experiments or wetland studies before inoculating filters with specific bacterial strains. To the authors knowledge it has not yet been seen at such high concentrations with such a short EBCT with such a short biomass growth period (Badawi, Rosenbom, Jensen, & Sørensen, 2016; Escolà Casas & Bester, 2015; Chen, et al., 2024; Timmers, Siegers, Ferreira, Lousada, & van der Wielen, 2024; Wang, et al., 2022).

The removal of Imidacloprid in C#3-GAC-E-IOCS deviates from the results found in the other two columns and the other compounds. In both C#1-GAC-N and C#2-GAC-E there is no initial nor later removal of Imidacloprid by either physical, chemical, or biological capture. In C#3-GAC-E-IOCS where the compound first encounters the IOCS, there is increased removal from week 5 onwards, peaking at 70 % in week 12. A similar removal rate is visible in the SSF layer following the IOCS layer, which removes an additional 70 % of the effluent of the IOCS filter. The combined IOCS-SSF removal of Imidacloprid reached 90 % versus filter influent concentrations at the end of the study. Previous studies using isolated bacteria have proven high removal rates of Imidacloprid under laboratory conditions, but to the authors' knowledge have not been confirmed in column studies with either SSF or IOCS (Pallavi & Suresh Kumar, 2022; Tiwari, Tripathi, Mohan, & Singh, 2023). The contribution is suspected to come from biodegradation as it appears from week 6 onwards and increases over time, plateauing at 70 % for each separate layer at the end of the study, though longer-term studies would be needed to confirm this definitively. No conclusion was found as to why the IOCS allowed for suspected biodegradation, although it is possible that the IOCS substrate allows for the successful development of a type of bacteria that cannot cultivate in a standalone SSF as in C#1-GAC-N and C#1-GAC-E. The removal of Imidacloprid in SSF C#3-GAC-E-IOCS could stem from the inoculation of washed-out IOCS biomass, though. More research into this would be highly advised; these findings have not been reported before to the author's knowledge, and this column study shows that removal rates on par with GAC filters can be attained for Imidacloprid in normal operating conditions given the correct substrate (IOCS in this case). Using this is a sandwich filter configuration that significantly reduces GAC loading, making it a potentially good addition to the current pilots in Texel and Boskoop, where the use case is originally centered around the removal of phosphate and NOM.

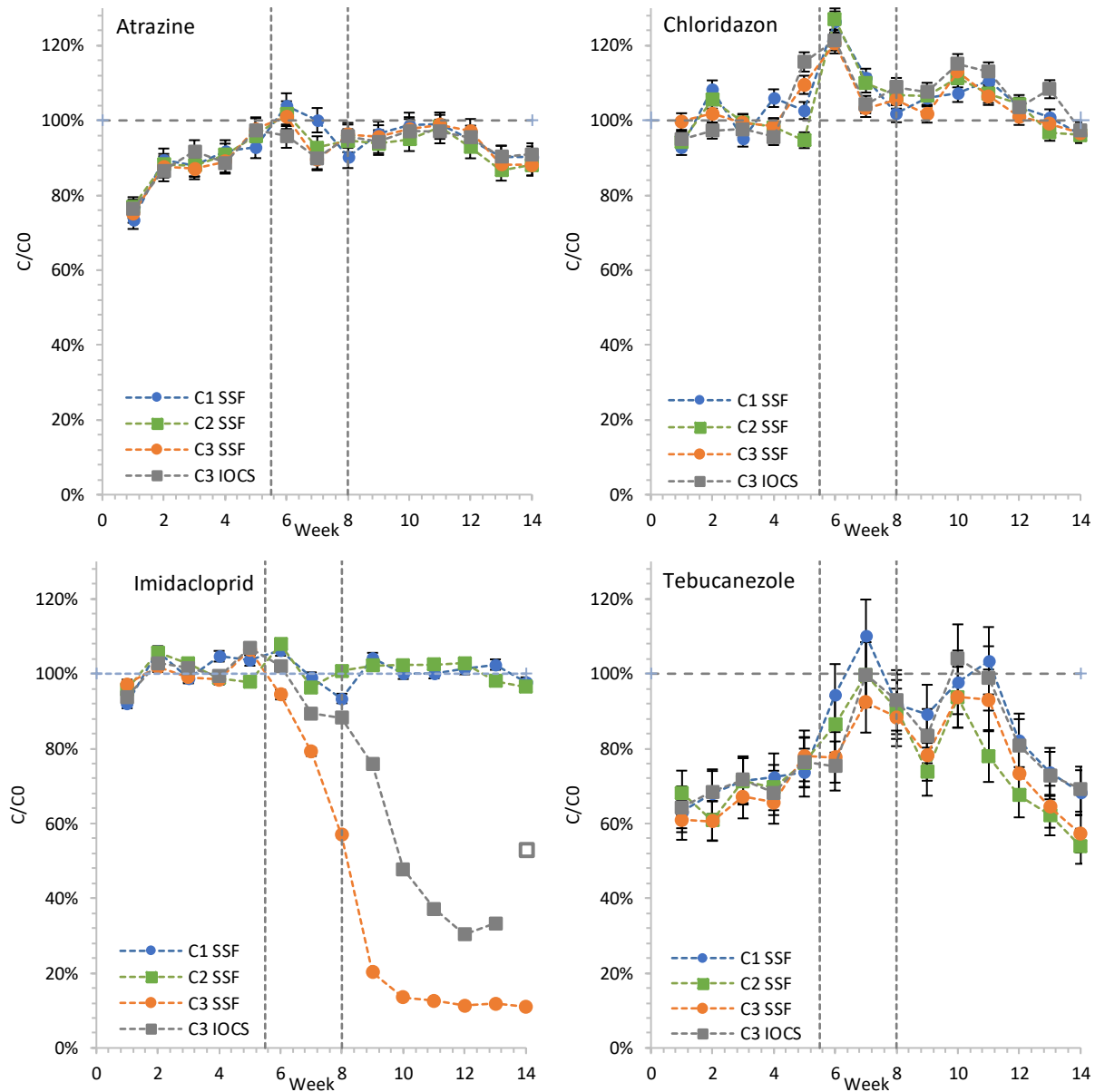


Figure 22A-D Breakthrough curves for the SSF and IOCS layer in each column during the 14-week study. Vertical lines indicate the start and end of weekly flushing. Error bars indicate variance between influent measurements (Table 23).

Pesticide adsorption over the GAC layer shows that the addition of the IOCS layer in C#3-GAC-E-IOCS increased adsorption of all compounds onto the GAC-E versus the otherwise identical C#2-GAC-E column (Figure 23). This is a result of the lower concentration in NOM-UV254 (Table 22) and lower overall pesticide competition due to the high removal of Imidacloprid in the IOCS layer (Figure 22C). Chloridazon shows the least difference between all compounds, as it had the highest adsorption of all compounds tested in the isotherm studies, it is likely influenced less by the difference in competition. This is the first material that has been found to augment the SSF-GAC sandwich filter's performance for pesticide removal (Li, Campos, Zhang, & Xie, 2022).

The low difference in C/C0 percentage removal of Imidacloprid despite the large concentration difference (10 vs 1 µg/L) between the influent of the GAC layers for the two columns (C#3-GAC-E-IOCS vs C#2-GAC-E) from week 10 onwards (Figure 22) indicate that the mass transfer zone is the limiting factor in this study and also explains why the breakthrough curves show a linear increase over time. This is likely due to the small scale of the columns and associated wall effects and preferential flow paths mentioned earlier as a result of the gas entrapment, both reducing the effective EBCT. Longer EBCT or deeper GAC beds would be advised in future studies to get a more accurate sorption profile.

When comparing removal between the two different carbon types it can be seen that C#2-GAC-E outperforms C#1-GAC-N (Figure 23), as predicted by the isotherm experiments. The difference is largest for Atrazine and decreases in the same order as found with the isotherm experiments (Figure 11), where the type of bonding appeared to be the determining factor in total sorption capacity. At the end of the columns study, C2#-GAC-E had sorbed 56% more Atrazine then C#1-GAC-N while showing a significant lower breakthrough (~26% vs ~60%) (Table 24). However, when taking the difference in density between GAC-N (250 kg/m³) and GAC-E (500 kg/m³) into account, it can be seen that the Norit had the highest pesticide sorption per gram of GAC. This contrasts with the isotherm studies, where Norit showed lower total sorption capacity and affinity for all compounds. The difference could be attributed to the too-short EBCT, as both GACs might have different kinetics. If Norit has higher kinetics, it could explain the higher overall sorption in combination with the lower total sorption capacity observed in the column experiments. It is recommended that kinetic experiments are performed in future studies to verify this.

Table 24 Mass pesticide removed in each GAC layer, both absolute and per gram of GAC used. Note that the majority of Imidacloprid is removed in the IOCS layer, resulting in a low total loading.

pesticide removed		Atrazine	Chloridazon	Imidacloprid	Tebuconazole
C#1-GAC-N	µg	779,79	1055,31	1046,39	913,73
C2#-GAC-E	µg	1217,64	1264,52	1312,37	1007,61
C#3-GAC-E-IOCS	µg	1311,88	1273,76	821,03	1077,96
pesticide removed /g GAC		Atrazine	Chloridazon	Imidacloprid	Tebuconazole
C#1-GAC-N	µg/g	245,99	332,91	330,09	288,24
C2#-GAC-E	µg/g	208,50	216,53	224,72	172,54
C#3-GAC-E-IOCS	µg/g	238,52	231,59	149,28	195,99
Breakthrough		Atrazine	Chloridazon	Imidacloprid	Tebuconazole
C#1-GAC-N	%	60,39%	30,27%	31,89%	39,29%
C2#-GAC-E	%	25,87%	7,29%	8,01%	25,25%
C#3-GAC-E-IOCS	%	25,26%	8,07%	11,57%	21,38%

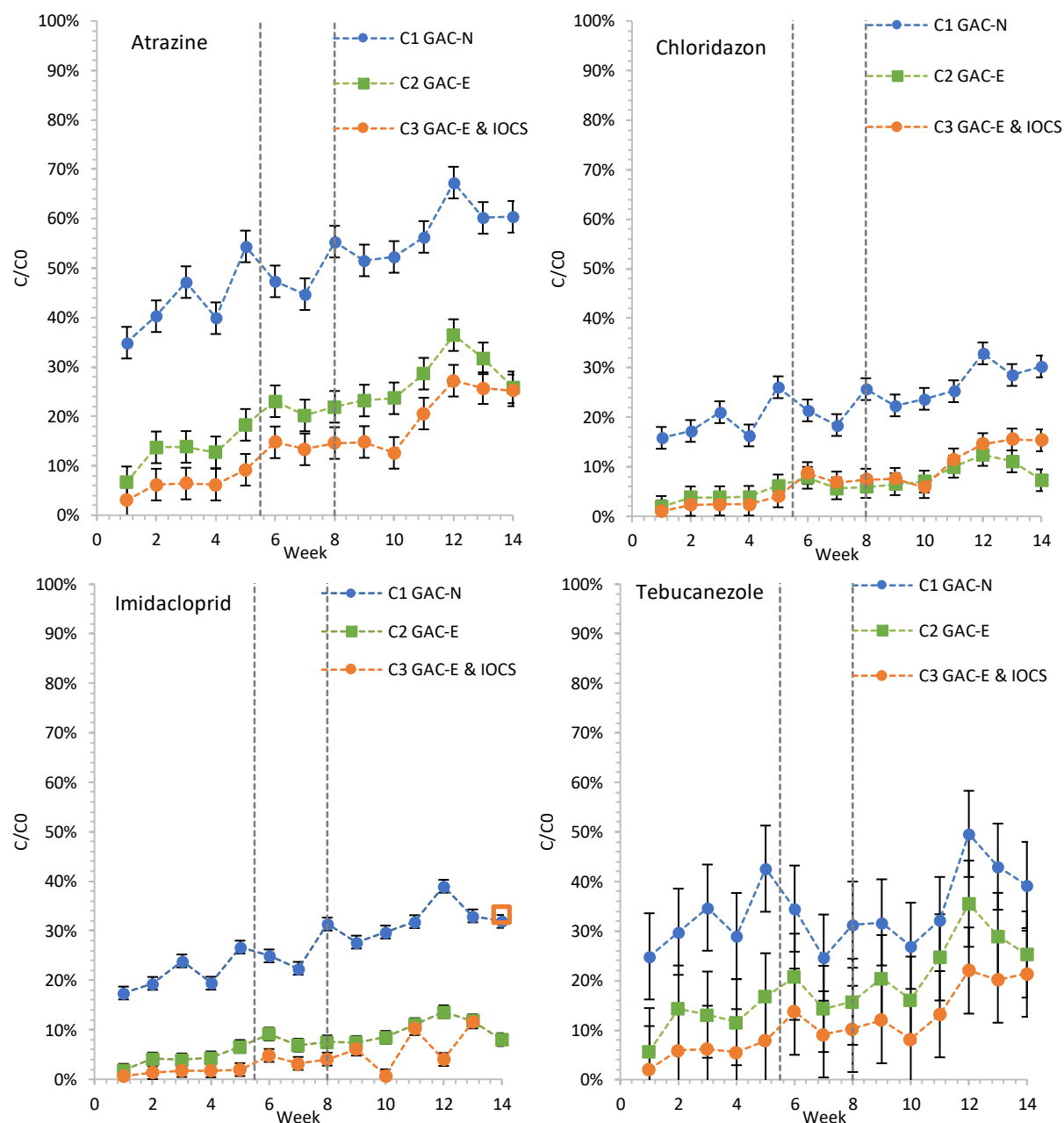


Figure 23A-D Breakthrough curves for the GAC layers in each column during the 14-week study. Vertical lines indicate the start and end of weekly flushing. Error bars indicate variance between influent measurements (Table 25).

Combining the pesticide removal in the IOCC-SSF and GAC layers provides the full overview of the workings of each lab scale column (Figure 24). The (IOCS)-SSF-GAC filters were all successful in the removal of pesticides from the influent water, with large differences between the timing of breakthrough between the compounds. The difference between C#2-GAC-E & C#1-GAC-N originates from the difference in carbon type, as the SSF layers in both columns show similar removal rates for all compounds (Figure 22). The addition of the IOCS layer in C#3-GAC-E-IOCS primarily increases the removal of Imidacloprid. The removal of the other compounds is increased due to the lower NOM loading (Figure 18) and lower overall pesticide loading due to the lower Imidacloprid influent concentrations (Figure 22). This translates in

slower breakthrough for all compounds and a higher total overall removal of the Atrazine, Chloridazon, and Tebuconazole by the C#-GAC-E layer compared to the C#2-GAC-E layer.

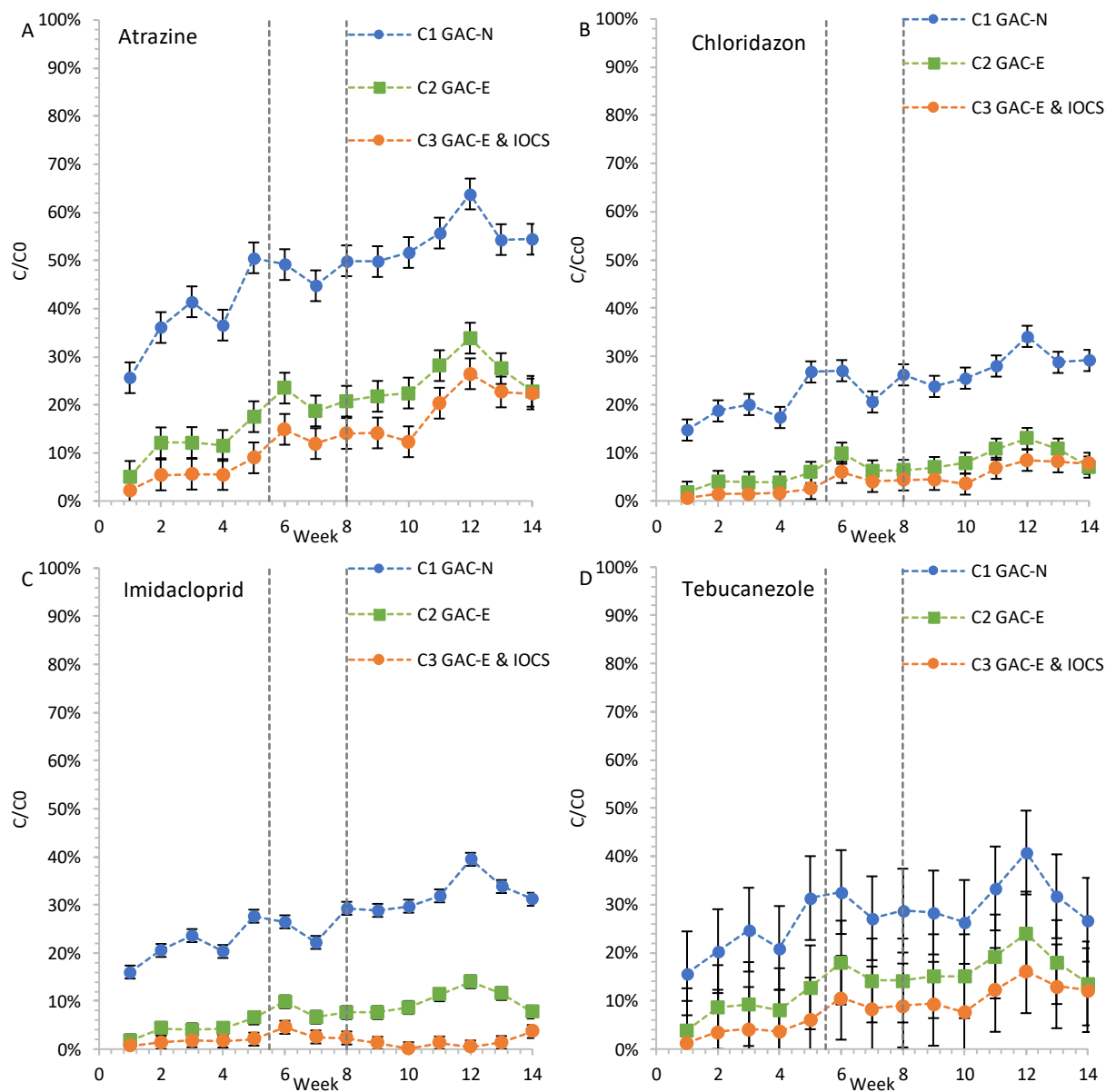


Figure 24 A-D Breakthrough curves for each column during the 14-week study. Vertical lines indicate the start and end of weekly flushing. Error bars indicate variance between influent measurements (Table 26).

It was not possible to model the total sorption capacity of the combined SSF-GAC-IOCS filters as the reduction in EBCT/Mass transfer zone resulted in the pesticides being pushed through the GAC layers too fast for the kinetics to reach equilibrium, the resulting linear breakthrough curves do not allow for conventional methods to calculate the total sorption capacity (Geankoplis, 1993). Conventional calculations will greatly underestimate the column's adsorption capacity as the column showed breakthrough from week 1 onwards. Furthermore, it is unclear if the suspected biodegradation has reached its peak contribution as the contribution of biomass appears to be significant for Tebuconazole and most notably Imidacloprid (Figure 22). These issues could be resolved by using wider columns with deeper GAC beds in combination with long-term experiments to obtain full breakthrough curves. By running long term experiments, the final contribution of biodegradation can be determined.

However, not all is lost. Of the two carbon types, GAC-E shows higher adsorption, in line with the isotherm experiments. The increase in pesticide removal due to the addition of the IOCS layer is clearly visible and highly recommended for further study and/or implementation in field tests. The pilots in Texel and Boskoop would benefit most from the use of GAC-E over GAC-N, the augmentation of the existing filters with IOCS would be beneficial for phosphate, NOM, and most importantly, pesticide removal. The augmentation of the lab scale SSF-GAC filter with an IOCS layer resulted in almost 90% reduction in the GAC influent concentrations for Imidacloprid, significantly lowering the overall pesticide load and extending filter lifetime. It is currently unclear whether the increased removal by IOCS is constrained to Imidacloprid or can be similarly obtained with other compounds found in TDW, for which additional research would be warranted.

6. Conclusion and Recommendations

The results of this study show that a lab scale SSF-GAC sandwich filter augmented with an IOCS layer has higher removal of pesticides, NOM, and phosphate in synthetic tile drainage water, leading to improved bed life versus a regular SSF-GAC filter. From the 5 pesticides used (Atrazine, Bentazone, Chloridazon, Imidacloprid and Tebuconazole), Bentazone was the only component that showed weak adsorption to the point that it did not yield suitable isotherm data. The column study showed a rapid initial breakthrough (20 - 50%) and quickly reached 100% breakthrough for GAC-N after 10 weeks. For GAC-E, the breakthrough reached a plateau at 80% after 11 weeks. This is compared to other compounds, which showed 10 - 30% breakthrough at the end of the 14-week study. Bentazone was the only charged compound used in the experiments. It is unknown if the weak adsorption is related to Bentazone alone or to it being a charged compound. More research is needed to confirm this as it could indicate that the pilots that currently employ both GAC-E and GAC-N can suffer from a rapid breakthrough of charged compounds.

Two different GAC types, one mesoporous (GAC-E) and one microporous (GAC-N), both employed in the pilot in Texel and used to investigate the influence of pesticide adsorption onto GAC in high nutrient, high NOM TDW. The isotherm results showed Freundlich-type adsorption with a higher affinity and total adsorption capacity ($\mu\text{g}/\text{mg}$) for GAC-E versus GAC-N, while the adsorption of NOM was equal for both GAC types in an identical water matrix. The adsorption of pesticides appeared to be dependent on the type of bonding between the GAC surface functional groups and pesticide molecules (Figure 11). Isotherm experiments examining the impact of different water matrices on GAC-N showed that an increase of TOC from 13.85 mg/L to 23.35 mg/L more than doubled (+117%) the TOC uptake by the GAC-N. An increase of the ionic strength from 9.38 mmol/L to 27.46 mmol/L resulted in a 17x higher uptake of ions in terms of mg/L. The increase in NOM and ionic strength resulted in decreasing Freundlich parameters, but much less pronounced than the difference in carbon type did (Figure 12). As such, it was determined that matching the surface functional groups of the GAC to the molecular bonding of the target pollutants molecules played a larger role in the filter performance than the influence of the water matrix composition for pesticide removal in this setting.

The column experiments used similar bed volumes for all layers of the SSF and GAC columns and were set up to investigate the performance of the GAC in SSF-GAC sandwich filters. Additionally, a separate sandwich filter was augmented with an IOCS layer to investigate the influence of the top-up layer. During the experiments, GAC-N showed faster breakthrough and lower overall pesticide sorption versus GAC-E. However, compensated for the difference in density between the two carbon types, GAC-N ($\rho = 250\text{kg}/\text{m}^3$) showed higher loading per gram GAC for all compounds versus GAC-E ($\rho = 500\text{kg}/\text{m}^3$) (Table 24), which contradicted the earlier isotherm experiments. The columns suffered from gas entrapment between GAC grains in combination with wall effects due to the small column diameter in correlation to the large GAC grain diameter, resulting in a reduced EBCT & mass transfer zone. It is theorized that the decrease in EBCT resulted in a mass transfer zone that was too short for the pesticides to reach equilibrium, as indicated by the equal percentage removal of imidacloprid despite a logarithmic order difference in influent concentration between columns (Figure 23C). If the kinetics for pesticide adsorption onto GAC-N are faster than GAC-E, it could explain the higher total GAC-N loading. Kinetic

experiments using the GACs could confirm this theory. Future column studies are advised to operate with wider diameters and deeper beds to prevent wall effects with the large-grained GACs. The downside of this is that it will lead to longer operating times before a breakthrough occurs. The columns were run in an upflow to prevent gas entrapment, but downflow should be investigated to see if it suffers less from gas entrapment.

Phosphate isotherm results showed Freundlich type adsorption, from which HSDM modelling showed that if 10 ton IOCS would be used on Texel it could treat 23.500m³ of water assuming 10m³/h containing 5 mg PO₄³⁻ /L at 55 minutes EBCT before effluent concentration would exceed the legal limit (Omgevingswet, 2024). However, the column experiments have shown that breakthrough occurred faster than expected (week 2 vs prediction of 4 - 11) , despite losing sorption capacity slower than expected. The breakthrough curve could not be reproduced by adjusting the parameters of the model. Literature suggests that reducing the EBCT further can significantly postpone the initial breakthrough, which is recommended for further studies (Zhang, Wang, Lakho, Yang, & Depuydt, 2022). The IOCS removed 12.6 mg PO₄³⁻ /g IOCS at 55 mins EBCT showing 50% breakthrough at the end of the study.

The removal of NOM was higher for the IOCS layer compared to the SSF layers (10 % vs 5 %), resulting in higher uptake of pesticides in the GAC layer due to lower NOM loading. Additionally, the NOM removal (measured by UV254) in the GAC layer following the IOCS-containing column was higher compared to the non-IOCS columns, despite having lower NOM influent concentrations (Figure 23). This synergy has not been identified before and warrants further research. The isotherm experiments found that pre-loaded NOM was selectively displaced from the IOCS due to the adsorption of phosphate, yet this was not observed from the UV254 data during the column experiments.

After 6 weeks until the conclusion of the experiments (week 14), the IOCS showed continuous increasing removal of the pesticides Chloridazon (up to 25 %) , Tebuconazole (up to 40 %) and Imidacloprid (up to 70 %), which was suspected to originate from biodegradation by the growing biomass. Chloridazon and Tebuconazole were also removed in the SSFs of the other two columns, yet the IOCS was the only substrate that showed initial Imidacloprid removal (Figure 22). After a small delay, the SSF following the IOCS layer began showing Imidacloprid removal (up to 70%) and was suspected to have been inoculated with washed-out biomass from the IOCS column. The increased removal of Imidacloprid by the IOCS/SSF remained constrained to the column set containing IOCS, indicating that the IOCS is a suitable substrate that allows for the cultivation of the imidacloprid-degrading biomass while standalone SSF is not. The combined removal of Imidacloprid from the influent by the IOCS-SSF was 90%, which has to the author's knowledge has not been seen before with IOCS and/or SSF to date. While the biodegradation of these compounds has been mentioned in literature, to the author's knowledge, there have not been studies that have obtained such high removal rates at these concentrations and short EBCT (Badawi, Rosenbom, Jensen, & Sørensen, 2016; Escolà Casas & Bester, 2015; Chen, et al., 2024; Timmers, Siegers, Ferreira, Lousada, & van der Wielen, 2024; Wang, et al., 2022). Biodegradation of OMPs had earlier been proven in SSF-GAC sandwich filters by other researchers, yet they required EBCT of 10 hours with a rapid decline in performance if this was reduced to 5 hours, far exceeding EBCT used in this study (Li, Zhuo, & Campos, 2018; Li, Campos, Zhang, & Xie, 2022; Xu, Campos, Li, Karu, & Ciric, 2021).

The reduction in NOM and Imidacloprid loading due to the IOCS layer resulted in an 8-10 % increase in pesticide removal vs an otherwise identical SSF-GAC-E column without the IOCS layer, indicating that the augmentation of SSF-GAC filters with an IOCS layer increases the filters' bed life and sorption capacity. Longer duration experiments are recommended to further investigate the driving mechanisms of pesticide removal by IOCS and to determine whether removal is constrained to Imidacloprid or whether other OMPs can show such high removal rates. Additionally, it is recommended that the suspected inoculation of the SSF with Imidacloprid degradation biomass from the IOCS is investigated and confirmed.

Modelling the expected pesticide breakthrough with fixed bed simulation tools using HSDM models proved to be a challenge due to missing pore diffusion parameters. In addition to this, the earlier mentioned reduction of EBCT and mass transfer zone resulted in linear breakthrough curves as the mass transfer zone was too short to reach equilibrium during column adsorption. As such, it is not possible to make accurate predictions on the expected lifetime of the pilots currently in operation. However, this research shows that tailoring the GAC surface chemistry to the targeted pollutants resulted in higher adsorption than the differences in GAC pore structure. Increasing NOM and ionic strength decreased the carbons' sorption capacity, yet the difference was significantly smaller than the difference in performance between the two carbon types. From this research, it is recommended to use GAC-E over GAC-N in the pilots, as its surface chemistry showed higher affinity and sorption capacity for the pesticides investigated. Biodegradation appears to play a large role in the removal of pesticides in high nutrient, high NOM containing waters and warrants further research. The combined increase in removal of phosphate, NOM, and pesticides by IOCS makes it a suitable material to employ as a top-up layer in the treatment of TDW using sandwich filters, for which its implementation is recommended to investigate its performance in new or existing field scale pilots.

Bibliography

(n.d.). Retrieved from <http://www.fast-software.de/>.

Calgon Carbon Corporation. (2024, 5 7). *Data Sheet Filtrasorb 300*. Retrieved from Calgon Carbon: <https://www.calgoncarbon.com/app/uploads/DS-FILTRA30018-EIN-E1.pdf>

Abdelkader, O., & Youcef, L. (2016). Phosphates Removal by Activated Carbon. *Sensor letters*, 1-6.

Agboeze, E., & Chime, C. (2022). KINETIC AND EQUILIBRIUM ISOTHERM OF PESTICIDES (ATRAZINE) ADSORPTION UNTO ACTIVATED CARBON OF CALABASH (LAGENARIA SICERARIA). *EPRA International Journal of Multidisciplinary Research*, 1-16. doi:10.36713/epra10877

Ahn, Y. C. (2015.). Removal of Iopromide and its Intermediates from Ozone-Treated Water Using Granular Activated Carbon.

Aislabie, J., & Lloyd-Jones, G. (1995). A review of bacterial degradation of pesticides. *Australian Journal of Soil Research*, 925-942.

Alberghina, G., Bianchini, R., Fichera, M., & Fisichella, S. (2000). Dimerization of Cibacron Blue F3GA and other dyes: influence of salts and temperature. *Dyes and Pigments*, 129-137.

Aldoury, M. M. (2017). *Removal of heavy metals from liquid waste using granular activated carbon*. lab lambert academic publishing.

Arora, H. (2017). *Optimising the Ripening Period of Slow sand filters*. TuDelft.

Baccar, R., Blázquez, P., Bouzid, J., Feki, M., & Sarrà, M. (2010). Equilibrium, thermodynamic and kinetic studies on adsorption of commercial dye by activated carbon derived from olive-waste cakes. *Chemical Engineering Journal*.

Badawi, N., Rosenbom, A. E., Jensen, A. M., & Sørensen, S. R. (2016). Degradation and sorption of the fungicide tebuconazole in soils from golf greens. *Environmental Pollution*, 368-378. doi:<https://doi.org/10.1016/j.envpol.2016.10.045>

Baldauf, G., & Zimmer, G. (1986). Adsorptive Entfernung leichtfluchtiger Halogenkohlenwasserstoffe bei der Wasseraufbereitung. *Vom wasser*.

Bansal, R. C., & Goyal, M. (2005). *Activated Carbon Adsorption*. Taylor & Francis.

Barrett, M., Bryck, J., Collins, M., Janonis, B., & Logsdon, G. (1991). *Manual of Design for Slow sand Filtration*. American Water Works Association.

Bauer, M., Buchanan, B., Colbourne, J., Foster, D., Goodman, N., Kay, A., . . . Sanders, T. (1996). The GAC/Slow sand filter sandwich - from concept to commissioning. *Water Supply*, 14, 159-175.

- Bedrijfstechnische parameters*. (2024, September 25). Retrieved from Dunea:
<https://www.dunea.nl/drinkwater/waterkwaliteit-en-samenstelling/verschillende-normen/bedrijfstechnische-parameters>
- Bellamy, W., Silverman, G., Hendricks, D., & Logsdon, G. (1985a). Removing Giardia cysts with slow sand filtration. *Journal American Water Works Association*, 52-60.
- Bellamy, W., Hendricks, D., & Logsdon, G. (1985b). Slow sand filtration: influences of selected process variables. *Journal American Water Works Association*, 62-66.
- Benmahdi, F. S., Haddad, D., Mandin, P., Kolli, M., & Bouhelassa, M. (2018). Breakthrough Curves Analysis and Statistical Design of Phenol Adsorption on Activated Carbon. *Chemical Engineering Technology*.
- Benstöm, F., Nahrstedt, A., Böhler, M., Knopp, G., Montag, D., Siegrist, H., & Pinnekamp, J. (2017). Performance of granular activated carbon to remove micropollutants from municipal wastewater—a meta-analysis of pilot- and large-scale studies. *Chemosphere*, 105-118.
- Bertelkamp, C., Reungoat, J., Cornelissen, E., Singhal, N., Reynisson, J., Cabo, A., . . . Verliefde, A. (2014). Sorption and biodegradation of organic micropollutants during river bank filtration: A laboratory column study. *Water Research*, 231-241.
- Bijlage XIX Besluit kwaliteit leefomgeving*. (2024, June 13). Retrieved from Overheid.nl:
<https://wetten.overheid.nl/jci1.3:c:BWBR0041313&bijlage=XIX&z=2024-01-01&g=2024-01-01>
- Boeckaert, C. (2023, July 05). *The regeneration of P-loaded iron coated sand*. Retrieved from northsearegion: <https://northsearegion.eu/nuredrain/news/the-regeneration-of-p-loaded-iron-coated-sand/>
- Borrull, J., Colom, A., Fabregas, J., Borrull, F., & Pocurull, E. (2021, August). Presence, behaviour and removal of selected organic micropollutants through drinking water treatment. *Chemosphere*, 276.
- Brown, J. C., & Lauderdale, C. V. (2006). Efficient, simultaneous destruction of multiple Drinking Water Contaminants Using Biological Filtration. *Florida Water Resources Journal*, 28-30.
- Burkhardt, J. (2025, January 7). *Environmental-Technologies-Design-Option-Tool*. Retrieved from Github:
<https://github.com/USEPA/Environmental-Technologies-Design-Option-Tool>
- Cabot. (2024, 5 7). *NORIT® PK 1-3 Datasheet*. Retrieved from Labshop: <https://www.labshop.nl/wp-content/uploads/2019/12/O160-TDS.Norit-PK-1-3-Cabot-Norit.pdf>
- Calgon Carbon. (2022). *Start-up and conditioning instructions*. Calgon Carbon. Retrieved from
https://www.calgoncarbon.com/app/uploads/DataSheet_StartUpConditioningInstructions_FINAL_102822-1.pdf

- Calgon Carbon Corporation. (2024, 5 7). *Data Sheet FILTRASORB® 400*. Retrieved from calgon carbon: <https://www.calgoncarbon.com/app/uploads/DS-FILTRA40018-EIN-E1.pdf>
- Campos, L., Su, M., Graham, N., & Smith, S. (2002). Biomass development in slow sand filters. *Water Research*, 4543-4551.
- Carlson, G., & Silverstein, J. (1998). Effect of molecular size and charge on biofilm sorption. *Water Res*, 1580–92.
- Chan, S., Pullerits, K., Riechelmann, J., Persson, K., Rådstrom, P., & Paul, C. (2018). Monitoring biofilm function in new and matured full-scale slow sand filters using flow cytometric histogram image comparison. *Water Research*, 27-36.
- Chen, L., Zhai, Y., van der Mark, E., Liu, G., van der Meer, W., & Medema, G. (2021). Microbial community assembly and metabolic function in top layers of slow sand filters for drinking water production. *Journal of Cleaner Production*.
- Chen, Y., Hajslova, J., Schusterova, D., Uttl, L., Vymazal, J., & Chen, Z. (2024). Transformation and degradation of tebuconazole and its metabolites in constructed wetlands with arbuscular mycorrhizal fungi colonization. *Water Research*. doi:<https://doi.org/10.1016/j.watres.2024.122129>
- Chowdhury, I., Rohan, M., Stodart, B., Chen, C., Wu, H., & Doran, G. (2021). *Persistence of atrazine and trifluralin in a clay loam soil undergoing different temperature and moisture conditions*. Environ. Pollut.
- Clements, M., & Haarhoff, J. (2004). *Practical experiences with granular activated carbon (GAC) at the Rietvlei Water Treatment Plant*. Water SA.
- Collins, M. R., Eighmy, T. T., & Fenstermacher, J. M. (1992). Removing Natural Organic Matter by Conventional Slow Sand Filtration. *American Water Works Association*, 80-90.
- Crittenden, J. C., Rhodes Trussell, R., Hand, D. W., Howe, K. J., & Tchobanoglous, G. (2022). *Stantec's Water Treatment: Principles and Design*. John Wiley & Sons.
- Cullen, T. R., & Letterman, R. D. (1985). The Effect of Slow Sand Filter Maintenance on Water Quality. *American Water Works Associatiom*, 48-55.
- Cycoń, M., & Piotrowska-Seget, Z. (2006). Transformations of pesticides in soil environment - a review. *Pestycydy*.
- D'Alessio, M., Yoneyama, B., Kirs, M., Kisand, V., & Ray, C. (2015). Pharmaceutically active compounds: Their removal during slow sand filtration and their impact on slow sand filtration bacterial removal. *Science of the Total Environment*, 124-135.

- De Ridder, D., . Verliefde, A., Heijman, S., . Verberk, J., Rietveld, L., Van Der Aa, L., . . . Amy, J. (2011). Influence of Natural Organic Matter on Equilibrium Adsorption of Neutral and Charged Pharmaceuticals onto Activated Carbon 416–423. *Water Science & Technology*, 416-423.
- Dimitrios G. Karpouzas, A. F.-S. (2005). Non-specific biodegradation of the organophosphorus pesticides, cadusafos and ethoprophos, by two bacterial isolates . *FEMS Microbiology Ecology*, 369-378.
- Ding, C., & Shang, C. (2010). Mechanisms controlling adsorption of natural organic matter. *Water Research*, 3651-3658.
- Dinga, C., Yana, X., Liu, W., Chang, Y., & Shang, C. (2010). Removal of natural organic matter using surfactant-modified iron. *Journal of Hazardous Materials*, 567-572.
- Dong, L., Hou, L., Wang, Z., Gu, P., Chen, G., & Jiang, R. (2018). A new function of spent activated carbon in BAC process: removing heavy metals by ion exchange mechanism. *Hazard Mater*, 76-84.
- Dussert, B. W., & Van Stone, G. R. (1994). The biological activated carbon process for water purification. *Water Eng. Manag.*, 22.
- Edgar, M., Hamdan, N., Morales, D., & Boyer, T. H. (2022). Phosphorus removal by steel slag from tile drainage water: Lab and field evaluations. *Chemosphere*.
- Escolà Casas, M., & Bester, K. (2015). Can those organic micro-pollutants that are recalcitrant in activated sludge treatment be removed from wastewater by biofilm reactors (slow sand filters)? *Science of The Total Environment*, 315-322. doi:<https://doi.org/10.1016/j.scitotenv.2014.10.113>
- EVERS GmbH & Co. KG. (2024, 5 7). *Eversrob*. Retrieved from Evers: <https://www.evers.de/en/products/everzitr-filter-materials/adsorption/eversorb>
- FAST. (2024, 9 6). Retrieved from <http://www.fast-software.de/>: <http://www.fast-software.de/>
- Frank, J., Ruhl, A. S., & Jekel, M. (2015). Impacts of backwashing on granular activated carbon filters for advanced wastewater treatment. *Water Research*, 166-174.
- Fu, J., Lee, W.-N., Coleman, C., Nowack, K., Carter, J., & Huang, C.-H. (2019). Removal of pharmaceuticals and personal care products by two-stage biofiltration for drinking water treatment. *Science of The Total Environment*, 240-248.
- Fundneider, T., Acevedo Alonso, V., Abbt-Braun, G., Wick, A., Albrecht, D., & Lackner, S. (2021). Empty bed contact time: The key for micropollutant removal in activated carbon filters. *Water Research*.
- Gangola, S., Bhatt, P., Kumar, A. J., Bhandari, G., Joshi, S., Punetha, A., . . . Rene, E. R. (2022, June). Biotechnological tools to elucidate the mechanism of pesticide degradation in the environment. *Chemosphere*, 296.

- Gao, Y., Yue, Q., Gao, B., & Li, A. (2020). Insight into activated carbon from different kinds of chemical activating agents: A review. *Science of The Total Environment*.
- Geankoplis, C. (1993). *Transport Processes and Unit Operation* (3 ed.). New Jersey: PTR Prentice Hall.
- Germán-Heins, J., & Flury, M. (2000). Sorption of Brilliant Blue FCF in soils as affected by pH and ionic strength. *Geoderma*, 87-101.
- Gijn, K. v., Chen, Y., van Oudheusden, B., Gong, S., de wilt, H., Rijnaarts, H., & Langenhoff, A. (2021). Optimizing biological effluent organic matter removal for subsequent. *Journal of Environmental Chemical Engineering*.
- Gimbel, R., Graham, N., & Collins, M. R. (2006). Dissolved oxygen issues with granular activated carbon sandwich (TM) slow sand filtration. In R. Gimbel, N. J. Graham, & M. R. Collins, *Recent Progress in Slow Sand and Alternative Biofiltration Processes*. IWA Publishing.
- Ginn, T. J., Amirtharajah, A., & Karr, P. (1992). Effect of particle detachment in granular-media filtration. *American Water Works*, 84-86.
- Goux, S. J., Ibanez, M., Van Hoorick, M., Debongnie, P., Agathos, S. N., & Pussemier, L. (2000). Biodegradation of atrazine in sand sediments and in a sand-filter. *Applied Microbiology and Biotechnology*, 589-595.
- Guo, Y., Askari, N., Smets, I., & Appels, L. (2024). A review on co-metabolic degradation of organic micropollutants during anaerobic digestion: Linkages between functional groups and digestion stages. *Water Research*.
- Halle, C., Huck, P. M., & Peldszus, S. (2015). Emerging Contaminant Removal by Biofiltration: Temperature, Concentration, and EBCT Impacts. *American Water Works Association*.
- Hedegaard, M. J., & Albrechtsen, H.-J. (2014). Microbial pesticide removal in rapid sand filters for drinking water treatment – Potential and kinetics. *Water Research*.
- Hejazifar, M., Azizian, S., Sarikhani, H., Li, Q., & Zhao, D. (2011). Microwave assisted preparation of efficient activated carbon from grapevine rhytidome for the removal of methyl violet from aqueous solution. *Anal. Appl. Pyrolysis*, 258-266.
- Heo, J.-H., Lee, D.-H., Koh, D.-C., & Chang, H.-W. (2007). The effect of ionic strength and hardness of trichloroethylene-contaminated synthetic groundwater on remediation using granular activated carbon. *Geosciences Journal*, 229-239.
- Huisman, L. (1974). *Slow sand filtration*. Geneva: WHO.
- Jegatheesan, V., & Vigneswaran, S. (2009). Deep Bed Filtration: Mathematical Models and Observations. *Environmental Science and Technology*.

- Jennings, S., & Krueger, J. (n.d.). *Clean Tailing Reclamation: Tailing Reprocessing for Sulfide Removal and Vegetation Establishment*.
- Jeuken, A., van Beek, E., van Duinen, R., van der Veen, A., Bocalon, A. J., Pieter, S., . . . Paalman, M. (2012). *Balancing supply and demand of fresh water under increasing drought and Salinisation in the Netherlands*. Kennis voor Klimaat.
- K. Yapsakli, F. Ç. (2010). Effect of type of granular activated carbon on DOC biodegradation in biological activated carbon filters. *Process Biochem.*, 355-362.
- Kalam, S., Abu-Khamsin, S. A., Kamal, M. S., & Patil, S. (2021). Surfactant Adsorption Isotherms: A Review. *American Chemical Society*.
- Kalkan, Ç., Yapsakli, K., Mertoglu, B., Tufan, D., & Saatci, A. (2011). Evaluation of Biological Activated Carbon (BAC) process in wastewater treatment secondary effluent for reclamation purposes. *Desalination*, 266-273.
- Koffsky, W., & Lykins, B. (1999). Disinfection/disinfectant by-product optimisation with ozone, biological filtration and chloramines. *Journal of Water Supply: Research and Technology*, 92-105.
- Korotta-Gamage, & Shashika Madushi Sathasivan, A. (2017). A review: Potential and challenges of biologically activated carbon to remove natural organic matter in drinking water purification process. *Chemosphere*, 120-138.
- Korshin, G. V., Benjamin, M. M., & Sletten, R. S. (1997). Adsorption of Natural organic Matter (NOM) on Iron Oxide: effects on NOM composition and formation of Organo-Halide compounds during chlorination. *Water Research*, 1643-1650.
- Krijn, J. (2021). *Smaller faster better; investigating grain size dependent pollutant removal on granular activated carbon*. TuDelft.
- Kruisdijk, E. (2022). *Re-use of drainage water for agriculture Fate of agrochemicals and assessment of well clogging during aquifer storage and*. Tu-Delft.
- Lambert, S., & Graham, N. (1995). Removal of non-specific dissolved organic matter from upland potable water supplies—I. Adsorption. *Water Research*, 2421-2426.
- Langenbach, K., Kusch, P., Horn, H., & Kästner, M. (2009). Slow Sand Filtration of Secondary Clarifier Effluent for Wastewater Reuse. *Environmental Science & Technology*.
- Li, B., Yang, Y., Wu, H., Zhang, C., Zheng, W., & Sun, D. (2020b). Adsorptive removal and mechanism of monocyclic aromatics by activated carbons from water: effects of structure and surface chemistry. *Colloids Surfaces A: Physicochem. Eng. Aspects*.
- Li, J., Campos, L. C., Zhang, L., & Xie, W. (2022). Sand and sand-Gac filtration technologies in removing PPCPs: a Review. *Science of the Total Environment*.

- Li, J., Zhuo, Q., & Campos, L. C. (2018). The application of GAC Sandwich slow sand filtration to remove pharmaceutical and personal care products. *Science of the Total Environment*, 1182-1190.
- Li, L. Q. (2002). Effects of activated carbon surface chemistry and pore structure on the adsorption of organic contaminants from aqueous solution. *Carbon*, 2085-2100.
- Logsdon, G. (1987). Evaluating treatment plants for particulate contaminant removal. *American Water Works Association*, 82-92.
- Logsdon, G. S., Kohne, R., Abel, S., & LaBonde, S. (2002). *Slow sand filtration for small water systems*. NRC Research Press.
- Maliva, R., Guo, W., & T.M., M. (2006). Aquifer Storage and Recovery: Recent Hydrogeological Advances and. *Water Environment Research*, 2428-2435.
- Manocha, S. M. (2003). *Porous carbons*. Department of Materials Science, Sardar Patel University, Vallabh Vidyanagar. Retrieved from <https://www.ias.ac.in/article/fulltext/sadh/028/01-02/0335-0348>
- Masson, S., Gineys, M., Delpeux-Ouldriane, S., Reinert, L., Guittonneau, S., Beguin, F., & Duclaux, L. (2016). Single , binary , and mixture adsorption of nine organic contaminants onto a microporous and a microporous/mesoporous activated carbon cloth. *Microporous Mesoporous Mater*, 23-34.
- McMeen, C. R., & Benjamin, M. M. (1997). NOM Removal by slow sand filtration through iron oxide-coated olivine. *American Water Works Association*.
- Mengxue, L., Jianyong, L., Yunfeng, X., & Guangren, Q. (2016). Phosphate adsorption on metal oxides and metal hydroxides: A comparative review. *Environmental Reviews*, 319-332.
- Micromeritics. (2016, Sept). *Tristar II Plus Surface area and porosity analyser*. Retrieved from [www.micromeritics.com: https://www.micromeritics.com/Repository/Files/Calculations-3030-TriStarII-Plus-v2-x_0.pdf](https://www.micromeritics.com/Repository/Files/Calculations-3030-TriStarII-Plus-v2-x_0.pdf)
- Moll, D. M., & Summers, R. S. (1999). Assessment of drinking water filter microbial communities using taxonomic and metabolic profiles. *Water Science and Technology*, 83-89.
- Nacéra Yeddou, M., & Bensmaili, A. (April 2009). Kinetics and thermodynamic study of phosphate adsorption on iron hydroxide-eggshell waste. *Chemical Engineering Journal* , 147(2-3), 87-96. doi:10.1016/j.cej.2008.06.024
- Nazara, A. S., Kurade, M., Khan, M. A., & Jeon, B.-H. (2022). Effect of humic acid on adsorption of methylparaben from aqueous solutions onto commercially available granular activated carbons. *Chemistry and Chemical Engineering*.

- Newcombe, G., & Drikas, M. (1997). Adsorption of NOM activated carbon: electrostatic and non-electrostatic effects. *Carbon*, 1237-1250.
- Nguyen, D., Tran, H., Juang, R., Dat, N., Tomul, F., Ivanets, A., . . . Chao, H. (2020). Adsorption process and mechanism of acetaminophen onto commercial activated carbon. *Environ. Chem.*
- Omgevingswet (January 1, 2024). Retrieved from <https://wetten.overheid.nl/BWBR0037885/2024-01-01>
- Pallavi, G., & Suresh Kumar, D. (2022). Biodegradation of imidacloprid: Molecular and kinetic analysis. *Bioresource Technology*. doi:<https://doi.org/10.1016/j.biortech.2022.126915>.
- Paredes, L., Fernandez-Fontaina, E., Lema, J., Omil, F., & Carballa, M. (2016). Understanding the fate of organic micropollutants in sand and granular activated carbon biofiltration systems. *Science of The Total Environment*, 640-648.
- Piai, L., Dykstra, J., Adishakti, M., Blokland, M., Langenhoff, A., & van der Wal, A. (2019). Diffusion of hydrophilic organic micropollutants in granular activated. *Water Research*, 518-527.
- Piai, L., Dykstra, J., van der Wal, A., & Langenhoff, A. (2022). Bioaugmentation of Biological Activated Carbon Filters for Enhanced Micropollutant Removal. *ACS ES&T Water*.
- Pöpel, H., Schmidt-Bregas, M., & Wagner, M. (1988). Application of activated carbon in waste water treatment - Part II. *Korrespondenz Abwasser*, 377–379.
- Qi Zhou, X. W. (2012). Phosphorus removal from wastewater using nano-particulates of hydrated ferric oxide doped activated carbon fiber prepared by Sol–Gel method. *Chemical Engineering Journal*, 619-626.
- Riddler, D. J., Verliefde, A. R., Mcconville, M., & Heijman, S. G. (2009). Development of a Predictive Model to Determine Micropollutant Removal using Granular Activated Carbon. *Drinking Water Engineering and Science Discussions*.
- Salomón-Negrete, M., Reynel-Ávila, H., Mendoza-Castillo, D., Bonilla-Petriciolet, A., & Duran-Valle, C. (2018). Water defluoridation with avocado-based adsorbents: synthesis, physicochemical characterization and thermodynamic studies. *Journal of Molecular Liquids*, 188-197.
- Sands, G. R. (2024, 5 7). *How agricultural drainage works*. Retrieved from University of Minisota Extension: <https://extension.umn.edu/agricultural-drainage/how-agricultural-drainage-works>
- Scholz, M., & Martin, R. (1997). Ecological equilibrium on biological activated carbon. *Water Research*, 2959-2968.
- Simpson, D. R. (2008). Biofilm processes in biologically active carbon water purification. *Water Research*, 2839-2848.
- Sontheimer, H. C. (1988). *Activated Carbon for Water Treatment*. Karlsruhe: DVGW-Forschungsstelle am Engler-Bunte-Institut der Universität Karlsruhe.

- Sperlich, A., Schimmelpfennig, S., Baumgarten, B., Genz, A., Amy, G., Worch, E., & Jekel, M. (2008). Predicting anion breakthrough in granular ferric hydroxide (GFH) adsorption filters. *Water Research*, 2073-2082.
- Statista Research. (2023, 3 24). *Agricultural consumption of pesticides worldwide from 1990 to 2020*. Retrieved from Statista: <https://www.statista.com/statistics/1263077/global-pesticide-agricultural-use/>
- Stumm, W., & Morgan, J. (1981). *Aquatic Chemistry: An Introduction Emphasizing Chemical Equilibria in Natural Waters*. New York: Wiley.
- Suresh Kumar, P. (2018). *Phosphate recovery from wastewater via reversible adsorption*. Delft. doi:<https://doi.org/10.4233/uuid:f75d3713-8ef2-4f92-884f-06664b040f47>
- Takeuchi, Y., Mochidzuki, K., Matsunobu, N., Kojima, R., Motohashi, H., & Yoshimoto, S. (1997). Removal of organic substances from water by ozone treatment followed by biological activated carbon treatment. *Water Science and Technology*, 171-178.
- Timmers, P. H., Siegers, W., Ferreira, Lousada, M., & van der Wielen, P. W. (2024). Bioremediation of rapid sand filters for removal of organic micropollutants during drinking water production. *Water Research*. doi:<https://doi.org/10.1016/j.watres.2023.120921>.
- Tiwari, S., Tripathi, P., Mohan, D., & Singh, R. (2023). Imidacloprid biodegradation using novel bacteria *Tepidibacillus decaturensis* strain ST1 in batch and in situ microcosm study. *Environ Sci Pollut Res*. doi:10.1007/s11356-022-24779-8
- Tran, H., Nguyen, H., Woo, S., Nguyen, T., Vigneswaran, S., Hosseini-Bandegharaei, A., . . . Chao, H. (2019). Removal of various contaminants from water by renewable lignocellulose-derived biosorbents: a comprehensive and critical review. *Crit. Rev. Environ. Sci. Technol.*, 2155-2219.
- Trikannad, S. A., van Halem, D., Foppen, J. W., & van der Hoek, J. P. (2023). The contribution of deeper layers in slow sand filters to pathogens removal. *Water Research*.
- Uhl, W. (2000). Biofiltration Processes for Organic Matter Removal. *Biotechnology Set, Second Edition*, 457-478.
- University of Hertfordshire. (2023, March 11). *PPDB: Pesticide Properties DataBase* . Retrieved from <https://sitem.herts.ac.uk/aeru/ppdb/en/index.htm>:
<https://sitem.herts.ac.uk/aeru/ppdb/en/index.htm>
- Valderrama, C., Gamisans, X., de las Heras, X., Farran, A., & Cortina, J. (2008). Sorption kinetics of polycyclic aromatic hydrocarbons removal using granular activated Carbon intraparticle diffusion coefficients. *Journal of Hazardous Materials*, 386-396.

- Vale. (2019, January 27). *Vale Press Releases*. Retrieved from Vale:
<http://www.vale.com/EN/investors/information-market/Press-Releases/Pages/Vale-updates-information-on-the-dam-breach-in-Brumadinho.aspx>
- van Gaalen, F., Franken, R., Kirkels, F., Ibrahim, S. I., van Minnen, J., Bouwman, A., & Vonk, M. (2024). *Klimaatrisico's in Nederland*. Den Haag: Planbureau voor de Leefomgeving .
- Verweij, W., van der Wiele, J., van Moorselaar, I., & van der Grinten, E. (2010). *Impact of climate change on water quality in the*. RIVM.
- Wang, J., de Ridder, D., van der Wal, A., & Sutton, N. B. (2023). Harnessing biodegradation potential of rapid sand filtration for organic micropollutant removal from drinking water: A review. *Critical Reviews in Environmental Science and Technology*, 2086–2118.
doi:<https://doi.org/10.1080/10643389.2020.1771888>
- Wang, J., Zhang, C., A.J. Poursat, B., Ridder, D. d., Smidt, H., van der Wal, A., & Sutton, N. B. (2022). Unravelling the contribution of nitrifying and methanotrophic bacteria to micropollutant co-metabolism in rapid sand filters. *Journal of Hazardous Materials*.
doi:<https://doi.org/10.1016/j.jhazmat.2021.127760>.
- Wang, J., Zhang, C., Poursat, B. A., Ridder, D. d., Smidt, H., Wal, A. v., & Sutton, N. B. (2022). Unravelling the contribution of nitrifying and methanotrophic bacteria to micropollutant co-metabolism in rapid sand filters. *Journal of Hazardous Materials*.
- Weber, W. (2004). Preloading of GAC by natural organic matter in potable water treatment systems: Mechanisms, effects and design considerations. *Journal of Water Supply: Research and Technology*, 469-482.
- Weber-Shirk, M., & I. Dick, R. (1997, Januari). Physical-chemical mechanisms in slow sand filters. *American Water works association Journal*, 89(1).
- Wettenbank. (2023, 4 28). Retrieved from Overheid: <https://wetten.overheid.nl/BWBR0005957/2009-12-22>
- Xu, L., Campos, L. C., Li, J., Karu, K., & Ciric, L. (2021). Removal of antibiotics in sand, GAC, GAC sandwich and anthracite sandbiofiltration systems. *Chemosphere*.
- Xue, W., Wu, C., Xiao, K., Huang, X. Z., Tsuno, H., & Tanaka, H. (2010). Elimination and fate of selected micro-organic pollutants in a full-scale anaerobic/anoxic/aerobic process combined with membrane bioreactor for municipal wastewater reclamation. *Water Research*.
- Yapsakli, K., & Cecen, F. (2010). Effect of type of granular activated carbon on DOC biodegradation. *Process Biochemistry*, 355-362.
- Youcef, L., & Abdelkader, O. (2017). Nitrate Adsorption from Synthetic Solutions Using Granular Activated Carbon. *Materials Focus*, 525-530.

- Zenga, L., Lia, X., & Liub, J. (2004). Adsorptive removal of phosphate from aqueous solutions using iron oxide tailings. *Water Research*, 1318-1326.
- Zhang, R., Wang, L., Lakho, F. H., Yang, X., & Depuydt, V. (2022, Februari). Iron oxide coated sand (IOS): Scale-up analysis and full-scale application for phosphorus removal from goat farm wastewater. *Separation and Purification Technology*, 284.

Appendix 1 MSDS GAC

EVERSORB 520 – EN 12915

Technical data sheet 03/2020

Page 2 / 2



Physical and chemical characteristics

Appearance	Granular carbon
Grain size	0,5 – 2,5 mm (8x35 Mesh)
Bulk density (backwashed and drained)	500 ± 25 kg/m³
Water content, as packed	< 5 %
Ash content	< 5 %
Iodine no.	> 1050 mg/g
Specific surface area (BET)	approx. 1100 m²/g
Ball-pan hardness	> 97 %

Packaging and delivery

EVERSORB activated carbon is supplied in:

- 25 kg bag
- 500 kg Big Bag
- Bulk transport in silo trucks

Note

The information given in this technical data sheet is accurately put together, revised and updated if required. However, we cannot be held responsible for this information as being up-to-date, exact and complete. Apart from that, this information cannot replace a personal consultation in the specific case.



EVERS GmbH & Co. KG
WATER TECHNOLOGY and ANTHRACITE REFINING
Rheiner Str. 14a · 48496 Hopsten Germany
Tel.: +49 5458 9307-0 · Fax: +49 5458 9307-40
Email: info@evers.de · Internet: www.evers.de



NORIT® PK 1-3 M

Granular Activated Carbon

WHY CABOT

Cabot Norit Activated Carbon is a premier activated carbon manufacturer respected for experienced people, diverse products and strong customer relationships. Cabot's history of innovation, product performance, technical expertise and customer focus ensure that you receive the right products and solutions for your specific purification needs.



NORIT PK 1-3 M granular activated carbon is a highly macro porous, low density granular activated carbon, which can be used in a broad range of liquid phase applications including potable water and process water treatment. NORIT PK 1-3 M granular activated carbon is produced by steam activation of a renewable raw material.

NORIT PK 1-3 M granular activated carbon meets the requirements of the latest version of the U.S. Food Chemicals Codex, the Drinking Water Standard EN 12915 (European Normalisation, 2009) and meet the Halal and Kosher requirements.

SPECIFICATIONS

Iodine number	min. 800	-
Particle size > 3.35 mm	max. 10	mass-%
Particle size (0.71 mm)	max. 5	mass-%
Moisture (as packed)	max. 5	mass-%

GENERAL CHARACTERISTICS

Methylene blue adsorption	19	g/100 g
Total surface area (B.E.T.)	875	m ² /g
Apparent density	280	kg/m ³
Density, backwashed and drained	250	kg/m ³
Effective Size D ₅₀	1.5	mm
Uniformity coefficient	1.5	-
Ash content	9	mass-%
pH	alkaline	-
Moisture (as packed)	4	mass-%
Dechlorination halving value	5	cm

Appendix 2 Particle size distributions

Table 27 Particle size distribution for both carbon types

Eversorb					Norit Pk1-3M			
Sieve-	retained fraction	retained fraction in % of total mass	retained fraction in %		Sieve-	retained fraction	retained fraction in % of total mass	retained fraction in %
opening(in μm)	(in gram)	(per sieve)	(cum.)		opening(in μm)	(in gram)	(per sieve)	(cum.)
Totaal					Totaal			
3500	0.05	0.02%	100.00%		3500	3.86	3.17%	100.00%
2500	0.08	0.03%	99.98%		2500	35.35	29.06%	96.83%
1800	32.669	13.89%	99.94%		1800	50.61	41.61%	67.76%
1700	33.3	14.16%	86.05%		1700	11.1	9.13%	26.15%
1400	84.71	36.02%	71.89%		1400	13.51	11.11%	17.03%
1250	31.227	13.28%	35.87%		1250	2.93	2.41%	5.92%
1000	48.433	20.60%	22.59%		1000	3.176	2.61%	3.51%
850	3.347	1.42%	1.99%		850	0.33	0.27%	0.90%
425	1.021	0.43%	0.57%		425	0.38	0.31%	0.63%
335	0.018	0.01%	0.13%		335	0.027	0.02%	0.32%
106	0.076	0.03%	0.12%		106	0.16	0.13%	0.30%
<1	0.217	0.09%	0.09%		<1	0.2	0.16%	0.16%

Table 28 PSD for the IOCS

Sieve-	retained fraction in % of total mass	retained fraction in %
opening(in μm)	(per sieve)	(cum.)
900.0	0%	0.00%
1000.0	1%	0.83%
1120.0	0%	0.83%
1250.0	1%	1.34%
1400.0	1%	2.47%
1600.0	3%	5.29%
1700.0	0%	5.29%
1800.0	12%	17.20%
2000.0	19%	36.51%
2240.0	29%	65.82%
2500.0	21%	86.74%
2800.0	10%	97.22%
3550.0	1%	98.40%
4000.0	0%	98.43%
5000.0	0%	98.43%
D10	1847 μm	
D50	2342 μm	
D60	2431 μm	

Appendix 3 correction factor

Table 29 Theoretical vs measured concentration of pesticides in the stock solution and the correction factor derived

Stock solution 1	Mass added (mg)	Theoretical Concentration (mg/L)	Measured Concentration (mg/L)	Factor
Atrazine	2.06	1.03	0.19	5.48
Bentazone	2.06	1.03	0.22	4.72
Chloridazon	2.00	1.00	0.16	6.35
Imidacloprid	2.06	1.03	0.15	6.79
Tebuconazole	2.01	1.01	0.23	4.44
Stock solution 2	Mass added (mg)	Theoretical Concentration (mg/L)	Measured Concentration (mg/L)	Factor
Atrazine	1.98	0.99	0.18	5.57
Bentazone	2.10	1.05	0.22	4.77
Chloridazon	2.01	1.01	0.22	4.59
Imidacloprid	2.03	1.02	0.16	6.26
Tebuconazole	2.01	1.01	0.22	4.51
Average correction factor				
Atrazine				5.52
Bentazone				4.75
Chloridazon				5.40
Imidacloprid				6.52
Tebuconazole				4.48

Appendix 4 IOCS isotherms

Table 30 IOCS Isotherm data table

	Concentration IOCS (mg/L)	DOC (mg/L)	PO ₄ ³⁻	Ca ²⁺	NO ₃ ²⁻	K ⁺	Mg ⁺	Na ⁺	UV254	Notes
P0 T0	0	9.158	50.891	69.513	2.107	28.643	14.403	52.41	0.214	
P0 3W	0	8.47	50.342	69.05	2.325	28.899	14.234	52.753	0.195	
P1-1 3W	100	8.67	46.808	67.088	2.56	28.094	13.826	51.524	0.198	
P1-2 3W	100	8.95	46.918	67.921	2.553	28.452	13.871	51.436	0.196	
P1-3 3W	200	9.06	43.1	65.866	2.64	28.425	13.791	51.624	0.21	
P1-4 3W	600	9.76	35.049	61.836	2.786	28.406	13.203	51.375	0.256	
P1-5 3W	1000	10.48	24.423	54.775	2.994	28.092	12.675	51.478	0.297	
P1-6 3W	2000	12.55	13.029	54.44	3.347	27.748	0.105	51.336	0.33	Observed grinding
P1-7 3W	4000	13.58	3.045	50.716	4.088	27.919	11.942	51.212	0.314	
P1-8 3W	8000	13.59	1.025	46.498	5.265	26.653	11.11	51.031	0.287	
P1-9 3W	16000	13.03	0.564	43.256	7.943	26.124	10.455	50.698		

Table 31 Conversion of weeks to BV for IOCS breakthrough simulation based on Freundlich Isotherm data

Week	BV
1	183,19
2	366,39
3	549,58
4	732,78
5	915,97
6	1099,17
7	1282,36
8	1465,56
9	1648,75
10	1831,95
11	2015,14
12	2198,33
13	2381,53
14	2564,72

Appendix 5 Pesticide Isotherms

Table 32 Raw LC-MS data for all compounds. Note; values are not corrected for the correction factor (Table 29)

	Atrazine	Bentazone	Chloridazon	Imidacloprid	Tebuconazole
	µg/L	µg/L	µg/L	µg/L	µg/L
I0-0	1.86	2.15	1.63	1.51	2.33
I0-CONTROL	1.91	2.12	1.63	1.56	2.26
I1-0	1.89	2.16	1.51	1.47	2.34
I1-CONTROL	1.86	2.30	1.53	1.53	2.12
I1 Schiewater - GAC 1 - NORIT					
I1-1	1.59	2.22	1.37	1.28	1.72
I1-2	1.68	2.28	1.49	1.30	1.79
I1-3	1.47	2.12	1.14	1.07	1.25
I1-4	1.21	2.11	0.78	0.79	0.81
I1-5	1.35	2.07	0.94	0.89	1.16
I1-6	0.65	1.67	0.31	0.34	0.27
I1-7	0.25	1.30	0.08	0.11	0.04
I1-8	0.06	0.58	0.01	0.02	0.01
I2 Schiewater GAC 2 - EVERSORB					
I2-1	1.57	1.89	1.26	1.19	1.71
I2-2	1.50	2.15	0.98	0.91	1.58
I2-3	1.28	2.04	0.67	0.66	1.19
I2-4	0.83	1.92	0.17	0.19	0.37
I2-5	0.96	1.93	0.27	0.29	0.55
I2-6	0.38	1.78	0.05	0.06	0.11
I2-7	0.10	1.25	0.01	0.01	0.01
I2-8	0.03	0.34		0.00	0.00
I3 Boskoop GAC 1 - NORIT					
I3-1	1.74	2.21	1.39	1.33	2.00
I3-2	1.69	2.02	1.39	1.36	1.90
I3-3	1.55	2.08	1.20	1.21	1.56
I3-4	1.42	2.11	0.95	0.98	1.16
I3-5	1.33	1.93	0.83	0.87	1.06
I3-6	1.01	2.04	0.53	0.60	0.61
I3-7	0.52	1.80	0.19	0.25	0.12
I3-8	0.13	0.88	0.03	0.04	0.01

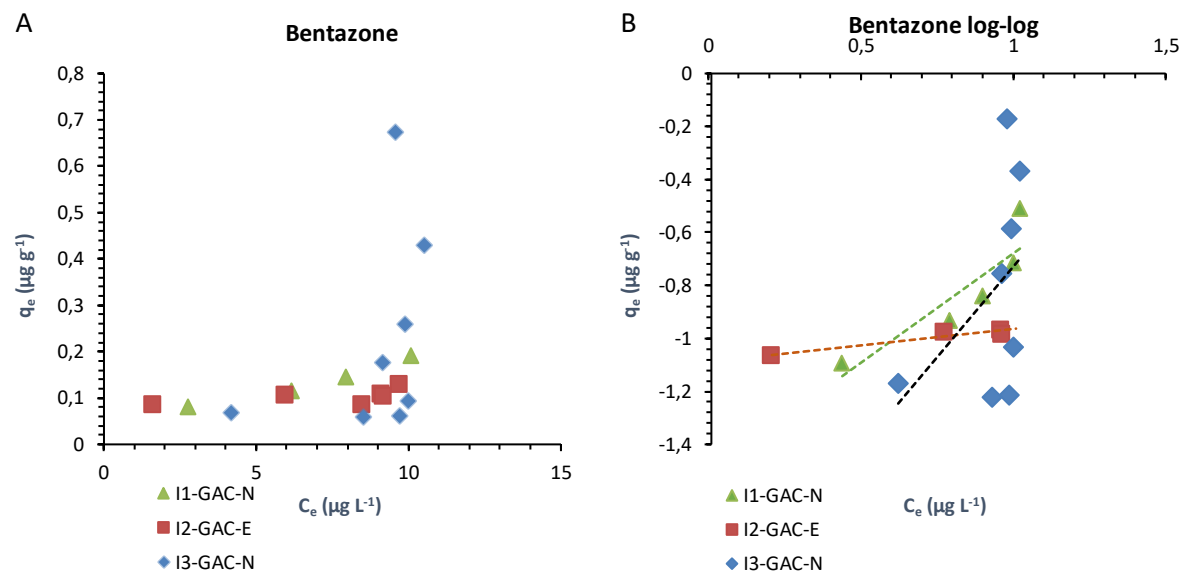


Figure 25A-B Bentazone C_e/Q_e (A) and log-log (B) plots. Plots where not suitable to model Freundlich or Langmuir isotherm parameters.

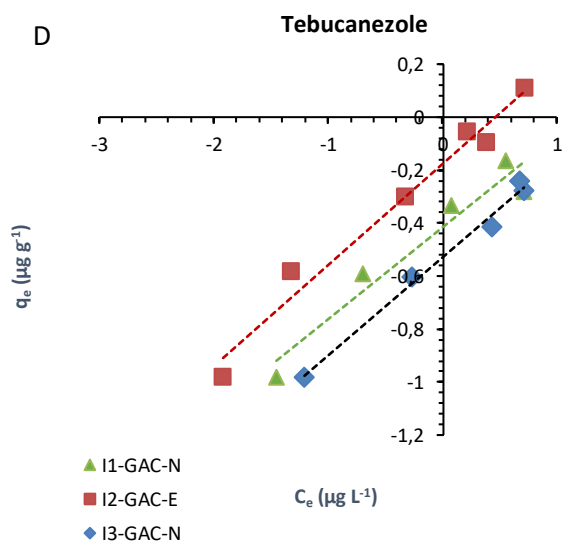
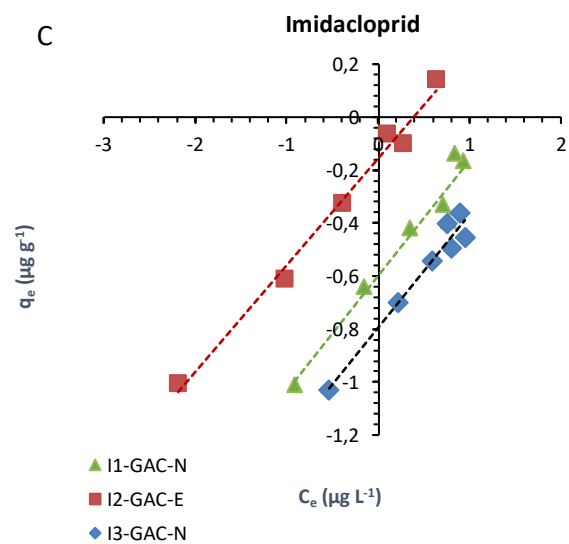
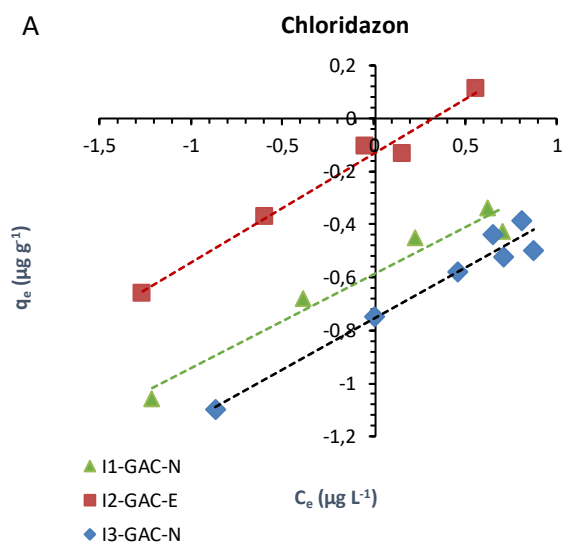
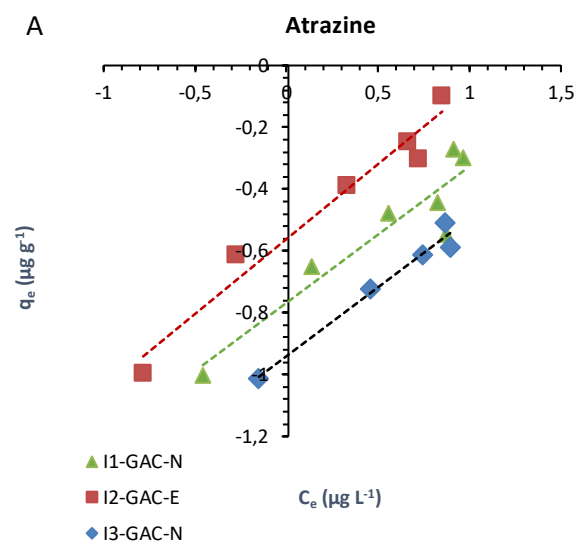


Figure 26A-D log-log plots for the 4 compounds used for Freundlich modelling

Appendix 6 Column studies

The salt tracer test was conducted using a 1mg/L NaCl solution. The pore volume can be estimated from the 50% breakthrough point of the salt tracer. As some fields of water research present their data as PV over BV, it is added as supplementary information.

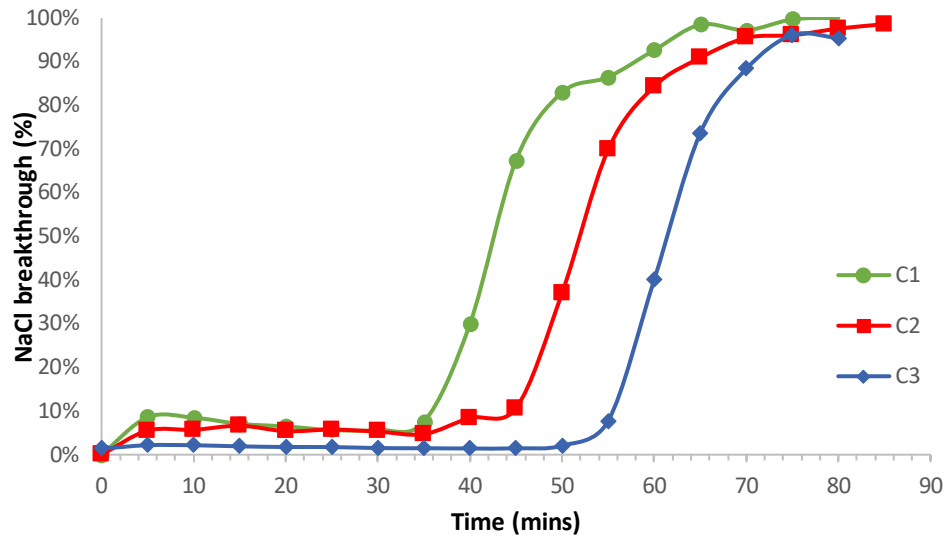


Figure 27 Salt tracer test (1mg/L NaCl) for all columns performed prior to the column experiments

Table 33 Salt tracer test data for all columns

	C1	C2	C3
Flow (ml/min)	2,08	1,92	1,91
First effluent flow (mins)	14,80	7,50	1,50
50% breakthrough (mins)	44,00	52,00	63,00
Volume pumped (mL)	122,01	114,10	123,06
Dead column volume (mL)	72,00	67,40	73,40
Effective pore space (mL)	50,01	46,70	49,66
Bed volume (mL)	129,26	129,26	129,26
bed porosity (mL)	0,39	0,36	0,38

Table 34 Bed volumes for all layers during the 14 weeks of operation of the column experiments

	C1		C2		C3		
Week	SSF	GAC	SSF	GAC	SSF	GAC	IOCS
1	216,94	911,16	216,60	909,73	222,42	934,16	203,08
2	435,94	1830,95	426,36	1790,71	438,85	1843,17	400,69
3	637,83	2678,88	623,11	2617,08	629,44	2643,67	574,71
4	838,00	3519,62	813,03	3414,71	817,64	3434,11	746,55
5	1031,54	4332,46	1001,83	4207,68	1001,78	4207,47	914,67
6	1250,87	5253,67	1216,34	5108,64	1214,27	5099,93	1108,68
7	1495,77	6282,24	1454,68	6109,64	1445,24	6070,02	1319,57
8	1692,65	7109,13	1654,87	6950,47	1647,34	6918,81	1504,09
9	1892,19	7947,18	1851,39	7775,86	1842,67	7739,22	1682,44
10	2085,37	8758,54	2058,87	8647,25	2041,05	8572,42	1863,57
11	2296,25	9644,26	2268,02	9525,70	2242,90	9420,18	2047,87
12	2499,21	10496,68	2478,66	10410,37	2441,09	10252,57	2228,82
13	2697,10	11327,84	2677,00	11243,39	2628,30	11038,84	2399,75
14	2883,97	12112,69	2864,91	12032,64	2819,06	11840,06	2573,93

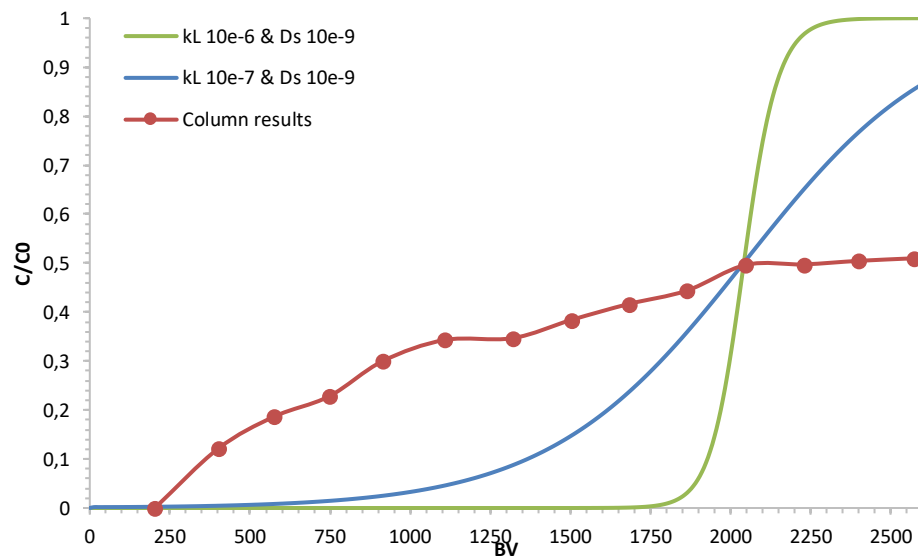


Figure 28 Phosphate breakthrough modelled with BV instead of weeks

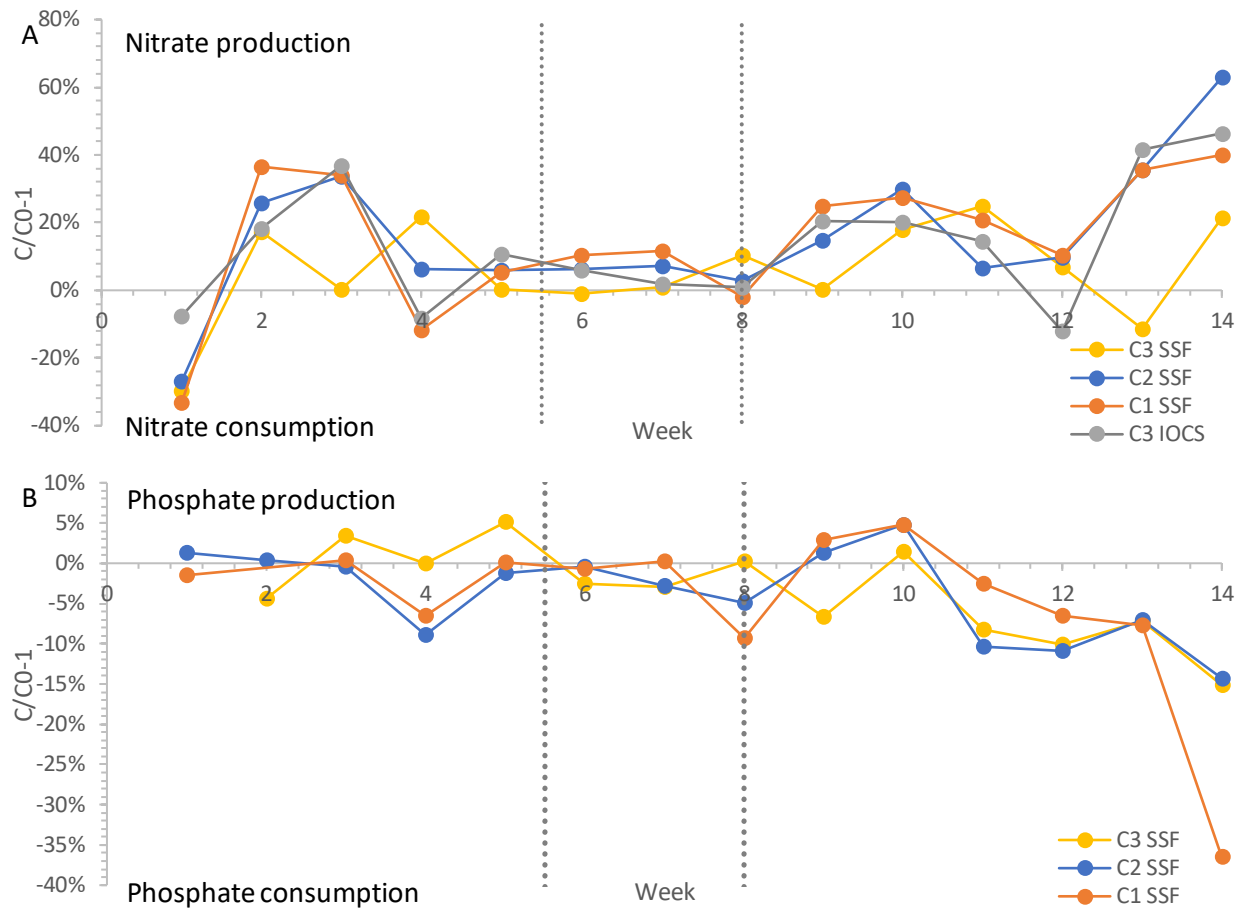


Figure 29 Nitrate and phosphate levels in the SSF and IOCS layers of the columns. Dashed lines indicate start and end of weekly flushing. Variance too small to be visible. Note the difference in C/CO axes.

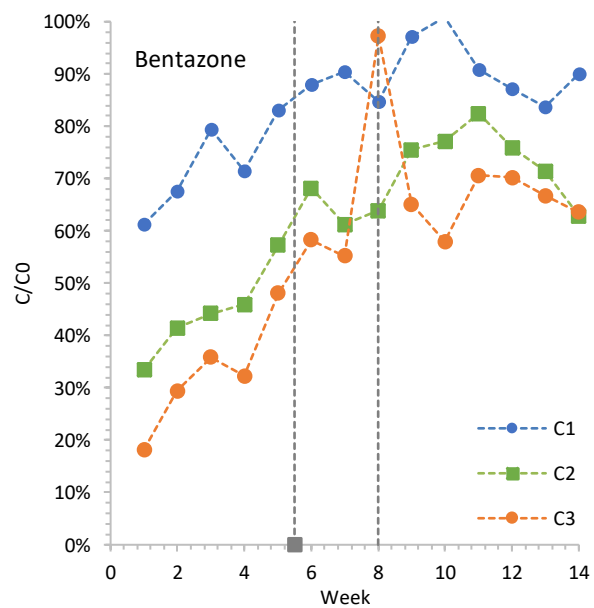
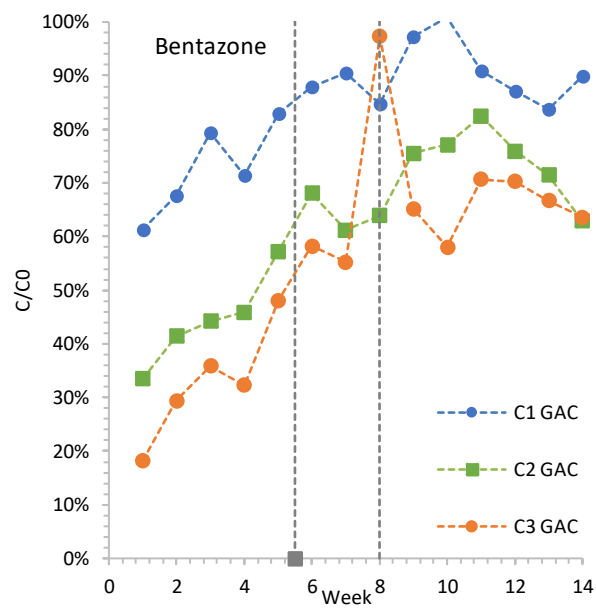
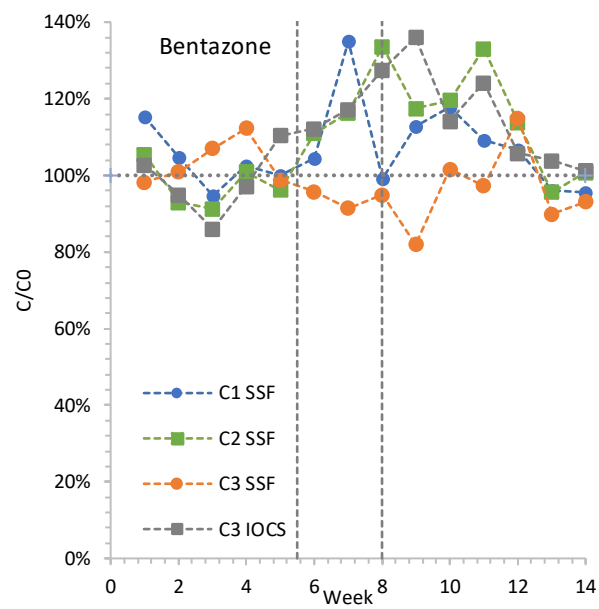


Figure 30A-C bentazone breakthrough curves for column studies. Breakthrough over SSF/IOCS (A), over GAC layer (B), over whole column (C)

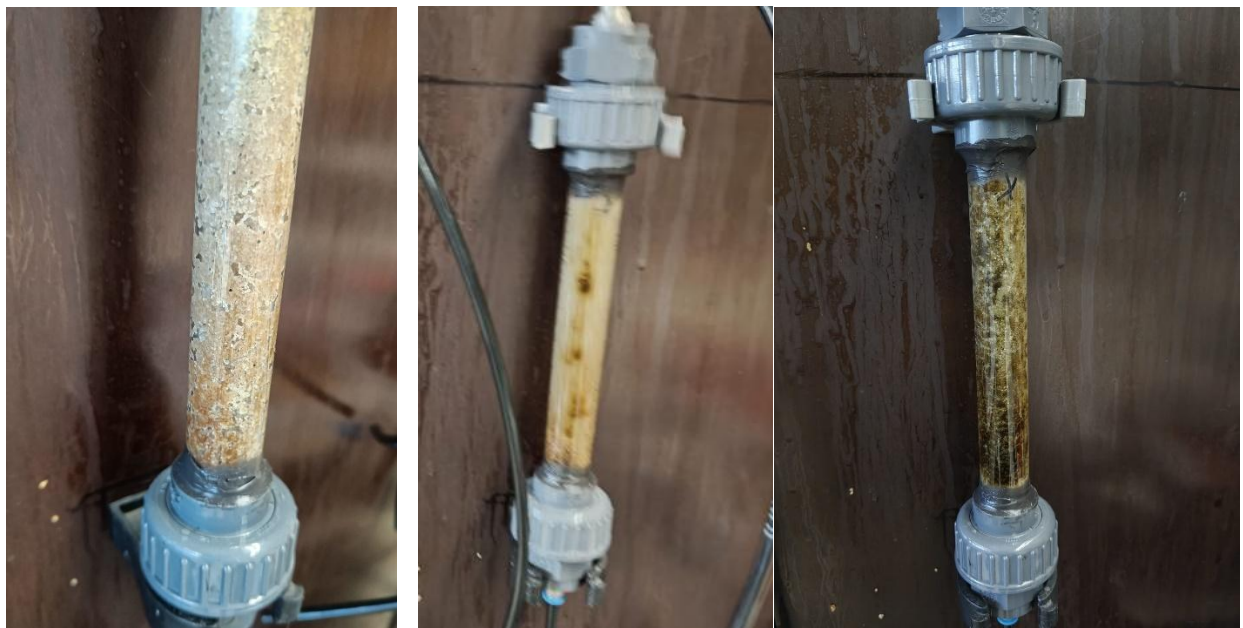


Figure 31 biogrowth on sand column. Photos taken after weeks 4,8,14